AD-A162 449 AUTOMATIC TARGET CLASSIFICATION USING HF MULTIFREQUENCY 1/3
RADARS(U) OHIO STATE UNIV COLUMBUS ELECTROSCIENCE LAB
J CHEN OCT 83 ESL-714190-3 N00014-82-K-0037

UNCLASSIFIED F/G 17/9 NL

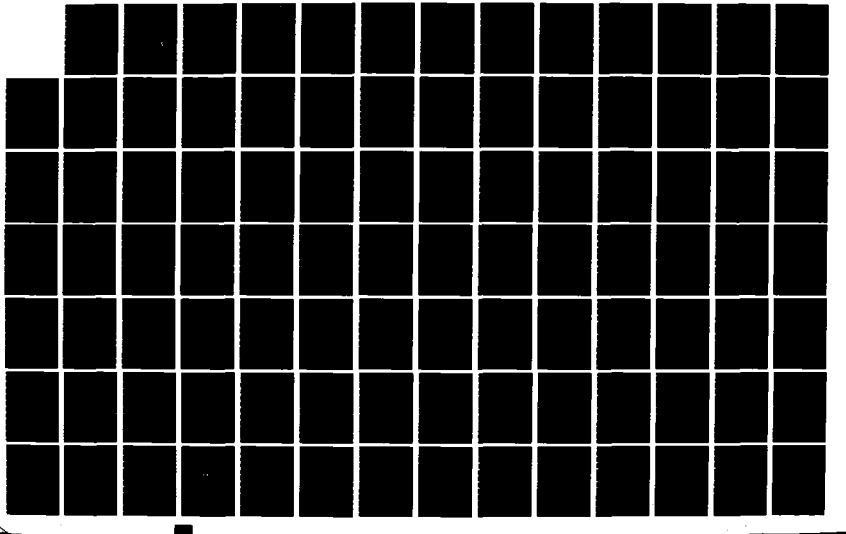

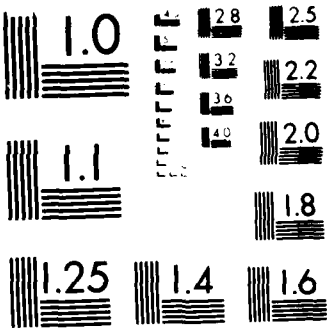

(12)

OSU

The Ohio State University

AUTOMATIC TARGET CLASSIFICATION USING HF MULTIFREQUENCY RADARS

Jenshiun Chen

The Ohio State University

ElectroScience Laboratory

Department of Electrical Engineering
Columbus, Ohio 43212

Technical Report 714190-3

Contract N00014-82-K-0037

October 1983

Department of the Navy
Office of Naval Research
800 North Quincy Street
Arlington, Virginia 22217

85

NOTICES

When Government drawings, specifications, or other data are used for any purpose other than in connection with a definitely related Government procurement operation, the United States Government thereby incurs no responsibility nor any obligation whatsoever, and the fact that the Government may have formulated, furnished, or in any way supplied the said drawings, specifications, or other data, is not to be regarded by implication or otherwise as in any manner licensing the holder or any other person or corporation, or conveying any rights or permission to manufacture, use, or sell any patented invention that may in any way be related thereto.

AD-A162 449

50272-101

REPORT DOCUMENTATION PAGE	1. REPORT NO.	2.	3. Recipient's Accession No

4. Title and Subtitle

AUTOMATIC TARGET CLASSIFICATION USING HF MULTIFREQUENCY RADARS

5. Report Date

October 1983

6.

7. Author(s)

Jenshiun Chen

8. Performing Organization Rept No

ESL 714190-3

9. Performing Organization Name and Address

The Ohio State University ElectroScience Laboratory
Department of Electrical Engineering
Columbus, Ohio 43212

10. Project/Task/Work Unit No

11. Contract(C) or Grant(G) No

(C)

(G) N00014-82-K-0037

12. Sponsoring Organization Name and Address

Department of the Navy
Office of Naval Research
800 North Quincy Street
Arlington, Virginia 22217

13. Type of Report & Period Covered

Technical Report

14.

15. Supplementary Notes

The work reported in this report was also used as a dissertation submitted to the Ohio State University Department of Electrical Engineering as part of the requirements for the degree Doctor of Philosophy.

16. Abstract (Limit: 200 words)

The classification of radar targets such as aircraft and ships using lower resonance-region radar returns has been of significant interest in recent years. The H.F. band is in the resonance region of such targets. The probability of misclassification depends upon the post-processing signal-to-noise power ratio.

Current techniques for measuring and processing the amplitude and phase of H.F. radar returns are reviewed. The post-processing SNR is determined as a function of coherent observation time. Based on features extracted from the radar returns, a frequency-domain Nearest-Neighbor classification algorithm and a time-domain Cross-Correlation classification algorithm are designed. A set of radar backscatter measurements of scale model ships and aircraft is used to generate a data base for testing the classification algorithms. Statistical techniques are applied to determine the probability of misclassification as a function of the post-processing SNR. The probability of misclassification for a reasonable amount of coherent observation time is determined.

17. Document Analysis a. Descriptors

b. Identifiers/Open-Ended Terms

c. COSATI Field/Group

18. Availability Statement

[illegible] for [illegible] distribution unlimited

19. Security Class (This Report) Unclassified

21. No. of Pages 207

20. Security Class (This Page) Unclassified

22. Price

(See ANSI-Z39.18) See Instructions on Reverse

OPTIONAL FORM 272 (4-77)
(Formerly NTIS-35)
Department of Commerce

TABLE OF CONTENTS

LIST OF TABLES

LIST OF FIGURES

Figure Page

Figure Page

Figure Page

CHAPTER I

INTRODUCTION

A. GENERAL NATURE OF THE PROBLEM

Radars operating at HF (3 to 30 MHz) have a unique capability of allowing propagation over long distance. Skolnik and Headrick [1, 2] indicated that over-the-horizon (OTH) HF radars using sky-wave propagation via refraction by the ionoshere are capable of detecting such targets as aircraft, ships, and missiles at distances beyond 4,000 km. The wavelengths of the HF band range from 10 to 100 m and are comparable to the dimensions of such targets. This means that the HF band is in the resonance region of such targets. Kennaugh and Moffatt [3, 4] found that low-frequency radar returns in the resonance region carried essential information regarding the overall dimensions and approximate shapes of the targets. Based on their work much research effort has been directed toward the identification of targets using resonance-region returns [4 - 13]. Ksienski and Lin [5, 8, 10] showed that reliable classification of aircraft can be achieved by processing resonance-region multi-frequency radar returns, and Walton and Young [13] demonstrated similar results for ships.

Fig. 1.1 shows a diagram of an HF target classification system. Possible targets include surface ships, aircraft, and missiles. The radar is capable of operating at several frequencies in the HF band. Two mechanisms of wave propagation are possible: sky wave and surface wave. The range of detection may vary depending on the propagation mechanism, frequency, weather, and other factors. The multi-frequency radar returns detected by the receiver are processed, and the target classifier then attempts to classify the detected target or targets based on the processed radar returns. The input to the target classifier is a set of amplitude and phase measurements of the target returns at selected frequencies. Conceptually the target classifier first extracts features from the radar returns then 'compares' the features with those in the catalog or data base, which is a set of ideal radar returns of a number of pre-selected targets. The target classifier can either identify an unknown target as one of the cataloged targets or claim that it is not listed in the catalog. The probability of misclassification depends on the post-processing signal-to-noise ratio of the radar returns, and the classification schemes used.

B. RESEARCH OBJECTIVES

Previous research work (e.g. ref. 4 - 13) usually assumed that amplitude and/or intrinsic phase were available. For HF radars the amplitude returns may vary widely as a function of the propagation loss,

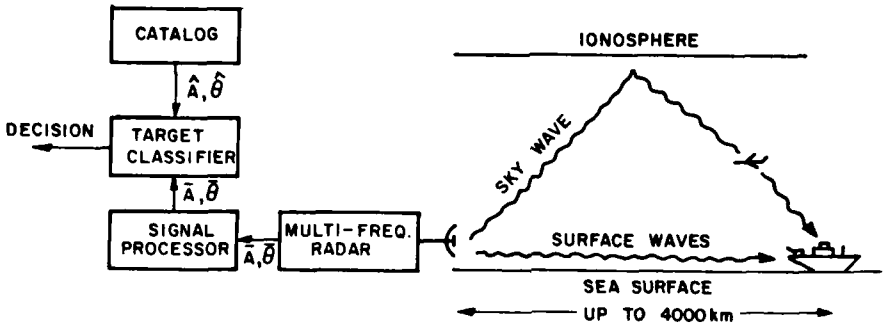

Figure 1.1. Block diagram of a typical target classification system. The catalog contains radar returns of some preselected targets $(\hat{A}, \hat{\theta})$. The output of the signal processor is a set of amplitude and phase returns of the unknown target.

antenna gains, and other factors. The phase returns are a function of wave path length and frequency, and can vary over the entire branch (e.g 0° to 360°). Therefore such radar returns must be processed extensively before reliable features can be extracted to classify the unknown targets. The probability of correctly classifying the unknown targets depends on the accuracy with which the radar returns are measured and the classification algorithms employed. The major purpose of this research is to

1. Study current techniques for measuring and processing the target returns.
2. Determine the approximate values of the post-processing signal-to-noise power ratio as a function of coherent observation time.
3. Develop target classification algorithms which utilize the processed amplitude and relative phase returns.
4. Determine the approximate values of the probability of misclassification as a function of post-processing signal-to-noise power ratio.
5. Determine the probability of misclassification achievable for a reasonable amount of coherent observation time.

C. ORGANIZATION OF THIS DISSERTATION

Chapter II will discuss two types of HF radars, namely, sky-wave and surface-wave radars [1, 2, 14]. The ionospheric and surface propagation effects will be briefly discussed [15, 16, 17]. Current techniques for measuring the amplitude returns [18] and relative phase returns [19] will also be reviewed. An estimation of the post-proscessing signal-to-noise power ratio as a function of total coherent observation time will be derived [20].

Chapter III will begin with a discussion of the basic classification process, and a brief discussion of Bayes decision theory [21, 22]. Based on the results of Chapter II, two non-parametric classification algorithms will be presented. The first algorithm will make use of the Nearest-Neighbor decision rule to classify targets in the frequency domain [5, 8, 10, 13]. The Nearest-Neighbor rule had been studied extensively in the literature and was proved to be very effective in identifying targets [5, 8, 10, 13]. The second will use cross-correlation processing to classify targets in the time domain [3, 9]. The correlation-processing is basically Matched-filtering, and has been used extensively in signal detection but has seldom been applied to target identification. Both algorithms require a catalog as mentioned above.

Chapter IV will discuss techniques for generating a data base [13]. Techniques for processing measured radar returns will be presented. Radar measurements of scale model targets, which were conducted in an

anechoic chamber, will be discussed. The processing of the measured data and the generation of an experimental database using the processed data will be discussed.

Chapter V will discuss testing of the classification algorithms using the experimental database. The targets selected include ships and aircraft. This chapter will estimate the probability of misclassification as a function of signal-to-noise ratio. All targets will be assumed to be listed in the database [23]. The design of a noise model and the scheme for estimating the classification probability using a finite number of samples will also be discussed [24]. The probability of misclassification as a function of coherent observation time will be determined.

Chapter VI will present a summary of the significance of the work, conclusions, and recommendations for future work.

CHAPTER II

MEASUREMENT OF H.F. RADAR RETURNS

A. INTRODUCTION

As discussed in Chapter I, our approach to target classification is to compare features extracted from radar returns of a target with those in the data base. It is evident that the probability of correctly classifying the targets is closely related to the accuracy with which we can measure the radar returns. Intuitively we know that the higher the signal-to-noise ratio, the lower the error. The use of HF frequencies for long distance detection further complicates the problem because of the large amount of noise that will accompany the radar returns. Therefore the design of identification algorithms must be facilitated by a knowledge of the characteristics of the post-processed H.F. radar returns. The purpose of this chapter is to examine, in general, how well we can estimate the H.F. radar returns. The post-processing signal-to-noise ratio will be estimated as a function of coherent observation time.

This will enable us to acquire an estimation of the probability of misclassification as a function of coherent observation time, and will give us an idea about the error probability we will likely have in practice.

Section B will discuss the characteristics of two types of HF radars, i.e., sky-wave and surface-wave HF radars, and a brief discussion on the propagation effects.

Section C will address the problem of measuring the radar cross section (RCS) of a target. It will examine and discuss the current techniques for calibrating the target cross section using the sea scatter as a reference. The post-processing signal-to-noise (SNR) power ratio will be evaluated statistically.

Section D will discuss measurement of the phase of radar returns using coherent radars, and determine the constituents of the coherent phase returns at the output of the receiver.

B. SOME CHARACTERISTICS OF HF RADARS

This section will first discuss sky-wave OTH H.F. radars [1, 2] and, then, discuss surface-wave OTH H.F. radars [14] and a comparison between the two types of radars.

1. H.F. Sky-Wave Radars

H.F. sky-wave radars make use of ionospheric refraction for the detection of targets at over-the-horizon distances. Ionospheric

conditions may vary with weather, season, time of day, solar activity, etc., and the optimum operating frequencies may change from time to time over a wide portion of the H.F. band.

There may be more than one refracting region in the ionosphere. The highest region, i.e., the F_2 layer, is at altitudes of from 230 to 400 km. A single refraction from such region allows radar ranges to be extended to almost 4000 km. Consider a figure from [15], as shown in Fig. 2.1. The figure is a diagram of transmission curves with the oblique transmission frequency as a parameter for a fixed distance of of 2,000 km superimposed on a vertical ionogram. Here the transmission curves describe the relationship between the oblique transmission and equivalent vertical transmission frequencies. Note that the equivalent vertical transmission frequency is the frequency of the vertically-transmitted waves which reach the same virtual height as the obliquely-transmitted waves do. In this case a plane reflector is used to model the ionosphere, and the transmission curves are given by the 'Secant Law' [15], i.e.,

$$f_{ob} = f_v \sec\phi_o$$

$$= f_v \sqrt{1 + \left(\frac{D}{2h'}\right)^2}$$

where h' = equivalent virtual height

D = distance

f_{ob} = oblique transmission frequency

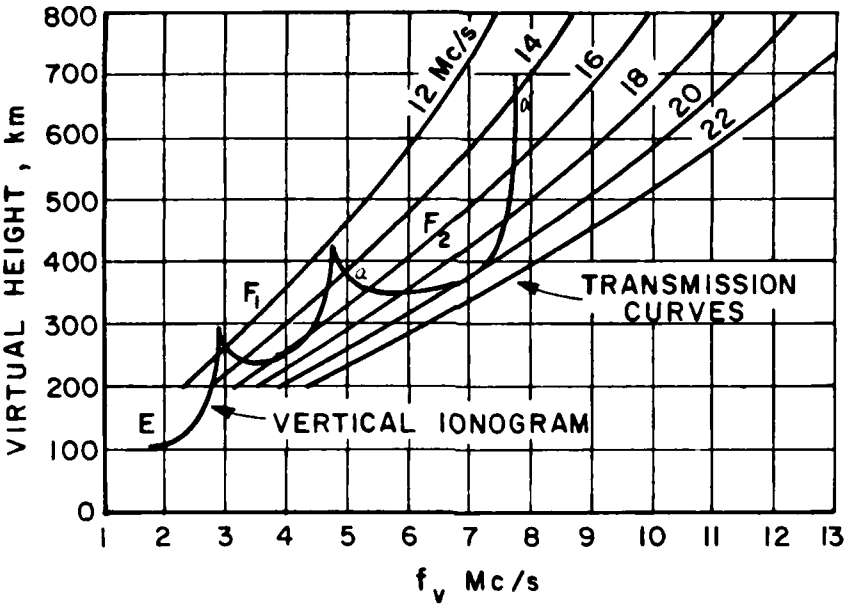

Fig. 2.1. Family of transmission curves parametric in frequency for a fixed distance of 2,000 km superimposed on a vertical ionogram (Davis [15]). The abscissa is the vertical transmission frequency, and the parameter is the oblique transmission frequency.

f_v = vertical transmission frequency

ϕ_0 = elevation angle.

The intersection of a transmission curve, for a given oblique transmission frequency f_{ob}, with the vertical ionogram gives the virtual heights of reflection of the transmitted curves. In Fig. 2.1 the three sections of the vertical ionogram would correspond to reflection from the E, F_1 and F_2 layers of the ionosphere. A frequency of 14 MHz, for example, for propagation over a distance of 2,000 km, could travel by several different paths, two of which would be reflected from the F_2 layer at heights corresponding to the intersections marked a and a' on the vertical ionogram. The corresponding ray paths are shown in Fig. 2.2 [15]. For values of f_v above 20 MHz there is no intersection, and, hence, no level of reflection. The distance for which a given frequency is the maximum frequency is called the skip distance. Within this distance no signals are received from the ionosphere. Waves with different frequencies may have different phase delays because they may propagate along different paths. The extraction of features from multi-frequency phase returns must therefore contend with this frequency-dispersion phenomenon.

In general, it is difficult to predict the received signal level because it may require a detailed knowledge of the ionosphere along the ray path together with elaborate ray-tracing [15]. Navon and Cory [16] showed that the received signal median for a one-way communication link of about 2000 km can be predicted with an accuracy of about 5 dB which is unfortunately, too high to be useful for target identification.

TABLE 2.1

SPECIFICATIONS OF HF RADARS

	SKY-WAVE RADAR	SURFACE-WAVE RADAR
TRANSMITTED POWER	SEVERAL HUNDRED kW	HIGHER
RANGE	1000 to 4000 km	about 300 km
Antenna gain	20 to 30 dB	same
Antenna horizontal length	about 1 km	about 1 km
Waveform	can be pulsed sinusoidal waves	can be pulsed sinusoidal waves
Bandwidth	5 to 100 kHz	can be wider
Pulse width	200 μs to 10 μs	can be narrower
Range resolution	2 to 40 km	can be smaller
Doppler resolution	about 0.1 Hz	can be less than 0.1 Hz
PRF	about 30 Hz	about 300 Hz
Targets	aircraft, ships, missiles	same
Antenna Azimuth beamwidth	about 1°	about 1°

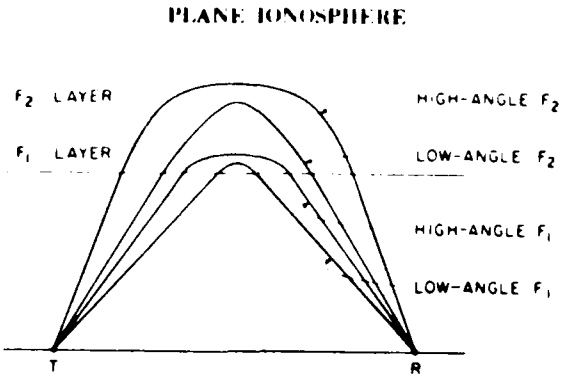

Fig. 2.2. Ray paths corresponding to intersections of transmission curves and the ionogram (Davis [15]).

The range of operation for sky-wave radar can be extended up to 4,000 km and beyond. However the range of operation is generally limited to a minimum of about 1,000 km due to the ionospheric skip-distance effect [15]. A specification of a typical HF sky-wave radars was given by Skolnik and Headrick [1, 2], and is shown in Table 2.1.

2. H.F. Surface-Wave Radars

Surface-wave radars rely on surface or ground wave propagation around the curvature of the earth. Because of high losses, propagation over long distances can best be achieved over the ocean surface [14]. The range of operation can vary from tens of kilometers up to about 500 kilometers. It covers the range-gap between line-of-sight radars and sky-wave radars. The specification for a typical surface wave radar is quite different from that of a sky-wave radar, as can be seen from Table 2.1. This will be briefly explained below.

Barrick [17] indicated that the sea state can significantly affect the ground-wave loss for propagation across the ocean at HF. The sea state is a measure of the wave height, as shown in Table 2.2 [1]. Figure 2.3 is a plot of the additional transmission loss due to sea state at 10 MHz [17]. It can be seen that the transmission loss increases rapidly as the ground distance increases. Table 2.3 is a list of additional transmission loss due to sea state for a fixed ground distance of 463 km (250 nmi). It can be seen that, for sea states of 4 and 5, the two-way losses at a frequency of 10 MHz can be as high as 23

TABLE 2.2

World Meteorological Organization Sea State [1].

Sea state	Wave height		Descriptive term
	Feet	Meters	
0	0	0	Calm, glassy
1	0–$\frac{1}{3}$	0–0.1	Calm, rippled
2	$\frac{1}{3}$–1$\frac{1}{2}$	0.1–0.5	Smooth, wavelets
3	2–4	0.6–1.2	Slight
4	4–8	1.2–2.4	Moderate
5	8–13	2.4–4.0	Rough
6	13–20	4.0–6.0	Very rough
7	20–30	6.0–9.0	High
8	30–45	9.0–14	Very high
9	over 45	over 14	Phenomenal

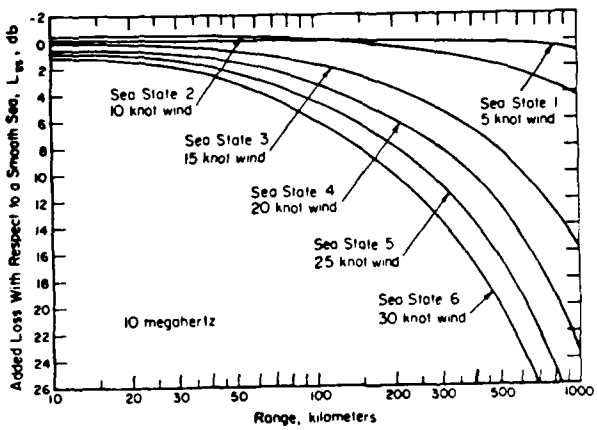

Fig. 2.3. Additional transmission loss due to sea state at 10 MHz (Barrick [17]).

TABLE 2.3

ADDITIONAL TRANSMISSION LOSS DUE TO SEA STATE (Barrick [17]).

FREQUENCY (MHz)	TWO-WAY LOSS (dB)*	
	SEA STATE = 4	SEA STATE = 5
5	< 2	< 6
7	< 10	< 16
10	< 23	< 31
15	< 34	< 40

*Ground distance < 250 nmi

dB and 31 dB, respectively, above the free-space loss. It can also be seen that the loss is less for low frequencies. Because of high propagation loss, surface-wave radars have a much shorter range of detection than sky-wave radars.

In most cases the incident elevation angle of surface waves on targets is equal to or slightly greater than zero, whereas the incident elevation angles of sky waves may vary widely, depending on target range. The latter may require a much larger data base containing backscatter data for a set of incident elevation angles, resulting in tremendous increase in complexity, ambiguity in look angles, and costs.

Finally in this section we would like to note that H.F. radars must employ doppler processing to seperate desired moving targets from surface clutter, because the clutter returns are usually much larger than the target returns [1]. The detection of low-speed targets such as ships requires more sophisticated processing and longer processing time to provide sufficient resolution in doppler frequency. Since a processing time of T seconds corresponds to a doppler frequency resolution of 1/T HZ, we can, ideally, obtain a very high doppler resolution if we increase the processing time. Trizna [5], however, indicated that there is a practical limit on the minimum spectral width which can be achieved.

He indicated that the most severe resolution limitation is provided by the ionosphere. Propagation in the ionosphere results in phase changes which may not be uniform across the phase fronts of the radar waves. The ionosphere condition may change with time, resulting in

change of wave paths with time. The maximum useful coherent observation time available for F-layer propagation is typically 25 seconds [18]. The E-layer is more stable and coherent observation times up to 100 seconds are possible [18].

C. MEASUREMENT OF H.F. AMPLITUDE RETURNS

The amplitude return of a target can be defined as the square root of the radar cross section σ of the target defined as

$$\sigma = \frac{\text{scattered power}}{\text{incident power density at the target}} \tag{2.1}$$

Let the incident power density at the target be given as

$$|E^i|^2 = \frac{P_T G_T}{4\pi R^2 L_p} \tag{2.2}$$

where

P_T = transmitted power

G_T = transmitting antenna gain

L_p = one-way propagation loss

R = one-way wave path length

Assume the scattered power is isotropic and L_p and R for both the incident field and the scattered field are the same, then the received power at the output of a radar receiver is given as

$$p^r = \left(\frac{P_T G_T}{4\pi R^2 L_p}\right) \sigma \left(\frac{1}{4\pi R^2 L_p}\right) Ae \left(\frac{G_a}{L_s}\right) \tag{2.3}$$

where,

L_s = system loss

G_a = receiver power gain

and A_e is the effective area of the receiving antenna, and is given as

$$A_e = \frac{G_R \lambda^2}{4\pi} \quad . \tag{2.4}$$

where

G_R = receiving antenna gain

λ = wavelength

The system loss L_s consists of loss in the antennas, transmission lines, and other losses in the transmitter and receiver. From equations (2.3) and (2.4) the target cross section σ can be given as

$$\sigma = \frac{p^r (4\pi)^3 R^4 L_p^2 L_s}{P_T G_T G_R \lambda^2 G_a} \tag{2.5}$$

and the amplitude return can be given as

$$A \equiv \bar{\sigma} = \sqrt{\frac{p^r (4\pi)^3 R^4 L_p^2 L_s}{P_T G_T G_R \lambda^2 G_a}} \tag{2.6}$$

Eq. (2.6) shows that the amplitude return is a function of many parameters, some of which may be difficult to estimate. For example the propagation loss L_p for either sky-wave or surface wave radars is difficult to estimate since, as discussed in section B, it may vary as the ionospheric condition or sea state changes. The amplitude as calculated by Eq. (2.6) cannot be used directly for target classification. One way to reduce the number of parameters is to use as a reference the signal return from another object which is close to the target, and whose radar cross section can be estimated independently. Suppose the reference signal power at the receiver output is given as

$$\sigma^{ref} = \frac{p^{ref}(4\pi)^3 R^4 L_p^2 L_s}{P_T G_T G_R \lambda^2 G_a} \tag{2.7}$$

where σ^{ref} is the radar cross section of the reference object. If the reference objects are close enough to the target, the propagation loss L_p and the wave path length R in Eq. (2.7) should be close to those in Eq. (2.5). Other parameters P_T, G_T, G_R, G_a, and L_s in both equations should be similar because the target and the reference are illuminated by the same radar at the same time. Taking the ratio of Eq. (2.5) and Eq. (2.7), we have

$$\frac{p^r}{p^{ref}} \approx \frac{\sigma}{\sigma^{ref}}$$

or

$$\sigma \approx \left(\frac{p^r}{p^{ref}}\right) \sigma^{ref} \tag{2.8}$$

Apparently Eq. (2.8) above is much simpler and more reliable than Eq. (2.5). Note that Eq. (2.8) is a calibration equation for a particular frequency. For multi-frequency returns the returns of each frequency must be calibrated individually. The parameters p^r and p^{ref} can be measured using Doppler processing, and σ^{ref} can be predicted, as discussed below.

Trizna [18] suggested that the sea scatter can be used as a reference for calibrating the target cross section. The sea may be regarded as composed of a large number of individual wave trains, each with a different wavelength and amplitude and travelling in different directions [1]. Assuming that the sea acts as a simple diffraction grating, Crombie [25] showed that, for radar waves incident on the sea surface with an incident angle of ϕ, the radar responds mainly to two resonant sea wave trains which are travelling radially toward and away from the radar, as shown in Fig. 2.4. From the figure, it is evident that the scattered signals are in-phase when

$$2\lambda\omega \cos\phi = n\lambda \; ; \; n = 1, 2, 3 \ldots$$

where

$\lambda\omega$ = water wave length

λ = radar wave length

ϕ = wave incident angle

The sea scatter is called first-order for n = 1, second-order for n = 2,

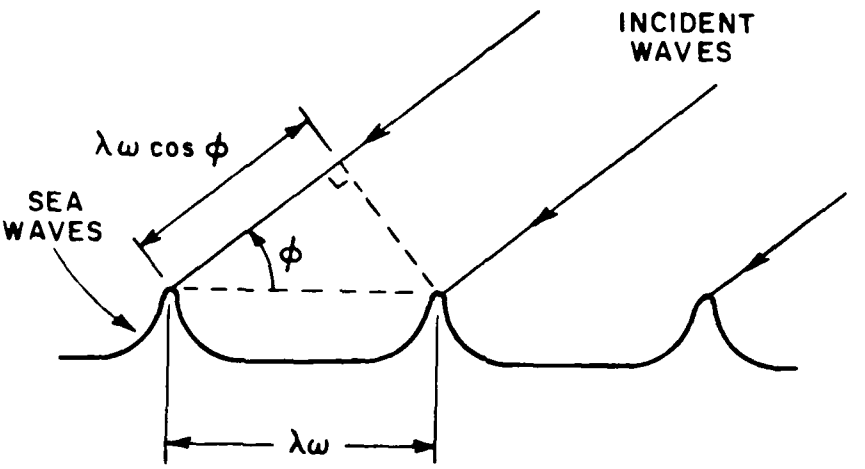

Fig. 2.4. A diffraction grating model for sea surface waves.

and so forth. The velocity of a water wave which is driven by gravity [26] is given by

$$v = \sqrt{\frac{g\lambda\omega}{2\pi}}$$

where g = acceleration due to gravity. Therefore the Doppler frequencies of the water waves are given by

$$f_d = \frac{2v}{\lambda} = \pm\sqrt{\frac{ng}{\pi\lambda\cos\phi}} \qquad (2.9)$$

After Crombie identified the mechanism of sea scatter, considerable research has been conducted on the analysis of sea scatter [18, 20, 26, 27, 28, 29, 30]. Now let's discuss the calibration of target cross section using sea scatter, as suggested by Trizna [18].

For convenience a figure from [18] is shown in Fig. 2.5, which is a radar spectrum of sea echo collected with a 17-second integration time and a 21.8-MHZ radar frequency, at a range of about 1600 KM. Note that the frequency in the figure is normalized to the first-order sea scatter. The area illuminated by the radar for a pulse length of τ and azimuth beam width θ_B is given by [1] (see Fig. 2.6)

$$A_C = R\theta_B \left(\frac{C\tau}{2}\right) \sec\phi$$

where

A_C = illuminated area

R = wave path length

θ_B = horizontal antenna beam width

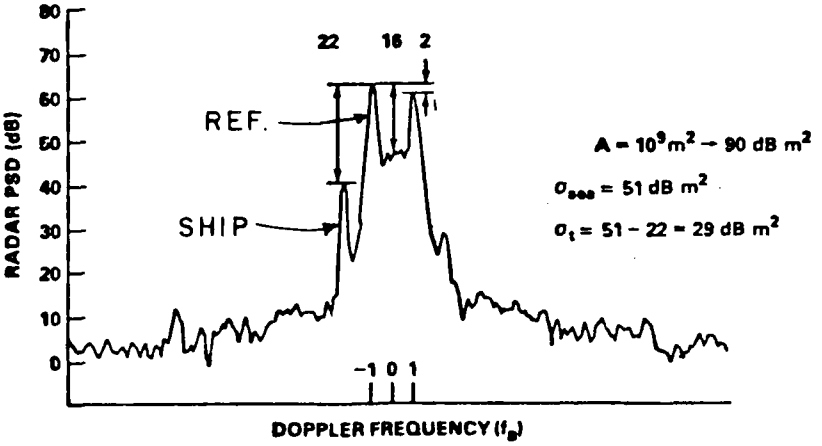

Fig. 2.5. A Doppler spectrum is shown in which a ship target return is separated from the clutter. The reference here is the larger first order sea scatter. The Doppler frequency here is normalized to the 1st order sea scatter Doppler frequency.

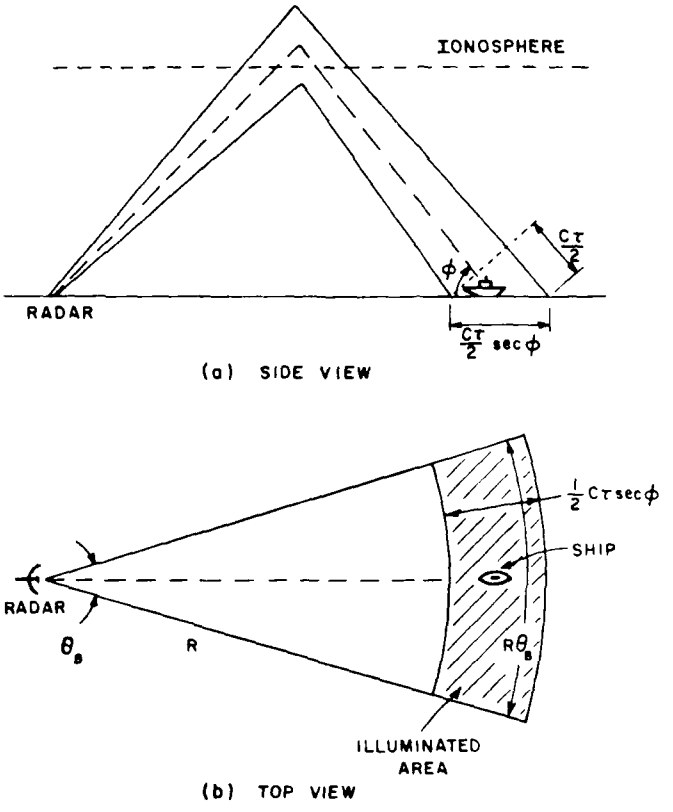

Fig. 2.6. The area illuminated by a radar is shown as the shaded area. Note here that

ϕ = grazing ange

τ = pulse width

C = speed of light

R = wavepath length

θ_B = antenna azimuth beam width

ϕ = elevation angle

τ = pulse width

The illuminated area (or scattering cell) in this case was of the order of 90 dB-square meters. As shown in the Doppler spectrum, the ship return is separated from the sea scatter, and the target return and the sea scatter can be readily obtained. It can be seen that the value of the cross section of the target is 22 dB below the greater first-order sea scatter located at f = -1. Based on a second-order model, Trizna [18] theoretically predicted that the magnitude of the sea scatter in this case is 51 dB-square-meters. Therefore he found that the target cross section is 29.2 dB-square-meters or 832 square meters.

Trizna indicated that the calibrated target cross section was sufficiently accurate to be applied to most conditions appropriate to HF propagation, in particular the high frequency portion of HF band. As the techniques are being updated and refined, the accuracy of measuring the target RCS will gradually improve.

The radar cross section of the sea is a function of wave height, current direction, wind speed, etc., and will vary as weather and sea state change [17, 18]. Barrick [20] experimentally found that the spectral component of the first-order sea scatter can be approximated by a Gaussian distribution. This enables us to analyze the error embedded in the calibrated target cross section σ in Eq. (2.8), as discussed below.

In order to increase the accuracy of the estimated target cross section we can increase the number of observations and then calculate the average of the received radar returns. Let $\bar{p}$ be the sample average defined as

$$\bar{p} = \frac{1}{M} \sum_{i=1}^{M} P_i \tag{2.10}$$

where P_i is the received power for the ith observation. From Eq. (2.8) and Eq. (2.10) we can estimate the target cross section σ_t^E as

$$\sigma_t^E \approx \frac{\sigma_B \bar{P}_t}{\bar{P}_B} \tag{2.11}$$

where

σ_B = theoretical value of the RCS of the reference

$\bar{p}_t$ = average power of the target returns

$\bar{p}_B$ = average power of the reference returns

In the following we will, under certain assumptions, attempt to estimate the difference between the estimated target cross section σ_t^E and the cataloged target cross section σ_t^c, and determine statistically the signal-to-noise power ratio.

We first assume that the total observation time does not exceed the interval over which the reference is statistically stationary. Barrick [20] indicated that, for sea scatter, this total observation time may vary between 1 and 12 hours.

Suppose the target cross section σ_t^c in the catalog can be expressed as

$$\sigma_t^c = \frac{\sigma_B \langle P_t \rangle}{\langle P_B \rangle} \tag{2.12}$$

where $\langle \cdot \rangle$ means expected value. For convenience assume that the actual value of σ_B can be estimated, and that the target return p_t is stationary so that

$$\bar{p}_t \approx \langle p_t \rangle \tag{2.13}$$

From Eqs. (2.11), (2.12), and (2.13) we have

$$\sigma_t^E \approx \frac{\sigma_B \bar{p}_t}{\bar{p}_B}$$

$$\approx \frac{\sigma_B \langle P_t \rangle}{\bar{p}_B}$$

$$= \frac{\sigma_B \langle P_t \rangle / \langle P_B \rangle}{\bar{p}_B / \langle P_B \rangle}$$

or

$$\sigma_t^E \approx \frac{\sigma_t^c}{\bar{P}_B/\langle P_B \rangle} \tag{2.14}$$

In general we can assume that the radar returns are narrow-band signals which can be expressed as follows.

$$f(t) = A(t)\cos(\omega_c t + \phi(t)) \tag{2.15}$$

where ω_c is the carrier frequency. For convenience define a phasor $\hat{f}(t)$ as

$$\hat{f}(t) \equiv A(t)\, e^{j\phi(t)} \tag{2.16}$$

Evidently

$$f(t) = \mathrm{Re}\{\hat{f}(t) e^{j\omega_c t}\} \tag{2.17}$$

Expand $\hat{f}(t)$ in terms of a Fourier series in the interval $[-T/2, T/2]$ and obtain

$$\hat{f}(t) = \sum_{k=-\infty}^{\infty} C_k\, e^{j(k\omega_c t + \phi_k)} \tag{2.18}$$

where $\omega_0 = 2\pi/T$ = fundamental frequency, and the Fourier coefficient is given by

$$C_k e^{j\phi_k} = \frac{1}{T} \int_{-T/2}^{T/2} \hat{f}(t)\, e^{-jk\omega_0 t}\, dt$$

with the variable C_k being real. Substitute Eq. (2.18) into Eq. (2.17) to get

$$f(t) = \mathrm{Re}\{\hat{f}(t)e^{j\omega_c t}\}$$

$$= \mathrm{Re}\{\sum_k C_k e^{j(k\omega_0 t+\phi_k)} e^{j\omega_c t}\}$$

$$= \sum_k C_k \cos[(\omega_c + k\omega_0)t + \phi_k]$$

$$= \sum_k C_k[\cos(\omega_c + k\omega_0)t \cos\phi_k - \sin(\omega_c + k\omega_0)t \sin\phi_k]$$

$$\equiv \sum_k [X_k \cos(\omega_c + k\omega_0)t - y_k \sin(\omega_c + k\omega_0)t] \qquad (2.19)$$

where

$$X_k \equiv C_k \cos\phi_k$$

$$Y_k \equiv C_k \sin\phi_k$$

The spectral component of f(t) at $\omega = \omega_c + k\omega_0$ is given by

$$P_k = X_k^2 + Y_k^2 \qquad (2.20)$$

Assume that X_k and Y_k are uncorrelated Gaussian variables with zero mean and variance α_k^2. This assumption is believed to be applicable in most cases. In fact Barrick [20] experimentally showed that the spectral components at the first-order sea scatter frequency can be approximated by Eq. (2.20), with X_k and Y_k being uncorrelated zero-mean Gaussian random variables. Suppose M independent spectral samples of the radar returns are collected, and define

$$\Gamma \equiv \frac{\bar{P}_B}{\langle P_B \rangle} \qquad (2.21)$$

then Eq. (2.14) can be rewritten as

$$\sigma_t^E = \frac{\sigma_t^c}{\Gamma} \tag{2.22}$$

Now

$$\begin{aligned} \langle P_B \rangle &= \langle X_B^2 + Y_B^2 \rangle \\ &= \langle X_B^2 \rangle + \langle Y_B^2 \rangle \\ &= 2\alpha_B^2 \end{aligned} \tag{2.23}$$

Let

$$\begin{aligned} \bar{P}_B &= \frac{1}{M} \sum_{n=1}^{M} P_{B,n} \\ &= \frac{1}{M} \sum_{n=1}^{M} (X_{B,n}^2 + Y_{B,n}^2) \end{aligned}$$

then Γ can be rewritten as

$$\begin{aligned} \Gamma &= \frac{\bar{P}_B}{\langle P_B \rangle} \\ &= \frac{1}{M 2\alpha_B^2} \sum_{n=1}^{M} (X_{B,n}^2 + Y_{B,n}^2) \\ &= \frac{1}{M} \sum_{n=1}^{M} \left(\frac{X_{B,n}}{\alpha_B}\right)^2 + \left(\frac{Y_{B,n}}{\alpha_B}\right)^2 \end{aligned} \tag{2.24}$$

Since $X_{B,n}/\alpha_B$ and $Y_{B,n}/\alpha_B$ are Gaussian-distributed with zero mean and variance 1, it can be shown [31] that Γ is Chi-Squared distributed with

M-1 degrees of freedom. The analysis will be greatly simplified if M is sufficiently large so that Γ can be approximately described by a Gaussian distribution by virtue of the Central-Limit Theorem. It has been shown that M = 12 would be sufficient [32]. Now let's calculate the expected value of Γ, namely $\langle\Gamma\rangle$, as follows.

$$\langle\Gamma\rangle = \left\langle \frac{\bar{P}_B}{\langle P_B\rangle} \right\rangle$$

$$= \frac{\langle\bar{P}_B\rangle}{\langle P_B\rangle} \qquad (2.25)$$

Now

$$\langle\bar{p}_B\rangle = \left\langle \frac{1}{M} \sum_{n=1}^{M} P_{B,n} \right\rangle$$

$$= \frac{1}{M} \left\langle \sum_{n=1}^{M} X_{B,n}^2 + Y_{B,n}^2 \right\rangle$$

$$= \frac{1}{M} \sum_{n=1}^{M} \langle X_{B,n}^2 \rangle + \langle Y_{B,n}^2 \rangle$$

$$= 2\alpha_B^2 \qquad (2.26)$$

where

$$\langle X_{B,n}^2 \rangle = \langle Y_{B,n}^2 \rangle \equiv \alpha_B^2$$

From Eq. (2.23) and Eq. (2.26) we have

$$\langle r \rangle = \frac{\langle \bar{P}_B \rangle}{\langle P_B \rangle}$$

$$= \frac{2\alpha_B^2}{2\alpha_B^2}$$

$$= 1 \qquad (2.27)$$

The variance of r can be calculated as follows.

$$\mathrm{Var}(r) = \mathrm{Var}\left(\frac{\bar{P}_B}{\langle P_B \rangle}\right)$$

$$= \frac{\mathrm{Var}(\bar{P}_B)}{\langle P_B \rangle^2}$$

Now

$$\mathrm{Var}(\bar{P}_B) = \mathrm{Var}\left(\frac{1}{M}\sum_{n=1}^{M} P_{B,n}\right)$$

$$= \mathrm{Var}\left(\frac{1}{M}\sum_{n=1}^{M} X_{B,n}^2 + Y_{B,n}^2\right)$$

$$= \left(\frac{1}{M}\right)^2 \sum_{n=1}^{M} \mathrm{Var}(X_{B,n}^2) + \mathrm{Var}(Y_{B,n}^2)$$

where

$$\mathrm{Var}(X_{B,n}^2) = \langle X_{B,n}^4 \rangle - \langle X_{B,n}^2 \rangle^2$$

and

$$\mathrm{Var}(Y_{B,n})^2 = \langle Y_{B,n}^4 \rangle - \langle Y_{B,n}^2 \rangle^2$$

Since $X_{B,n}$ and $Y_{B,n}$ are Gaussian with zero mean and variance α_B^2 we have, using moment expansion [21],

$$\langle X_{B,n}^4 \rangle = 3\langle X_{B,n}^2 \rangle^2 - 2\langle X_{B,n} \rangle^4$$

$$= 3\langle X_{B,n}^2 \rangle^2$$

and

$$\mathrm{Var}(X_{B,n}^2) = 3\langle X_{B,n}^2 \rangle^2 - \langle X_{B,n}^2 \rangle^2$$

$$= 2\langle X_{B,n}^2 \rangle^2$$

$$= 2(\alpha_B^2)^2$$

$$= 2\alpha_B^4$$

Likewise we have

$$\mathrm{Var}(Y_{B,n}^2) = 2\alpha_B^4$$

Hence

$$\mathrm{Var}(\bar{P}_B) = \left(\frac{1}{M}\right)^2 \sum_{n=1}^{M} (2\alpha_B^4 + 2\alpha_B^4)$$

$$= \left(\frac{1}{M}\right)^2 \cdot M \cdot 4\alpha_B^4$$

$$= \frac{4\alpha_B^4}{M}$$

Therefore the variance of Γ is

$$\mathrm{Var}(\Gamma) = \frac{\mathrm{Var}(\bar{P}_B)}{\langle P_B \rangle^2}$$

$$= \frac{\frac{4\alpha_B^2}{M}}{4\alpha_B^4}$$

$$= \frac{1}{M} \qquad (2.28)$$

We conclude that, for M sufficiently large, Γ is approximately Gaussian-distributed with mean 1 and variance 1/M. Let's rewrite Γ as

$$\Gamma = \Gamma_0 + 1 \qquad (2.29)$$

where Γ_0 is approximately Gaussian with zero mean and variance 1/M. If the absolute value of Γ_0 is less than 1 we can rewrite Eq. (2.22) in terms of a power series expansion as

$$\sigma_t^E = \frac{\sigma_t^c}{1+\Gamma_0}$$

$$= \sigma_t^c (1 - \Gamma_0 + \Gamma_0^2 - \Gamma_0^3 + \Gamma_0^4 - \ldots) \qquad (2.30)$$

It is seen that the estimated target cross section can now be expressed as the sum of the cataloged value σ_t^c and a noise term defined as

$$N_0 \equiv -\sigma_t^c \Gamma_0 + \sigma_t^c \Gamma_0^2 - \sigma_t^c \Gamma_0^3 + \ldots \qquad (2.31)$$

It can also be shown that for M greater than 3 the probability that the absolute value of Γ_o is greater than one is extremely small. Indeed, for M = 3,

$$\mathrm{Var}(\Gamma_o) = \frac{1}{M} = 1/3$$

The probability that $|\Gamma_o|$ is smaller than 1 is given as

$$p(|\Gamma_o| < 1) = p(|3\Gamma_o| < 3)$$

where the term $(3\Gamma_o)$ is a standard Gaussian variable. From the Standard Gaussian Distribution table we have

$$p(|\Gamma_o| < 1) \approx 99.74\% \tag{2.32}$$

The variance of the noise N_o can be calculated as follows.

$$\mathrm{Var}(N_o) = \sigma_t^2\mathrm{Var}(\Gamma_o) + \sigma_t^2\mathrm{Var}(\Gamma_o^2) + \sigma_t^2\mathrm{Var}(\Gamma_o^3) + \ldots \tag{2.33}$$

Eq. (2.28) already gives us the variance of Γ_o. Now let's use Gaussian moment expansion [21] to evaluate the higher order terms. From [21] we have

$$E\{\Gamma_o^n\} = \begin{cases} 1 \cdot 3 \ldots (n-1)\left(\frac{1}{M}\right)^{n/2} & \text{for n even} \\ 0 & \text{for n odd} \end{cases} \tag{2.34}$$

Now

$$\mathrm{Var}(\Gamma_o^2) = E\{\Gamma_o^4\} - E^2\{\Gamma_o^2\}$$

$$= 3 \cdot \left(\frac{1}{M}\right)^2 - \left(\frac{1}{M}\right)^2$$

$$= 2 \cdot \left(\frac{1}{M}\right)^2 \tag{2.35}$$

$$\mathrm{Var}(r_o^3) = E\{r_o^6\} - E^2\{r_o^3\} = 15\left(\frac{1}{M}\right)^3 \tag{2.36}$$

It is obvious that the third and higher order terms are negligibly small for large M. Therefore Eq. (2.33) becomes

$$\mathrm{Var}(N_o) \approx (\sigma_t^c)^2 \left(\frac{1}{M} + 2 \cdot \left(\frac{1}{M}\right)^2\right) \tag{2.37}$$

Define a signal-to-noise power ratio as

$$\frac{S}{N} \equiv \frac{\sigma_t^c}{\sqrt{\mathrm{Var}(N_o)}} \tag{2.38}$$

From Eq. (2.37) and Eq. (2.38) we have

$$\frac{S}{N} = \frac{\sigma_t^c}{\sqrt{\mathrm{Var}(N_o)}}$$

$$\approx \frac{\sigma_t^c}{\sigma_t^c \sqrt{\left(\frac{1}{M} + 2\left(\frac{1}{M}\right)^2\right)}}$$

$$= \frac{M}{\sqrt{M+2}} \tag{2.39}$$

As an example let's suppose the coherent integration time for each sample is 10 seconds, and we take M = 100 samples, which corresponds to a total observation time of about 16 minutes, then the post-processing signal-to-noise ratio is

$$\frac{S}{N} \approx \frac{100}{\sqrt{10\ 2}} \approx 10 = 10 \text{ dB}$$

In Chapter V we will determine the probability of misclassification corresponding to this observation period.

D. MEASUREMENT OF PHASE RETURNS

In this section we shall briefly analyze the phase returns measured by a typical coherent radar. Fig. 2.7 is a simplified block diagram of a coherent pulse radar system. Suppose the RF oscillator generates a sinusoidal waveform of frequency f_{RF}, and assume that the output signal is given by

$$E = |E_0| \cos(2\pi f_{RF} t) \tag{2.40}$$

The signal transmitted by the antenna can be given as

$$E_T = |E_T| \cos(2\pi f_{RF} t + \phi_T) \tag{2.41}$$

where ϕ_T is the total phase shift between the RF oscillator and the antenna. The received signal at the RF amplifier of the receiver will then be

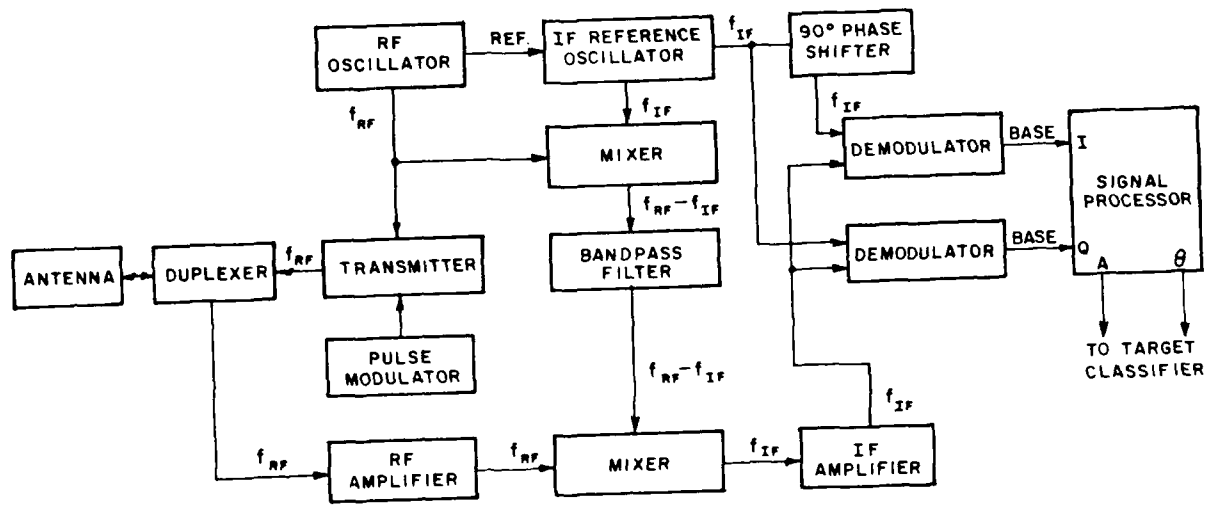

Fig. 2.7. Block diagram of a coherent radar system.

$$E_R = |E_R| \cos(2\pi f_{RF} t + \phi + \phi_R + \frac{4\pi R}{\lambda}) \tag{2.42}$$

where ϕ_R is the total equipment phase shift between the RF oscillator and the input to the receiver measured at the equipment operating frequency, ϕ is the intrinsic phase return induced by the target, and R is the one-way wave path length. The local oscillator frequency is obtained by mixing the output of the RF oscillator with the output of a stable IF reference oscillator and then selecting either the sum or difference frequency with a bandpass filter. The local oscillator signal is then mixed with the output of the RF amplifier to obtain the IF frequency, which is in turn amplified by the IF amplifier. At this point the signal is of the form

$$E_{IF} = |E_{IF}| \cos(2\pi f_{IF} t + \phi + \frac{4\pi R}{\lambda} + \phi_{IF}) \tag{2.43}$$

where ϕ_{IF} is the total equipment phase shift at the output of the IF amplifier. The output of the amplifier is coherently demodulated, with both in-phase and quadrature signals from the IF reference oscillator used as a reference.

This results in the following in-phase and quadrature components:

$$E_I = |E_{IF}| \cos(\frac{4\pi R}{\lambda} + \phi + \phi_{total}) \tag{2.44}$$

$$E_Q = |E_{IF}| \sin(\frac{4\pi R}{\lambda} + \phi + \phi_{total})$$

where ϕ_{total} is the total system phase shift. The phase output of the

signal processor is given by

$$\theta = \tan^{-1}\left(\frac{E_Q}{E_I}\right)$$

$$= \frac{4\pi R}{\lambda} + \phi + \phi_{total} \qquad (2.45)$$

The wave path length R for sky wave radars is a function of ionospheric condition and frequency, and the phase may vary widely as the frequency changes. For surface wave radars the wave path length is essentially independent of frequency.

Goggins and others [19] showed that it would be possible to recover the intrinsic phase returns under certain conditions. They [19] mathematically proved that for a smooth conducting body in the Rayleigh region the co-polarized terms of the scattering matrix have zero phase shift. Based on this, they suggested a differential phase technique to recover the intrinsic phase, as discussed below.

From Eq. (2.45) the phase return measured in the Rayleigh region can be given as

$$\theta_o = \frac{4\pi R}{\lambda_o} + \phi^o_{total} \qquad (2.46)$$

where λ_o is the wavelength in the Rayleigh region, R_o is the wave path length in the Rayleigh region, and the intrinsic phase ϕ is set to zero. The total equipment phase shift can be written as

$$\phi_{total} = \frac{2\pi D}{\lambda} \qquad (2.47)$$

where D = Total wave path length in the equipment. From Eq. (2.45) and Eq. (2.46) we have

$$\theta = \frac{4\pi R}{\lambda} + \phi + \frac{2\pi D}{\lambda}$$

$$\theta_o = \frac{4\pi R_o}{\lambda_o} + \frac{2\pi D}{\lambda_o}$$

or

$$\lambda\theta = 4\pi R + \lambda\phi + 2\pi D \tag{2.48}$$

$$\lambda_o\theta_o = 4\pi R_o + 2\pi D \tag{2.49}$$

Taking the difference between Eq. (2.48) and Eq. (2.49), we have

$$\lambda\theta - \lambda_o\theta o = 4\pi(R-R_o) + \lambda\phi$$

If $R = R_o$ then the intrinsic phase is given by

$$\phi = \frac{\lambda\theta - \lambda_o\theta_o}{\lambda} \tag{2.50}$$

For sky-wave radars the wave path length R is obviously not equal to R_o, and Eq. (2.50) does not hold. For surface-wave radars, R may be close to R_o, and the intrinsic phase may be recovered. In addition to the requirement that R be equal to R_o, this method needs phase measurements in the lower Rayleigh region, which, for targets like ships and aircraft, corresponds to frequencies much lower than the H.F. region. Because of such requirements, the classification alogorithms to be discussed in the next chapter do not directly utilize the intrinsic phase.

CHAPTER III

TARGET CLASSIFICATION ALGORITHMS

A. INTRODUCTION

The subject of pattern classification has been extensively studied in the literature (e.g., Duda and Hart [21]). The basic process of a pattern classification system is depicted in Figure 3.1. As shown in the figure, the measurement system (in our case a radar system) makes measurement of a physical object, and each measurement may contain a set of independent components and can be viewed as a vector y. In our case each measurement is a vector whose components are the amplitude and phase of the radar returns of a target at a number of frequencies. Each measurement vector is a point in the multi-dimensional measurement space. The purpose of the feature extractor is to reduce the dimensionality of the measurement vector by using certain features that distinguish the objects. The feature extractor transforms a measurement vector y to a point or feature vector in a multi-dimensional feature space. The feature vectors are passed to the object classifier that uses the features and assigns the object to an appropriate class.

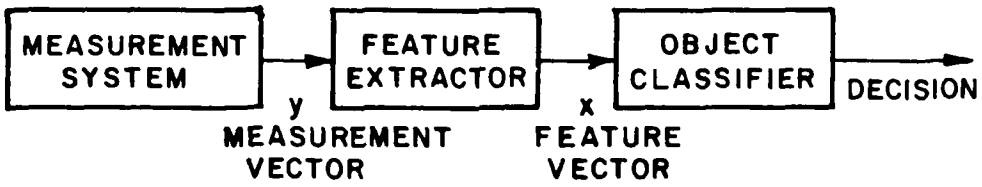

Figure 3.1. Basic process of a pattern classification system.

There are two types of classification problems, i.e., parametric and nonparametric. In parametric classification the probability distribution of the observation space is expressed as a functional form, such as that of the normal distribution, which is completely specified by at most a finite number of real-valued parameters [33]. In nonparametric classification, on the other hand, the probability distribution is not indexed by a finite number of parameters [33]. Note that the fundamental difference of the nonparametric classifier from the parametric classifier is that the parametric form of the underlying probability distribution is not assumed or used. The nonparametric method are important because parametric probabilistic information is usually not available or the assumption of it is not justified.

In Section B we will briefly discuss a fundamental classification theory, i.e., the Bayes decision theory [21,22]. As will be seen, such decision theory minimizes the average probability of error, but requires knowledge about the a posteriori probability of the feature vector X. For classification of radar targets, it is clear that parametric probabilistic information about the feature vector is not available or the assumption of it is not justified because of the lack of adequate information on system performance. Therefore, we must resort to nonparametric methods. Two classification methods which do not require knowledge of the probabilistic information will be discussed in Section C (the frequency-domain algorithm) and Section D (the time-domain algorithm).

B. BAYES DECISION THEORY

Suppose two classes of samples are to be classified. Let the first class be denoted as ω_1 and the second as ω_2. Let the probability of occurrence (a priori probability) of class ω_i, i=1.2, be denoted as $p(\omega_i)$. Let $p(X/\omega_i)$ denote the conditional probability of an observation X in the feature space, given that X belongs to class ω_i. Given an observation X, the probability that the observation belongs to class ω_i is given as $p(\omega_i/X)$, i.e., the a posteriori probability. Suppose that we know both the a priori probabilities $p(\omega_i)$ and the conditional densities $p(\omega_i/X)$, then the a posteriori probability can be calculated from the Bayes rule:

$$p(\omega_i/X) = \frac{p(X/\omega_i)\ p(\omega_i)}{p(x)} \tag{3.1}$$

where

$$p(x) = \sum_{j=1}^{2} p(x/\omega_j)\ p(\omega_j) \quad .$$

Because we have assumed that the decision rule must classify an observation X either as class 1 or class 2, we can view it as a rule for dividing the total observation space Z into two parts, Z_1 and Z_2. Whenever an observation falls in Z_1 it is classified as class 1, and whenever an observation falls in Z_2, it is classified as class 2. We can now write an expression for the average cost or risk in terms of the decision regions

$$\text{RISK} = P(W_1) \int_{Z_2} P(X/W_1)dX + P(W_2) \int_{Z_1} P(X/W_2)dx \qquad (3.2)$$

where we have assumed that there is no cost for making right decisions, and the costs for making wrong decisions are unity. Now, to find the Bayes decision rule we must choose the decision regions Z_1 and Z_2 in such a manner that the risk will be minimized [21,22]. Since

$$Z = Z_1 + Z_2$$

Eq. (3.2) can be rewritten as

$$\text{RISK} = P(W_1) \int_{Z-Z_1} P(X/W_1)dx + P(W_2) \int_{Z_1} P(X/W_2)dx$$

or

$$\text{RISK} = 1 + \int_{Z_1} [P(W_2)\, P(X/W_2) - P(W_1)\, P(X/W_1)]\, dx$$

In order to minimize the risk all values of X where the second term in the above integral is larger than the first should be included in Z_1 because they contribute a negative amount to the integral. Similarly, all values of X where the first term is larger than the second should be excluded from Z_1 (assigned to Z_2) because they would contribute a positive amount to the integral. Values of X where the two terms are equal have no effect and may be assigned arbitrarily. Thus, the decision regions are defined by the statement:

$$\text{If} \quad P(W_2)\, P(X/W_2) > P(W_1)\, P(X/W_1)$$

assign X to Z_2 and consequently classify X as class 2. Otherwise assign X to Z_1 and classify X as class 1. In terms of the a posteriori probability, the Bayes decision rule is given as follows.

$$\text{classify } X \text{ as } \omega_1 \text{ if } p(\omega_1/X) > p(\omega_2/X)$$
$$\text{classify } X \text{ as } \omega_2 \text{ if } p(\omega_2/X) > p(\omega_1/X) \quad . \tag{3.3}$$

If there are more than two classes, say, N classes, the Bayes decision rule becomes [21,22]

$$\text{classify } X \text{ as } \omega_i \text{ if}$$
$$p(\omega_i/X) > p(\omega_j/X) \text{ for } j = 1,2,\ldots, N \text{ and } i \neq j \quad . \tag{3.4}$$

It is evident that the Bayes decision rule requires knowledge about the a posteriori probability density function which is not available for application to this problem. In the following two sections two classification algorithms which do not require the probabilistic information will be discussed.

C. CLASSIFICATION IN THE FREQUENCY DOMAIN

The first classification algorithm makes use of features extracted from the multi-frequency radar returns of a target. The measurement

vector may be chosen as a set of amplitude $A(f_i)$ and phase $\theta(f_i)$ of the backscatter of a target, measured at frequencies $f = f_1, f_2, \ldots, f_N$. Note that the amplitude is defined as the square root of the measured target cross section. From Equation (2.45) we know that the relative phase return θ is a function of the wave path length R and the total equipment phase shift ϕ_{total}, i.e.,

$$\theta = \frac{4\pi R}{\lambda} + \phi + \phi_{total} \tag{3.5}$$

As discussed in Chapter II, section D, the intrinsic phase return ϕ can be recovered by the differential phase technique when the phase path length R is independent of the frequency. The technique also requires that a phase return be measured in the Rayleigh region.

Instead of using either the relative phase return θ or the intrinsic phase return ϕ, we can define a "*differential quantity*" W as follows:

From Equation (3.5) we have

$$\theta_i \lambda_i = 4\pi R_i + \phi_i \lambda_i + \phi_i^{total} \lambda_i$$

$$\theta_{i+1} \lambda_{i+1} = 4\pi R_{i+1} + \phi_{i+1} \lambda_{i+1} + \phi_{i+1}^{total} \lambda_{i+1} \tag{3.6}$$

where θ_i = measured phase return at $\lambda = \lambda_i$

R_i = one-way wave path length at $\lambda = \lambda_i$

ϕ_i = intrinsic phase at $\lambda = \lambda_i$

ϕ_i^{total} = total equipment phase shift at $\lambda = \lambda_i$

The above two equations can also be written as

$$\theta_i \lambda_i = 4\pi R_i + \phi_i \lambda_i + \frac{2\pi D}{\lambda_i} \lambda_i$$

$$\theta_{i+1} \lambda_{i+1} = 4\pi R_{i+1} + \phi_{i+1} \lambda_{i+1} + \frac{2\pi D}{\lambda_{i+1}} \lambda_{i+1} \tag{3.7}$$

where D is the total phase path length in the radar system as defined in Equation (2.47). Taking the difference between the two equations we have

$$\theta_i \lambda_i - \theta_{i+1} \lambda_{i+1} = 4\pi(R_i - R_{i+1}) + (\phi_i \lambda_i - \phi_{i+1} \lambda_{i+1}) \tag{3.8}$$

Except for the factor $4\pi(R_i - R_{i+1})$, the quantity $(\theta_i \lambda_i - \theta_{i+1} \lambda_{i+1})$ is directly related to the quantity $(\phi_i \lambda_i - \phi_{i+1} \lambda_{i+1})$, which is a function of only the wavelengths and the intrinsic phases. For surface wave radars, we have $R_i \approx R_{i+1}$, so that

$$\theta_i \lambda_i - \theta_{i+1} \lambda_{i+1} \approx \phi_i \lambda_i - \phi_{i+1} \lambda_{i+1} \tag{3.9}$$

For sky wave radars, R_i and R_{i+1} may differ by a large amount. However if λ_i and λ_{i+1} differ by only a small amount and the radar operating frequencies are properly chosen, the difference between R_i and R_{i+1} may be made very small. Define W as

$$W_i = \theta_i \lambda_i - \theta_{i+1} \lambda_{i+1}$$
$$i = 1, 2, \ldots, N-1 \tag{3.10}$$

where N is the total number of frequency components available. Since the phase θ_i in Equation (3.5) is multiply valued, i.e.,

$$\theta_i \equiv \theta_i + 2n\pi \quad ; n = 1, 2, 3, \ldots, \tag{3.11}$$

the variable W_i in the equation has also multiple values. This problem can be solved as follows.

Let the phase difference $\Delta\theta$ be defined as

$$\Delta\theta = \theta_i - \theta_{i+1} \tag{3.12}$$

It is evident that the variable W_i is uniquely defined if we require that the phase difference be confined to the region:

$$-\pi < \Delta\theta \leq \pi \tag{3.13}$$

Since

$$\begin{aligned} \Delta\theta &= \theta_i - \theta_{i+1} \\ &\equiv (\theta_i - \theta_{i+1}) + 2n\pi \quad ; n = \text{integer} \end{aligned}$$

the phase difference $\Delta\theta$ can be confined to the region defined in Equation (3.13) by repeatedly subtracting 2π or adding 2π to $\Delta\theta$ until Equation (3.13) is satisfied.

Define a feature space as

$$(A_1, A_2, \ldots, A_N, kW_1, kW_2, \ldots, kW_{N-1}) \tag{3.14}$$

where K is a normalization constant such that the variances of A and W are related as

$$VAR(A) = \beta \cdot VAR(kW) \tag{3.15}$$

If β is set to 1 then both the amplitude and the phase are assigned equal weightings. If the phase is not reliable or contains large amounts of error, as is the case for ionospheric propagation, we can set β to be a large number so that the amplitude is given more weight. On the other hand β can be set to be a small number so that the phase is given higher weighting. Thus, by setting β, we can determine the reliable weights of the amplitude and phase. Note that if β is set to infinity, then, only the amplitude is used for classification, and if $\beta = 0$, then, only the phase is used for classification. Once β is selected the normalization constant K can be computed as

$$K = \sqrt{\frac{VAR(A)}{\beta \cdot VAR(W)}} \tag{3.16}$$

The problem now is how to estimate the variance of the amplitude and W. Our approach here is to calculate the variance of A and of W in the data base, and use the result as an estimate of the true variance. It is noted that such estimates may contain errors, and further research into finding an optimum K is needed.

Once the constant K is calculated, the distance between any two points in the feature space Equation (3.14) can be defined as

$$d_{a,b} = \sqrt{\sum_{i=1}^{N} (A_i^a - A_i^b)^2 + \sum_{i=1}^{N-1} (kW_i^a - kW_i^b)^2} \tag{3.17}$$

where

A^a and W^a define one of the two points and, A^b and W^b define the other point.

Once the feature space is defined, the Nearest Neighbor Decision rule [21] can be applied to classify the targets. The N.N. rule is non-parametric, yet its error rate is close to the error rate of the Bayes decision rule. In fact, it has been shown [21] that the error rate of the N.N. rule is never worse than twice the Bayes error rate. An algorithm for classification in the frequency-domain is given below.

Suppose we choose the frequencies $f = f_1, f_2, \ldots, f_N$. Let the amplitude and phase returns of the unknown target be given as $A_t(f_i)$ and $\theta_t(f_i)$, respectively, where $i = 1, 2, \ldots, N$. Also suppose there are M classes in the data base. Let the amplitude and phase returns of each class in the database be given as $A_j(f_i)$ and $\theta_j(f_i)$, where f_i means the i^{th} frequency, $i = 1, 2, \ldots, N$, and j means the j^{th} target, $j = 1, 2, \ldots, M$.

1. Compute the W's as follows

$$W_i^t = \lambda_i \theta_t(f_i) - \lambda_{i+1} \theta_t(f_{i+1})$$

$$W_i^j = \lambda_i \theta_j(f_i) - \lambda_{i+1} \theta_j(f_{i+1})$$

$i = 1, 2, \ldots, N-1$

$j = 1, 2, \ldots, M$

2. Calculate the means of A and W in the database.

$$\overline{A} = \frac{1}{MN} \sum_{j=1}^{M} \sum_{i=1}^{N} A_j(f_i)$$

$$\overline{W} = \frac{1}{M(N-1)} \sum_{j=1}^{M} \sum_{i=1}^{N-1} W_i^j$$

Calculate the variance of A and W in the database.

$$\text{Var}(A) = \frac{1}{MN} \sum_{j=1}^{M} \sum_{i=1}^{N} (A_j(f_i) - \bar{A})^2$$

$$\text{Var}(W) = \frac{1}{M(N-1)} \sum_{j=1}^{M} \sum_{i=1}^{N-1} (W_i^j - \bar{W})^2$$

Use the variances above as estimates of the true variance of A and W. Select a value for β, and compute the normalization constant as

$$K = \sqrt{\frac{\text{Var}(A)}{\text{Var}(W) \cdot \beta}} \tag{3.18}$$

3. Compute in the feature space the distance between the target and each class in the database.

$$d_{t,j} = \sqrt{\sum_{i=1}^{N} (A_t(f_i) - A_j(f_i))^2 + \sum_{i=1}^{N-1} (kW_i^t - kW_i^j)^2}$$

$$j = 1, 2, \ldots, M$$

4. Apply the Nearest Neighbor rule:

Classify the target as class j if $d_{t,j} > d_{t,k}$

$$k = 1, \ldots, M \quad ; \quad k \neq j$$

D. CLASSIFICATION IN THE TIME DOMAIN

In the last section we tried to reduce the phase error caused by the variation of the effective phase path length. Since this phase error is equivalent to time-shifting of the corresponding time-domain waveform, it may also be removed in the time domain. It was shown [12] that the time-domain ramp response, obtained by integrating twice the impulse response, is proportional to the cross-sectional area of a target along the line-of-sight. Here the impulse response waveform is the time-dependent electro-magnetic field intensity produced at a fixed point in space when a plane electromagnetic shock wave strikes an object [3], and can be obtained by synthesizing the frequency-domain response [12]. It is therefore feasible to use the time-domain data as features for identification of targets.

Let X(m) be a set of complex frequency-domain data defined by

$$X(m) = A(f_k)\, e^{j\theta(f_k)} \quad ; k = 1, 2, \ldots, M \tag{3.20}$$

where A is the amplitude and θ is the phase of the target returns

$$m = f_1/\Delta f \ , \ f_2/\Delta f \ , \ \ldots, \ f_M/\Delta f \tag{3.21}$$

and the frequencies are equally-spaced, i.e.,

$$f_i - f_{i-1} = \Delta f \quad ; i = 1, 2, \ldots, M \tag{3.22}$$

Define the time-domain data as the Discrete Inverse Fourier Transform (DIFT) of the frequency domain data X(m) [34], i.e.,

$$X(n) \equiv X(n\Delta t) = \text{DIFT}\ \{X(m)\} \tag{3.23}$$

where

$$n = 1, 2, \ldots, N$$

$$\Delta t = \frac{1}{N\Delta f}$$

and

$$\Delta f = \frac{1}{M\Delta t} \tag{3.24}$$

Note here the time-domain data should be real, and the amplitude of the frequency-domain data are symmetric around f = 0, i.e.,

$$X(m) = X^*(-m) \tag{3.25}$$

where X* is the complex conjugate of X. Suppose the time-domain data of two targets, x(n) and y(n), respectively, are synthesized from their respective frequency-domain response. Define a Correlation Function of x(n) and y(n) as

$$R_{xy}(k) = \sum_{n=1}^{N} x(n)\, y(n-k) \tag{3.26}$$

From the Cauchy-Schwartz inequality, i.e.,

$$|\Sigma_i a_i b_i|^2 \leq (\Sigma_i |a_i|^2)\ (\Sigma_i |b_i|^2) \tag{3.27}$$

we have

$$[R_{xy}(k)]^2 = \left[\sum_{n=1}^{N} x(n)\, y(n-k)\right]^2 \leq \left(\sum_{n=1}^{N} x^2(n)\right)\left(\sum_{n=1}^{N} y^2(n)\right) \tag{3.28}$$

where the equality holds if and only if

$$\frac{x(i)}{y(i-k)} = \text{constant} \tag{3.29}$$

for i = 1, 2, ..., N. Now

$$[R_{xx}(k)]^2 = \left[\sum_{n=1}^{N} x(n)\, x(n-k)\right]^2$$

$$< \left(\sum_{n=1}^{N} x^2(n)\right)\left(\sum_{n=1}^{N} x^2(n-k)\right)$$

$$< \left(\sum_{n=1}^{N} x^2(n)\right)\left(\sum_{n=1}^{N} x^2(n)\right)$$

$$= \left(\sum_{n=1}^{N} x^2(n)\right)^2 \tag{3.30}$$

Since

$$R_{xx}(0) = \sum_{n=1}^{N} x(n)\, x(n)$$

$$= \sum_{n=1}^{N} x^2(n) \tag{3.31}$$

we have, from Equation (3.27),

$$[R_{xx}(k)]^2 < [R_{xx}(0)]^2$$

or

$$|R_{xx}(k)| < R_{xx}(0) \tag{3.32}$$

Define a correlation coefficient of x(n) and y(n) as

$$\rho_{xy}(k) = \frac{Rxy(k)}{\sqrt{R_{xx}(0)}\sqrt{R_{yy}(0)}} \tag{3.33}$$

It is evident from Equations (3.28) and (3.32) that

$$\rho_{xy}(k) \leq 1 \tag{3.34}$$

and the equality holds if

$$x=y \text{ and } k=0 \tag{3.35}$$

i.e., if the two waveforms coincide and the relative time-shift between the two waveforms is zero.

A time-domain classification algorithm is given below. Suppose the time-domain data x(n) of a target is derived from its frequency-domain response, and the time-domain data of each class in the data base are derived from their respective frequency-domain data, and are given as $y_i(n)$; i=1,2,..., C.

1. Compute the Correlation Function

$$\rho_{xy_i}(k) = \frac{R_{xy_i}(k)}{\sqrt{R_{xx}(k)}\sqrt{R_{y_iy_i}(k)}}$$

$$i = 1, 2, \ldots, C \tag{3.36}$$

2. Choose the time-shift constant K such that

$\rho_{xy_i}(k)$ is maximized, i.e.,

$$\rho_{xy_i}^{max} = \underset{k}{MAX} \{ \rho_{xy_i}(k) \} \text{ for each } i \tag{3.37}$$

Note that this would remove the relative time-shift between the two waveforms, and $\rho_{xy_i}^{max}$ is independent of the time-shift.

3. Identify the unknown target as class i if

$$\rho_{xy_i}^{max} > \rho_{xy_j}^{max} \quad ; \; j = 1, 2, \ldots, C \quad ; \quad j \neq i \tag{3.38}$$

Note that from the theories of Discrete Fourier Transform [34]

$$R_{xy}(k) = DIFT \{x(m)\ y^*(m)\} \tag{3.39}$$

and

$$R_{xx}(0) = \sum_{n=1}^{N} x^2(n) = 2 \sum_{m=1}^{M} |X(m)|^2 \tag{3.40}$$

Thus it is more efficient to calculate the correlation coefficient as

$$\rho_{xy}(k) = \frac{DIFT\{x(m)\ y^*(m)\}}{2\sqrt{\sum_{m=1}^{M} |X(m)|^2}\ \sqrt{\sum_{m=1}^{M} |y(m)|^2}} \tag{3.41}$$

CHAPTER IV

GENERATION OF A DATA BASE

A. INTRODUCTION

The testings of classification algorithms require a data base which is representative of the data to be expected in practice. A set of radar backscatter measurements made by The Ohio State University ElectroScience Laboratory of scaled models of ships and aircraft was used to generate a data base for testing. The data base was designed to simulate a full scale data base for target classification using H.F. multifrequency radars.

In section B we will discuss the measurement of scaled models at scaled frequency and the calibration of measured radar returns. Due to limitations on the measurement system, backscatter of the models was measured in a number of small frequency bands respectively, e.g., 2-4 GHz, 4-8 GHz, and 8-12 GHz. Target locations may be slightly changed from one measurement to another, therefore, when these data were connected together to form a wider band of data, e.g., 2-12 GHz, phase offsets were found to be present at the junction of two adjacent frequency bands. In section C we will discuss the connection of two data sets and techniques for removing the phase offsets. After

calibration and phase correction, the data were interpolated and smoothed to obtain data values at desired frequencies. The interpolation and smoothing made use of a Hamming window which had zero phase in both the frequency domain and the time domain [35], and was equivalent to a low-pass filter in the time domain. The interpolation will be the subject of Section D.

In summary, the measured data were first calibrated, then connected together in bands and, then, interpolated and smoothed. The resulting data formed the data base which was used for testing the algorithms discussed in Chapter III. In section E we will present plots of the post-processed waveforms in the data base.

B. MEASUREMENT AND CALIBRATION

The measurement facility used to obtain scattering data on the model targets was a monostatic swept-frequency radar system. Operation of the system was interactively controlled by a FORTRAN program on a minicomputer. A simplified diagram of the system is shown in Fig. 4.1. Model targets were placed on a low-RCS pedestal. The range was configured so that the far-field criterion was approximately satisfied. The elevation angles of the incident waves were approximately zero. For ship models a large ground plane is needed to simulate the reflection from the sea surface. Instead of building such a ground plane, a replica was attached to each ship model, as shown in Fig. 4.2. This effectively simulated the image created by the reflection from the sea surface. By rotating the targets, the aspect angles of the incident

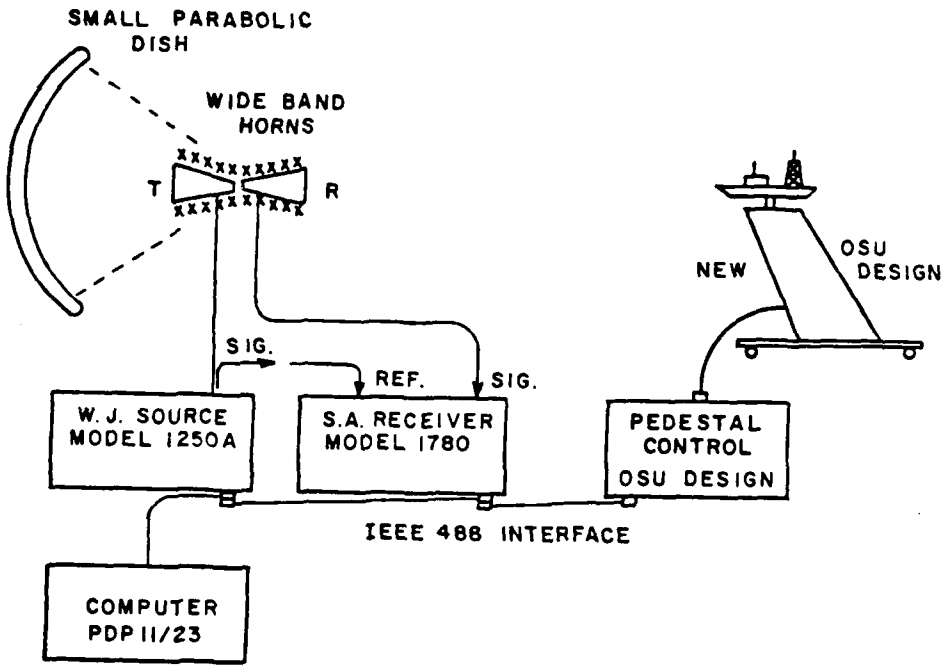

Fig. 4.1. Diagram of the radar measurement facility.

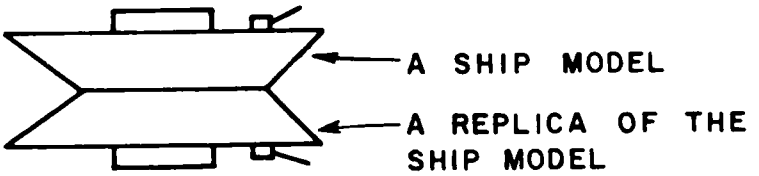

Fig. 4.2. Simulation of the reflection from the sea surface. A replica is attached to each ship model.

waves were varied. For each particular aspect angle, the radar returns were measured in a number of frequency bands, which included 1-2 GHZ, 2-4GHZ, 4-8GHZ, and 8-12GHZ. In each band there were 201 equally-spaced points. The frequency increments of the data points were 0.005GHZ for the 1-2GHZ band, 0.01GHZ for the 2-4GHZ band, .02GHZ for the 4-8GHZ band, and .02GHZ for the 8-12GHZ band. The frequency increments were chosen to be small to provide enough data points for the interpolation and smoothing of the data waveform.

The aspect angles and the frequency bands chosen for each model might be different. In most cases, the aspect angles varied from 0 to 180 degrees at 15 degree increments, and the frequency bands were chosen as 2-4GHZ, 4-8GHZ, and 8-12GHZ. In most cases, vertical polarization was used.

The calibration of measured data made use of reference spheres whose theoretical radar returns were readily available. Prior to calibration by spheres, background returns were subtracted from the data. The background returns were measured separately after the targets were removed. They included returns from the antenna's supporting structures, the building's walls and ceilings, wave absorbers, etc. It was noted that the subtraction of background returns would not remove couplings between targets and the background itself. Therefore a Hamming Window, which is equivalent to a time-domain low-pass filter, was applied to alleviate the coupling effects. The voltage amplitude of the received target return was proportional to the square root of the target cross section. The received voltage amplitude A and phase θ for

a particular frequency $f = f_i$ formed a complex number given by

$$s(f_i) = A(f_i)\cos\theta(f_i) + j\, A(f_i)\sin\theta(f_o) \tag{4.1}$$

The radar return of a target at $f = f_i$ was calibrated as

$$T_c(f_i) = (T_m(f_i) - B_m(f_i)) \cdot \frac{S_t(f_i)}{S_m(f_i) - B_m(f_i)} \tag{4.2}$$

where all items were complex numbers, and

$T_c(f_i)$ = calibrated radar return of the target

$T_m(f_i)$ = measured radar return of the target

$B_m(f_i)$ = measured radar return of the background

$S_m(f_i)$ = measured radar return of a sphere

$S_t(f_i)$ = theoretical radar return of the sphere

Eq. (4.2) is a calibration equation which employs the backscatter from a sphere as a reference, and is similar in principle to the calibration equation (2.8), which employs the backscatter from the sea surface as a reference. The phase reference of the calibrated return of the target is the same as that of the theoretical return of the sphere, i.e., the center of the target.

C. CONNECTION OF TWO FREQUENCY BANDS

This section is concerned with the connection of two sets of data measured in two adjacent frequency bands to create a data set of a wider bandwidth.

Suppose two sets of multi-frequency noise-contaminated radar returns measured at adjacent frequency bands are to be connected as shown in Fig. 4.3. Let the frequency range of the first set of data be $f_{-1} \leq f \leq f_0$ and that of the second set of data be $f_0 \leq f \leq f_1$. The junction of the two sets is at $f = f_0$. Suppose the positions of the target in these two measurements differ by only a small amount. Note a 2-milimeter position offset at a frequency of 6 GHZ yields almost 30 degrees of electrical phase discontinuity (Eq. (4.4)). Since the target is assumed to be in the far-zone, there is no significant amplitude offset at $f = f_0$. Therefore, the amplitude data can be connected directly without correction. The phase offset, however, is significant even if the position offset is only a fraction of a wavelength. The position offset causes a ramp-type offset in phase as the frequency increases or decreases. This type of offset can be approximately corrected as follows.

Let the phase offset $\Delta^*\theta(f_0)$ at $f = f_0$ be estimated as

$$\Delta^*\theta(f_0) = \overset{*}{\theta}_2(f_0) - \overset{*}{\theta}_1(f_0) \tag{4.3}$$

where $\overset{*}{\theta}_2(f_0)$ and $\overset{*}{\theta}_1(f_0)$ are estimates of the true phase $\theta_2(f_0)$ and $\theta_1(f_0)$, respectively. Since the phase offset and the position offset δ are related by

$$\Delta\theta(f_0) = \frac{2\pi \cdot 2\delta}{\lambda_0} \; ; \quad \lambda_0 = c/f_0 \tag{4.4}$$

The position offset δ can be estimated as

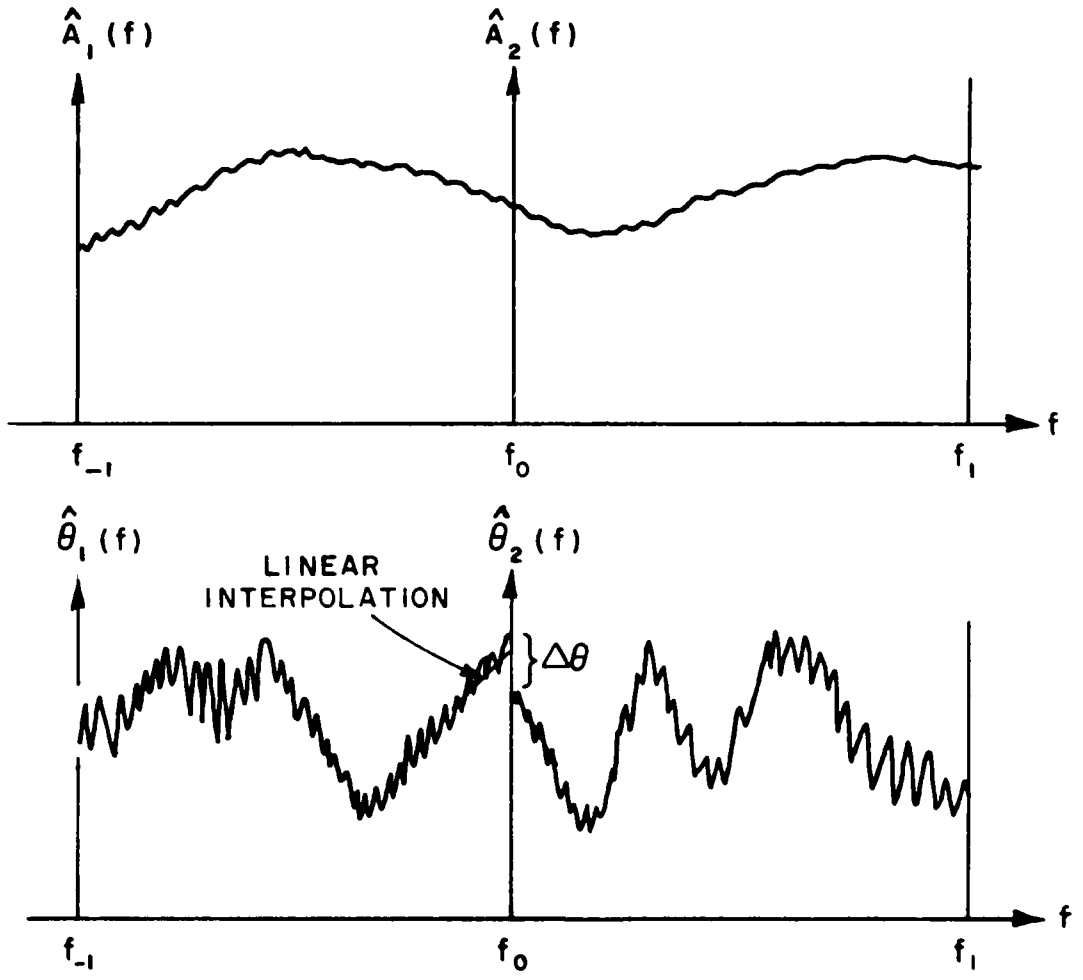

Fig. 4.3. Connection of two frequency bands.

$$\delta^* = \frac{\Delta^*\theta(f_0)\lambda_0}{4\pi} \tag{4.5}$$

and one of the two sets of data, say $\hat{\theta}_2(f)$, can be corrected as follows.

$\hat{\theta}_2^c$ = corrected phase

$$= \hat{\theta}_2(f) - \Delta^*\theta(f)$$

$$= \hat{\theta}_2(f) - \frac{2\pi \cdot 2\delta^*}{\lambda}$$

$$= \hat{\theta}_2(f) - \frac{4\pi\ (\Delta^*\theta(f_0)/4\pi)\ .\ (c/f_0)}{c/f}$$

i.e.,

$$\hat{\theta}_2^c(f) = \hat{\theta}_2(f) - \Delta^*\theta(f_0)\ \frac{f}{f_0} \tag{4.6}$$

When using Eq. (4.6) we must be careful to avoid the branch-cut problem. Since

$$\Delta^*\theta(f_0) \text{ is equivalent to } \Delta^*\theta(f_0) + 2n\pi; \quad n = \text{integer} \tag{4.7}$$

Eq. (4.6) can be rewritten as

$$\hat{\theta}_2^c(f) = \hat{\theta}_2(f) - (\Delta^*\theta(f_0) + 2n\pi) \cdot \frac{f}{f_0} \tag{4.8}$$

or

$$\hat{\theta}_2^c(f) = \hat{\theta}_2(f) - (\Delta^*\theta(f_0)\ \frac{f}{f_0}) - 2n\pi\ \frac{f}{f_0} \tag{4.9}$$

Now if f/f_0 is not an integer $\hat{\theta}_2^c(f)$ has different values for different values of n. A principal branch must therefore be chosen for $\Delta^*\theta(f_0)$. A convenient choice would be

$$-\pi < \Delta^*\theta(f_0) \leq \pi \tag{4.10}$$

In order to calculate $\Delta^*\theta(f_0)$ two parameters $\theta_1^*(f_0)$ and $\theta_2^*(f_0)$ must be estimated first. One approach is to interpolate $\theta_1^*(f)$ and $\theta_2^*(f)$ using data points in the vicinity of $f = f_0$. The minimum-squared-error linear interpolation can be chosen to estimate $\theta_1^*(f_0)$ and $\theta_2^*(f_0)$ as follows [36].

$$\theta_i^*(f_0) = A_i f_0 + B_i; \quad i = 1,2 \tag{4.11}$$

where

$$A_i = \frac{\sum_{j=1}^{n} \hat{\theta}_i(f_j)(f_j - \bar{f})}{\sum_{j=1}^{n} (f_j - \bar{f})^2}$$

$$B_i = \bar{\hat{\theta}}_i - A_i \bar{f}$$

and

$$\bar{f} = \frac{1}{n} \sum_{j=1}^{n} f_j$$

$$\bar{\hat{\theta}}_i = \frac{1}{n} \sum_{j=1}^{n} \hat{\theta}_i(f_j) \tag{4.12}$$

An empirical value for n is 5 or 6. A higher-order interpolation can be used so that it fits better the data points. However it would likely be distorted by the noise already contained in the data.

The disadvantage of the interpolation is that a few of the data points used might be so enormously distorted by noise that the interpolation results become unacceptable. A remedy to this dilemma is to estimate the phase offset $\Delta^*\theta(f_0)$ in the time domain. A ramp-type phase-shift in the frequency domain is equivalent to a constant time-shift in the time domain. If

$$m(t) \overset{F}{\longleftrightarrow} A(f)e^{j\theta(f)} \tag{4.13}$$

form a Fourier transform pair then

$$m(t-\tau) \overset{F}{\longleftrightarrow} A(f)e^{j(\theta(f)-2\pi f\tau)} \tag{4.14}$$

From Eq. (4.5) we have

$$\tau = \frac{\Delta^*\theta(f_0)}{2\pi f_0} \tag{4.15}$$

or

$$\Delta^*\theta(f_0) = 2\pi f_0\tau \tag{4.16}$$

Suppose the time-domain waveform is given by

$$m(t) = F^{-1}\{A(f)e^{j\theta(f)}\}$$

and

$$\hat{m}_1(t) = F^{-1}\{\hat{A}_1(f)e^{j\hat{\theta}_1(f)}\}$$

$$\hat{m}_2(t) = F^{-1}\{\hat{A}_2(f)e^{j\hat{\theta}_2(f)}\} \qquad (4.17)$$

where $\hat{m}_1(t)$ and $\hat{m}_2(t)$ are band-limited approximations to the time domain waveform m(t) using different frequency bands. A plot of $\hat{m}_1(t)$ and $\hat{m}_2(t)$ is shown in Fig. 4.4. The amount of time-shift τ can be approximated in two ways. The first is to roughly estimate the distance between the peaks of $\hat{m}_1(t)$ and $\hat{m}_2(t)$. The second is to cross-correlate the two waveforms, and find the time-shift which maximizes the cross-correlation function. The time approach uses the contribution from all available frequency data points, and the overall shapes of the time domain waveforms cannot be adversely affected by a few distorted data points in the frequency domain. A drawback is the additional processing time required. It was decided that the frequency-domain linear interpolation approach would be appropriate for our application. Therefore the frequency-domain approach was used.

D. INTERPRETATION AND SMOOTHING

In this section we will discuss the use of Hamming Windows for interpolating and smoothing data points to estimate the values of the data at selected frequencies. Suppose the data points are a set of complex numbers c(f) given as

$$c(f_k) = X(f_k) + j\ Y(f_k) \qquad (4.18)$$

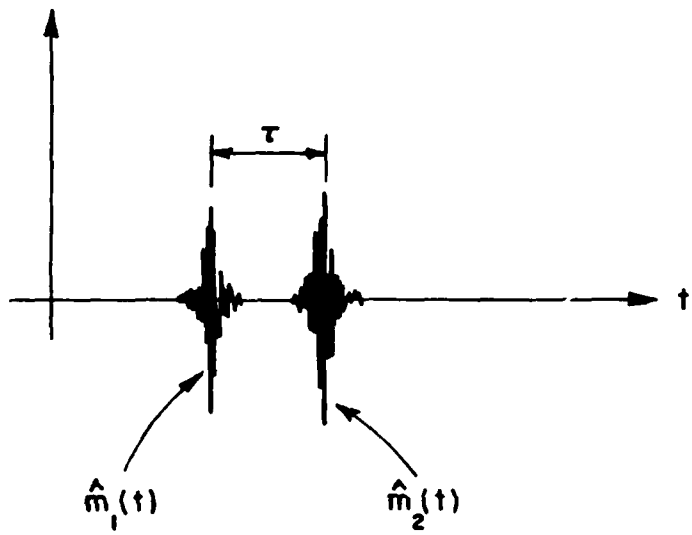

Fig. 4.4. Determination of the relative position offset in the time domain.

where

$$k = 1, 2, \ldots, L$$

The real part X and the imaginary part Y are real functions of frequency, as shown in Fig. 4.5. Define a Hamming Window as follows [24]

$$H(f,\tau) = \begin{cases} 0.54 + 0.46 \cos(\pi f/\tau); & -\tau/2 < f < \tau/2 \\ 0 & ; \text{elsewhere} \end{cases} \tag{4.19}$$

Note that the Hamming window is symmetric, therefore, when convolved with a waveform, the result is equivalent to shifting the window to specific locations of the waveform, then taking the weighted average of neighboring points covered under the window, as shown in Fig. 4.5. The complex data points can be interpolated and smoothed by convolving the Hamming Window with the data itself as shown in the following equation.

$$\tilde{c}(\tilde{f}_j) = \frac{\sum_{k=n}^{m} H(f_k, \tilde{f}_j, \tau)\, W_s(f_k) c(f_k)}{\sum_{k=n}^{m} H(f_k, \tilde{f}_j, \tau)\, W_s(f_k)} \tag{4.20}$$

where

$$\tilde{f}_j - \tau/2 < f_n, \ldots, f_m < \tilde{f}_j + \tau/2; \quad m > n$$

$$H(f_k, \tilde{f}_j, \tau) = 0.46 + 0.54 \cos\left(\frac{\pi(f_k - \tilde{f}_j)}{\tau}\right)$$

$$W_s(f_k) = (f_{k+1} - f_{k-1})/2 \tag{4.21}$$

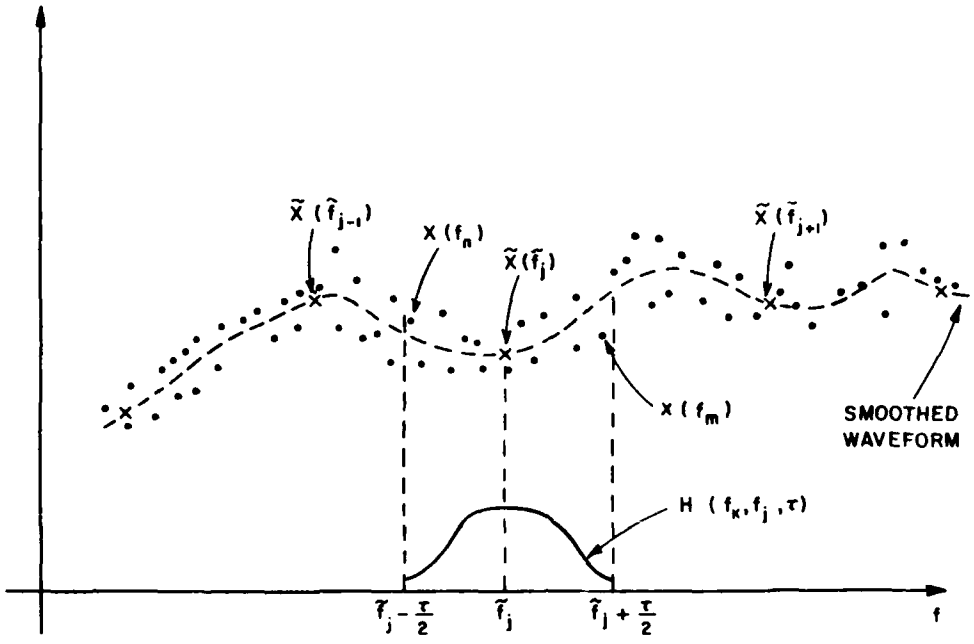

Fig. 4.5. Interpolation and smoothing of a noisy waveform using a Hamming Window.

The value of the waveform at $f = \tilde{f}_j$, i.e., $\tilde{c}(\tilde{f}_j)$ is estimated by calculating the weighted average of the data values covered under the Hamming window $H(f_k, \tilde{f}_j, \tau)$. The weight for each data point under the window is determined by the Hamming window; the further the data from the center the smaller the weight.

Note that the weighting function $W_s(f_k)$ is added to compensate for possible errors caused by uneven distribution of data points, as will be shown numerically in an example. The term in the numerator of Eq. (4.20) is a normalization factor so that the sum of the weights is 1. The necessity of using the normalization factor becomes evident when the waveform $c(f_x)$ is constant. In this case the interpolated values $\tilde{c}(\tilde{f}_j)$ remain constant, as expected.

Now let's interpret Eq. (4.20) in the time domain. The inverse Fourier Transform of the Hamming Window is a low-pass filter given by [35]

$$\hat{H}(t,\tau) = \frac{\tau \sin(t\pi\tau)}{t\pi\tau} \cdot \left(\frac{0.54 - 0.08(t\tau)^2}{1 - (t\tau)^2}\right) \qquad (4.22)$$

The convolution in Eq. (4.20) therefore is equivalent to a time-domain low pass filtering as shown in Fig. 4.6. Note that the time-domain Hamming window is real and its amplitude has a maximum at t=0, and is about 8 db down at $t = 1/\tau$. Since our calibration scheme as shwon in Eq. (4.2) sets the phase center to be located at the center of the targets, the time-domain returns at time equal to zero would

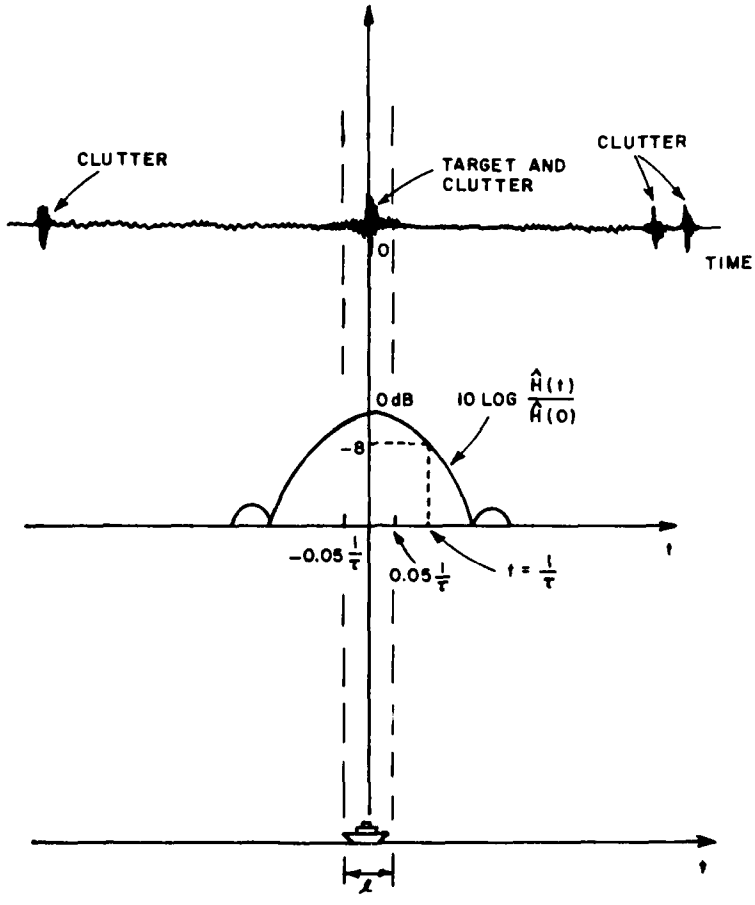

Fig. 4.6. Interpretation of the interpolation in the time domain. The Hemming window becomes a low-pass filter in the time domain.

correspond to the centers of the targets. The time t and the target range R are related by

$$t = 2R/c \tag{4.23}$$

where c is the speed of light. For a target of length ℓ, a major part of the time-domain returns is confined to a zone given by

$$-\ell/c < t < \ell/c \tag{4.24}$$

In addition most of the clutter is greatly removed in distance (or time) from the target. Note that the clutter here is very different from random noise, and is confined to specific mechanisms such as reflections from walls. Therefore, the clutter can be removed by the Hamming window if the window width is chosen properly. For example, if τ is chosen as 300 MHZ, then $1/\tau$ is equivalent to a range of 50 cm. Since model lengths are about 10 cm, a major part of the returns comes from the zone below (see Fig. 4.6).

$$-0.05\,\frac{1}{\tau} < t < 0.05\,\frac{1}{\tau} \tag{4.25}$$

Therefore most clutter will be removed. The effectiveness of this algorithm is illustrated in the following example.

Suppose we are given 6 data points, which are sampled from a waveform defined as

$$c(f) = f$$

The waveform is a ramp, as shown in Fig. 4.7. Note that the dots on the the waveform indicate sample points. Note that the spacing between each sample is not constant. Suppose that we want to estimate the value of the waveform at f = 3 based on the 6 data points. The true value at f = 3 should be C = 3. Now we apply a Hamming window on the data points with its center located at f = 3. Since there are four data points on one side of the window, and only two on the other side, the window is unbalanced, i.e., the contribution from one side is larger than the other. From Eq. (4.20), the waveform value at C = 3 can be estimated as

$$\tilde{c}(3) = 2.9489$$

and the error is given as

$$\% \text{ error} = \frac{c(3) - \tilde{c}(3)}{c(3)} = 1.7\%$$

Now suppose the weighting function $W_s(f_k)$ is not used, despite the data points are not equally spaced, then

$$\tilde{c}(3) = 3.35$$

and the error is given as

$$\% \text{ error} = \frac{\tilde{c}(3) - c(3)}{c(3)} = 11.7\%$$

which is several times higher. The weighting function $W_s(f_k)$ in Eq. (4.20) is obviously very effective.

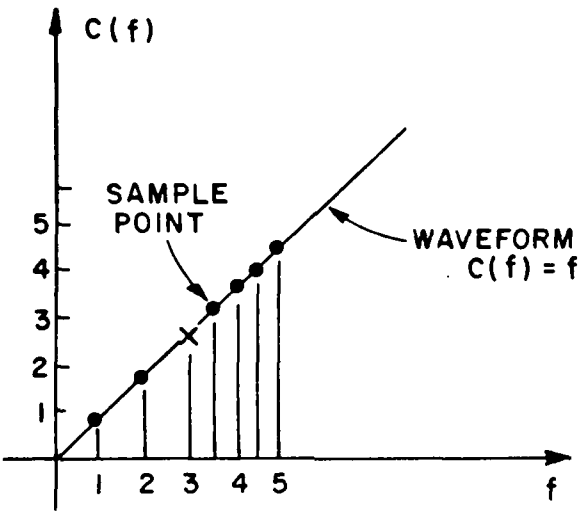

Fig. 4.7. An example of the interpolation. There are 6 data points located at f = 1, 3, 3.5, 4, 4.5, and 5. The underlying function is c(f) = f. It is desired to estimate the data value at f = 3.

E. POST-PROCESSED RADAR RETURNS

The accuracy of the post-processed data can be examined by comparing processed returns of spheres with the theoretical returns of the spheres. An example is given in Fig. 4.8 for a 3.5 inch (diameter) sphere calibrated by a 6 inch reference sphere. It is seen that the error in the amplitude waveforms is small. The error in the phase waveforms is also small except for a ramp-type phase offset. The offset is caused by a difference in positions between the center of the 3.5 inch sphere and the 6 inch sphere. Based on this type of comparison, we found that, in general, the accuracy of the measured data is enough for our application here.

Plots of the processed radar returns of five model ships and four model aircraft are shown in Appendix A. The aspect angles of the targets are 0, 90 and 180 degrees, and the polarization is vertical. Smoothed and unsmoothed waveforms are shown at the same time for comparison. Note that, for this modelling, the amplitude, frequency, and phase are scaled as follows:

$$A_s = A\eta$$
$$f_s = f/\eta$$
$$\theta_s = \theta$$

where

η = scale factor
A_s = scaled amplitude
f_s = scaled frequency
θ_s = scaled phase.

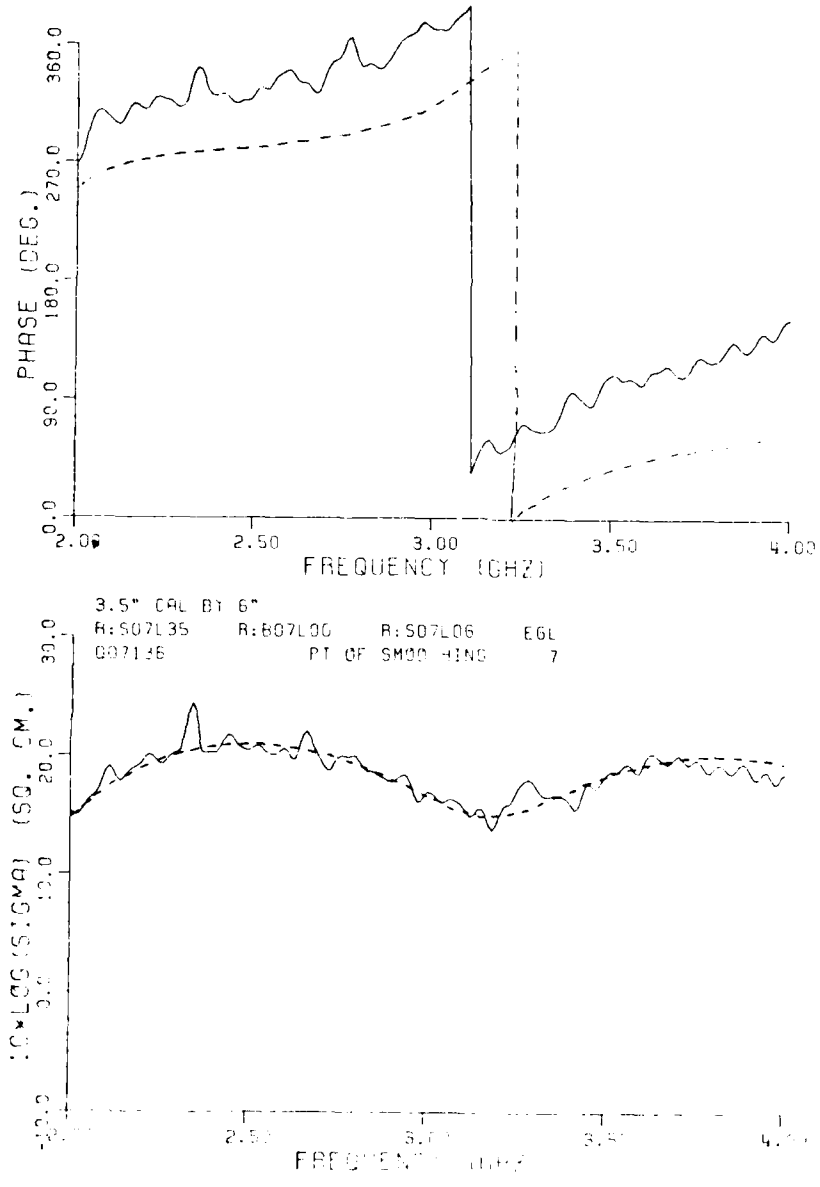

Fig. 4.8. Comparison between measured and theoretical returns of a 3.5 inch sphere at f = 2-4GHZ.

CHAPTER V

TESTING OF CLASSIFICATION ALGORITHMS

A. INTRODUCTION

This chapter will discuss the experiment which were conducted to test the performance of the target classification algorithms developed in Chapter III.

Figure 5.1 is a flowchart showing the experimental process for testing the classification algorithms. As shown in the figure a data base is comprised of multi-frequency amplitude data $A_k(f_j)$ and phase data $\theta_k(f_j)$, where K means the K^{th} target, and f_j means the j^{th} frequency. Two data bases were generated, each consisting of multi-frequency radar data for five ships and four aircraft. Techniques for generating these two experimental data bases have been discussed in Chapter VI, section C. Based on the data bases, we generated catalogs of features for time-domain classification and for frequency-domain classification. Features for test targets were generated by injecting noise into the data stored in the data base. In section B we will discuss the generation of the test data and the noise model used. The test target data were then classified either in the frequency domain or in the time domain, as discussed in Chapter III. By performing the

AD-A162 449 AUTOMATIC TARGET CLASSIFICATION USING HF MULTIFREQUENCY RADARS(U) OHIO STATE UNIV COLUMBUS ELECTROSCIENCE LAB J CHEN OCT 83 ESL-714190-3 N00014-82-K-0037 2/3

UNCLASSIFIED F/G 17/9 NL

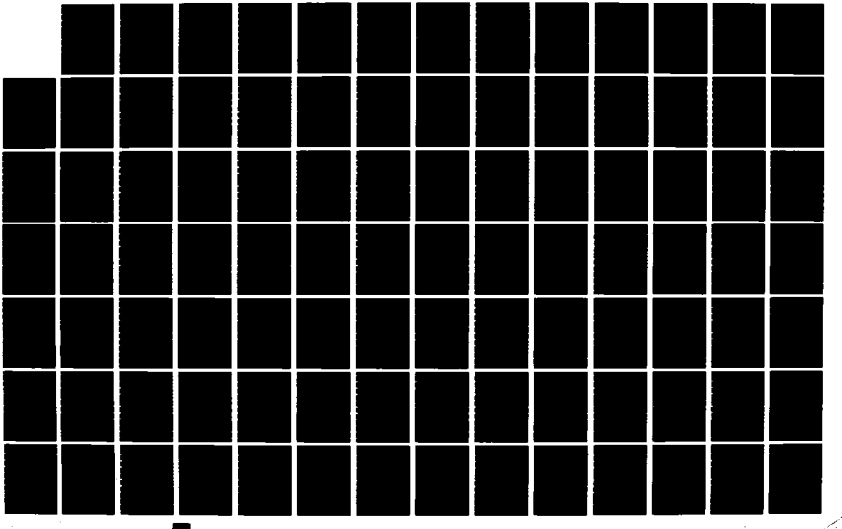

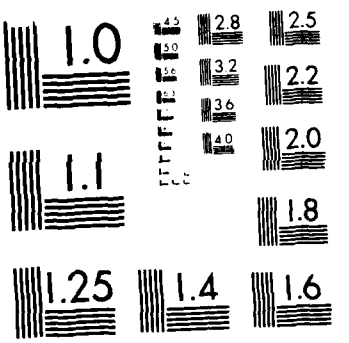

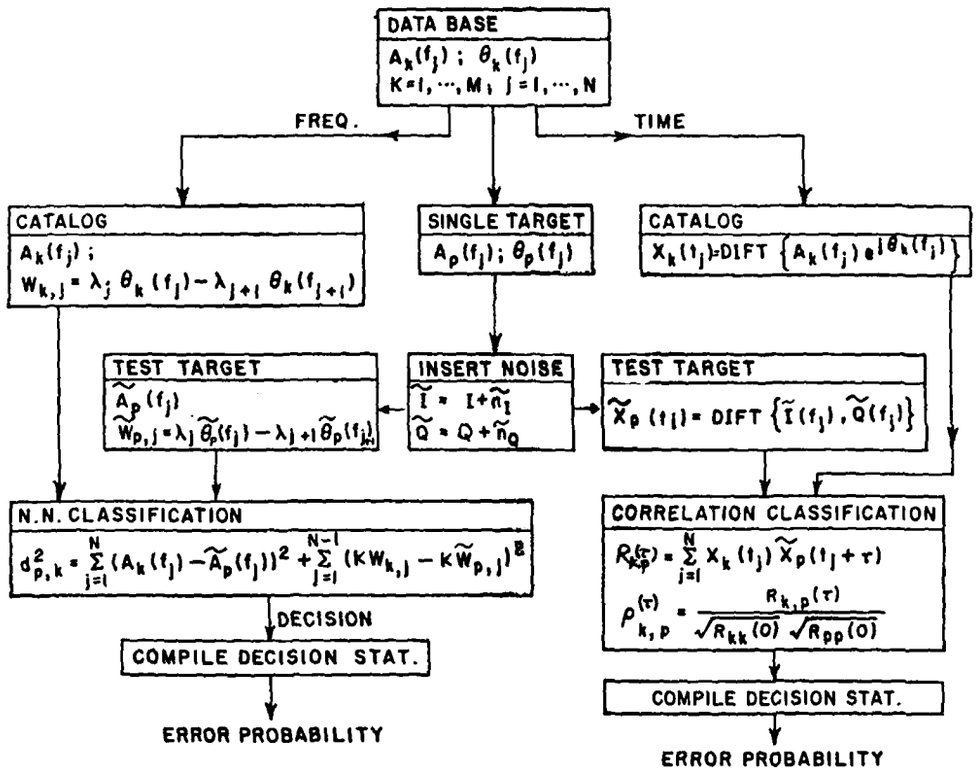

Figure 5.1. A flowchart showing the experimental process for testing the classification algorithms.

classifications of test target data several times, where each experiment is statistically independent, we can obtain an estimate of the probability of misclassification. Section C will discuss the statistical techniques for estimating the probability of misclassification. In section D we will present experimental results for the classification of ships, and, in section E, results for the classification of aircraft.

B. NOISE MODEL

There are a lot of factors which affect the noise present in the post-processed radar returns. In general, noise models which can precisely describe the characteristics of the noise in practice are too complex to be treated with available mathematical methods, or are too cumbersome to compute.

Consider three noise models as shown below.

1. $\tilde{s} = s + \tilde{\varepsilon}_0$ (additive noise)
2. $\tilde{s} = \tilde{\varepsilon}_1 s$ (multiplicative noise)
3. $\tilde{s} = \tilde{\varepsilon}_2 s + \tilde{\varepsilon}_3$ (additive and multiplicative noises)

where, s is the original signal, $\tilde{s}$ is the noise-contaminated signal, and $\tilde{\varepsilon}_0$, $\tilde{\varepsilon}_1$, $\tilde{\varepsilon}_2$ and $\tilde{\varepsilon}_3$ are Gaussian-distributed random noise terms.Based on the noise models and a data base, we calculated the probabilities of misclassification as a function of signal-to-noise power ratio. The result showed that the probability of misclassification for each model for a given signal-to-noise ratio was similar to each other. This indicates that the total power of the noise, rather than its specific

characteristics, has more impact on the performance of the classification algorithms. Furthermore, since there are numerous independent noise sources, none of which is dominant, the statistics of the sum of these noises can be approximately described as Gaussian by virtue of the Central Limit Theorem. Therefore an additive Gaussian noise model would be appropriate for our application here.

A noise-free data point at a particular frequency is a vector consisting of an in-phase component I and a quadrature-phase component Q, which are defined as

$$I = A \cos \theta$$
$$Q = A \sin \theta \qquad (5.1)$$

where A is the amplitude and θ is the phase. The in-phase component and the quadrature-phase component of a noise-contaminated data point can be generated by adding Gaussian noise to the noise-free data point, i.e.,

$$\tilde{I} = I + \tilde{n}_I$$
$$\tilde{Q} = Q + \tilde{n}_Q \qquad (5.2)$$

where $\tilde{n}_I$ and $\tilde{n}_Q$ are independent, Gaussian-distributed random variables with zero mean and variance α^2. The relation between the noisy data point and the noise-free data point is illustrated in Figure 5.2, where, on a I-Q plane, it is shown that the noise-free data point may be scattered by the noise vector over a circular region (shaded). Here we assume that the power of each noise components, $\tilde{n}_I$ and $\tilde{n}_Q$, is the same

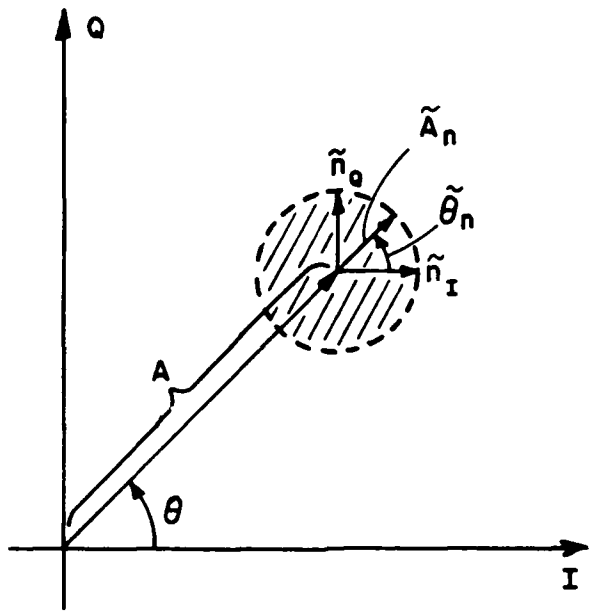

Figure 5.2. The distribution of the noise on an I-Q plane.

so that the shaded region is circular. It is noted that the amplitude of the noise vector is given as

$$\tilde{A}_n = \sqrt{\tilde{n}_I^2 + \tilde{n}_Q^2} \tag{5.3}$$

which is Rayleigh-distributed, and the phase of the noise vector is given as

$$\tilde{\theta}_n = \tan^{-1}\left(\frac{\tilde{n}_Q}{\tilde{n}_I}\right) \tag{5.4}$$

which is uniformly distributed [31]. From Equation (5.2) we can calculate a noisy amplitude and a noisy phase as

$$\begin{aligned}\tilde{A} &= \sqrt{\tilde{I}^2 + \tilde{Q}^2} \\ &= \sqrt{(I + \tilde{n}_I)^2 + (Q + \tilde{n}_Q)^2}\end{aligned} \tag{5.5}$$

$$\begin{aligned}\tilde{\theta} &= \tan^{-1}\left(\frac{\tilde{\theta}}{\tilde{I}}\right) \\ &= \tan^{-1}\left(\frac{Q+\tilde{n}_Q}{I+\tilde{n}_I}\right)\end{aligned} \tag{5.6}$$

The noisy phase in the above equation can be used to calculated a noisy W, i.e.,

$$\tilde{W}_i = \tilde{\theta}_i \lambda_i - \tilde{\theta}_{i+1} \lambda_{i+1} \tag{5.7}$$

In the case where only amplitude is available the amplitude in the presence of the noise is given by

$$\tilde{A} = \sqrt{(I+\tilde{n}_I)^2 + \tilde{n}_Q^2} \tag{5.8}$$

Noisy time-domain data can be obtained by taking the inverse discrete Fourier transform of the noisy frequency-domain data defined in Eq. (5.2).

All of the noise-contaminated features above are defined based on the additive Gaussian noise model defined in Eq. (5.2). A signal-to-noise power ratio (SNR) for such a model can be defined as the ratio of total signal power and total noise variance, i.e.,

$$\frac{S}{N} = \frac{I^2 + Q^2}{VAR(\tilde{n}_I) + VAR(\tilde{n}_Q)}$$

$$= \frac{A^2}{2\alpha^2} \tag{5.9}$$

In our classification experiments, the signal power A^2 was first estimated using the data in the data base. By varying the noise power α^2 the SNR was varied over a range, and the probability of misclassification was determined for each SNR value.

C. ESTIMATION OF THE PROBABILITY OF MISCLASSIFICATION

Analytical calculations of error probabilities for our classification schemes here are rather involved because they may require integrations of multi-dimensional probability density functions with extremely complicated boundaries. Furthermore the density functions may not be readily obtainable. Therefore one has to resort to statistical methods for estimating the probability of misclassification.

Suppose there are M targets, and the probability of occurrence of each target C_j, i.e., the a priori probability, is given by $p(c_j)$, $j = 1, 2, \ldots, M$. The probability of misclassification can be given as

$$P(\text{Error}) = \sum_{j=1}^{M} P(\text{Error}/c_j)P(c_j) \tag{5.17}$$

where $P(\text{Error}/c_j)$ is the conditional probability of error given target j. A good statistical estimate for the conditional probability $p(\text{Error}/c_j)$ is the Maximum Likelihood Estimate (MLE) [24].

Now let's derive the MLE of $P(\text{Error}/c_j)$. Let

$$P(\text{Error}/c_j) \equiv P_j \tag{5.18}$$

Suppose n_j independent classification experiments are performed on target j. This can be done by using different seeds for generating

noises in each experiment so that the noises are independent of each other. In each experiment the probability of misclassifying target j is p_j. It is evident that the probability of misclassifying target j m_j times can be described by a binomial probability distribution, i.e., m_j is Binomial-distributed with parameter p_j, and

$$p\{m_j/p_j\} = \binom{n_j}{m_j} p_j^{m_j} (1-p_j)^{n_j-m_j} \tag{5.19}$$

A feasible choice of the Likelihood Function would be the term $p\{m_j/p_j\}$ defined by Eq. (5.19) [24]. The MLE of p_j is the one which maximizes the Likelihood Function, i.e.,

$$\hat{p}_j = \max_{p_j} p\{m_j/p_j\} \tag{5.20}$$

or

$$\frac{\partial}{\partial p_j} \log p\,(m_j/P_j) \Big|_{P_j=\hat{P}_j} = 0 \tag{5.21}$$

where $\hat{p}_j$ is the MLE of p_j. Now

$$\frac{\partial}{\partial p_j} [\log p\,\{m_j/p_j\}]$$

$$= \frac{\partial}{\partial p_j} \log \{\binom{n_j}{m_j} p_j^{m_j} (1-p_j)^{n_j-m_j}\}$$

$$= \frac{\partial}{\partial p_j} \{\log\binom{n_j}{m_j} + m_j \log p_j + (n_j-m_j)\log(1-p_j)\}$$

$$= \frac{m_j}{p_j} - \frac{(n_j-m_j)}{(1-p_j)} \tag{5.22}$$

From Eq. (5.21) and Eq. (5.22) we have

$$\frac{m_j}{n_j} - \frac{n_j - m_j}{(1-\hat{p}_j)} = 0$$

or

$$\hat{p}_j = \frac{m_j}{n_j} \tag{5.23}$$

When the sample size n_j is large (normally $n_j p_j > 5$), a $(1 - \alpha)$ confidence interval for p_j can be approximately given as [24]

$$\hat{p}_j \pm \xi_\alpha \sqrt{VAR(\hat{p}_j)}$$

or

$$p\left(\hat{p}_j - \xi_\alpha \sqrt{VAR(\hat{p}_j)} < p_j < \hat{p}_j + k_\alpha \sqrt{VAR(\hat{p}_j)}\right) = (1 - \alpha)$$

where ξ_α is defined by $\Phi(\xi_\alpha) = 1-\alpha/2$, where Φ is the standard normal distribution, and

$$\Phi(\xi_\alpha) = \frac{1}{2\pi} \int_{-\infty}^{\xi_\alpha} e^{\frac{-x^2}{2}} dx$$

and

$$VAR(\hat{p}_j) = \frac{\hat{p}_j(1-\hat{p}_j)}{n_j}$$

Note that the $(1 - \alpha)$ confidence interval for P_j means that the probability of P_j falling in the interval is $(1 - \alpha)$.

Suppose the probability of occurrence for each target is the same, i.e.,

$$p(c_j) = \frac{1}{M}$$

then the probability of misclassification P_E can be estimated as

$$P_E = \sum_{j=1}^{M} p(Error/c_j)\, p(c_j)$$

$$\approx \frac{1}{M} \sum_{j=1}^{M} \hat{p}_j$$

$$\equiv \hat{P}_E \qquad (5.24)$$

Note that $\hat{P}_E$ is also an MLE of P_E[24]. A $(1-\alpha)$ confidence interval for P_E is given as [24]

$$\hat{P}_E \pm \xi_\alpha \sqrt{VAR(\hat{P}_E)}$$

where ξ_α is defined as $\Phi(\xi_\alpha) = 1-\alpha/2$.

Now

$$VAR(\hat{P}_E) = VAR\left(\frac{1}{M}\sum_{j=1}^{M} \hat{p}_j\right)$$

$$= \frac{1}{M^2}\sum_{j=1}^{M} VAR(\hat{p}_o)$$

$$= \frac{1}{M} VAR(\hat{p}_o)$$

$$= \frac{1}{M}\frac{\hat{p}_o(1-\hat{p}_o)}{n}$$

where $\hat{p}_1, \hat{p}_2, \ldots, \hat{p}_M$ are assumed to be mutually independent and

$$VAR(\hat{p}_1) = VAR(\hat{p}_2) = \ldots = VAR(\hat{p}_M) \equiv VAR(\hat{p}_o)$$

Therefore the $(1-\alpha)$ confidence interval for P_E becomes

$$\hat{P}_E \pm \xi_\alpha \sqrt{\frac{\hat{P}o(1-\hat{P}_o)}{Mn}} \qquad (5.25)$$

An algorithm for estimating the probability of misclassification is given below.

Suppose there are M data files in the data base representing, respectively, M classes, and each containing N complex frequency components, i.e., the I-data and Q-data.

1. Create M targets by injecting noise into the M data files respectively, i.e., for each I data and Q data of each of the N frequencies of each file, generate two Gaussian random numbers, and contaminate the data as shown in Eq. (5.2). Use different seeds for each file.
2. Classify the M targets according to the algorithms in Section C of Chapter III (frequency-domain classification) and in Section D of Chapter III (time-domain classification).
3. Repeat the above experiments (steps 1 and 2) a number of times, using different seeds for each experiment.
4. Calculate the probability of misclassification using Eq. (5.24).

D. CLASSIFICATION OF SHIPS

In this section we will discuss our experiments on the classification of ships and the results.

The experiments made use of a data base consisting of 15 classes as defined in Table 5.1. The aspect angles of the ships were chosen to be 0, 90, and 180 degrees so that data of the same ships at different aspect angles (e.g., class 1, 2, and 3) would be independent of each other. Since data of different ships (e.g., class 1 and 4) were also independent, all classes in the data base would be

independent of each other. The number of frequencies N employed for the classifications were N = 2, 4, and 8, with a frequency increment of Δf = 0.4 MHZ. Young and Walton found [13] that the duration of a time-domain ramp response R(t) was less than 6 transit time across the length ℓ of a target, i.e.,

$$R(t,t_0) \approx 0 \text{ for } t < t_0 \text{ or } t > t_0 + (6\ell/c) \tag{5.26}$$

where C is the speed of light and t_0 is a time reference. For the above time-limited function, the Shannon's sampling theorem requires that the frequency-sampling rate Δf satisfy

$$\Delta f < c/6\ell \tag{5.27}$$

The ships have dimensions of the order of 100 meters, which implies that the sampling rate for the ship returns should satisfy

$$\Delta f < 0.5 \text{ MHZ} \tag{5.28}$$

Based on the criterion in Eq. (5.28) we chose the frequency-increment Δf as 0.4 MHZ. The minimum frequency available in the data base was 1.67 MHZ, therefore, the frequency ranges were chosen as 1.7 MHZ < f < 2.1 MHZ for N = 2, 1.7 MHZ < f < 2.9 MHZ for N = 4, and 1.7 MHZ < f < 4.5 MHZ for N = 8. The corresponding range of wavelengths for 1.7 MHZ < f < 4.5 MHZ is 67 m < λ < 176 m, and the ratios of the ship's dimensions D and the wavelengths are of the order of

TABLE 5.1

A LIST OF SHIPS USED IN THE CLASSIFICATION EXPERIMENTS

CLASS	TARGET	ASPECT ANGLE (degrees)
1	A	0
2	A	90
3	A	180
4	B	0
5	B	90
6	B	180
7	C	0
8	C	90
9	C	180
10	D	0
11	D	90
12	D	180
13	E	0
14	E	90
15	E	180

Elevation angle = 0°

Polarization: Vertical

$$D/\lambda \approx 1 \tag{5.29}$$

which means the radar returns are in the lower Resonance region. For frequency-domain classifications the parameter β in Eq. (3.15) was chosen as $\beta \approx \infty$, $\beta = 0$, and $\beta = 1$, corresponding, respectively, to uses of 'amplitude features only', 'phase features only', and 'both amplitude and phase features'. A feature called 'relative amplitude' was also employed for classifications in the frequency domain, and was defined as follows.

$$\bar{A}_i = A_i/A_{i+1} \; ; \; i = 1, 2, \ldots, N - 1 \tag{5.30}$$

where

$\bar{A}_i$ = ith relative amplitude

A_i = ith amplitude

N = number of frequencies

The division undertaken in Eq. (5.30) was designed for the removal of possible multiplicative bias embedded in the amplitude data.

For time-domain classification, the Discrete Inverse Fourier Transform (DIFT) was applied to obtain real numbers for the time-domain signals. Frequency-domain data were assumed to be symmetric around $f = 0$, i.e.,

$$c(f) = c^*(-f) \tag{5.31}$$

where, C*(f) is the complex conjugate of the frequency-domain data C(f), so that the corresponding time-domain signals would be real numbers.

It is known that we can reduce the error probability if the target aspect angles are known. In practice the aspect angles should be estimated with some accuracy otherwise the probability of misclassification may increase sharply. Let's consider the effects of an error of 15 degrees in the estimated target aspect angles, as shown in Fig. 5.3. The change in path length ΔP for a change in aspect angles by 15 degrees is given by

$$\Delta p = 2 \cdot \Delta \ell$$

$$= 2 \cdot \left(\frac{D}{2} - \frac{D}{2} \cos 15° \right)$$

or

$$\Delta p = 3.4\% \; D \tag{5.32}$$

which is only a fraction of the total target dimension D. Consider a data base as shown in Table 5.2, where the aspect angles are 15 degrees apart. Tables 5.3 - 5.5 are matrices which show the N.N. distances between any two classes in the data base for $\beta = \infty$ (amplitude only),

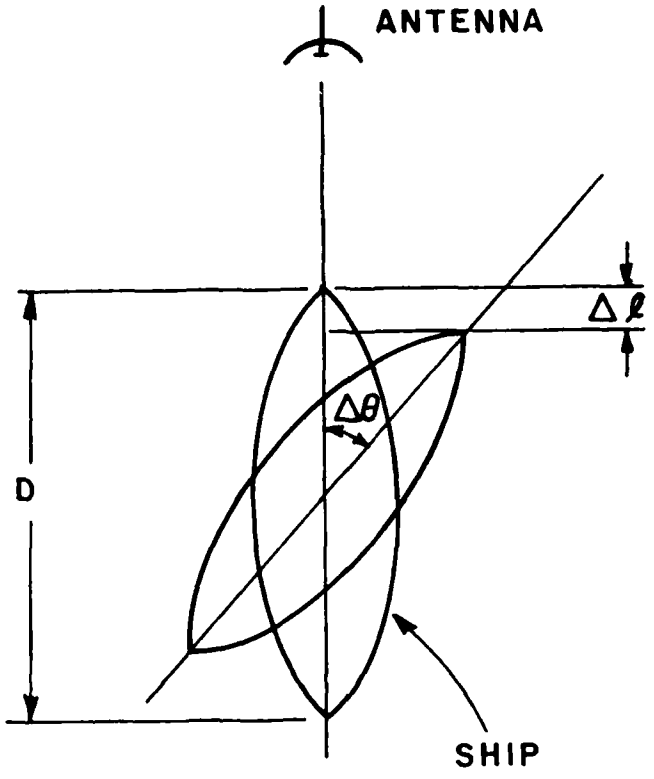

Fig. 5.3. Change of wavepath length Δp for a change in aspect angles by 15°. Note $\Delta p \approx 2\Delta\ell = 2 \cdot (\frac{D}{2} - \frac{D}{2}\cos\Delta\Theta)$.

TABLE 5.2

A LIST OF SHIPS USED IN THE CLASSIFICATION EXPERIMENTS

CLASS	TARGET	ASPECT ANGLE (degrees)
1	A	0
2	A	15
3	A	30
4	B	0
5	B	15
6	B	30
7	C	0
8	C	15
9	C	30
10	D	0
11	D	15
12	D	30
13	E	0
14	E	15
15	E	30

Elevation angle = 0°

Polarization: Vertical

TABLE 5.3

A MATRIX SHOWING THE DISTANCE BETWEEN ANY TWO CLASSES.
THE ENTRY AT ROW I AND COLUMN J IS THE N.N. DISTANCE BETWEEN CLASS I AND CLASS J. ONLY AMPLITUDE DATA ARE USED TO CALCULATE THE DISTANCE.

CLASS	1	2	3	4	5	6	7	8	9	10	11	12	13	14	15
1	0.	18.	23.	162.	155.	150.	276.	291.	203.	62.	53.	20.	166.	181.	230.
2	18.	0.	10.	164.	158.	157.	277.	294.	205.	69.	57.	30.	164.	175.	232.
3	23.	10.	0.	166.	160.	160.	280.	297.	208.	66.	54.	32.	167.	175.	231.
4	162.	164.	166.	0.	20.	89.	199.	206.	125.	193.	191.	179.	120.	140.	158.
5	155.	158.	160.	20.	0.	73.	199.	204.	121.	186.	184.	170.	119.	144.	153.
6	150.	157.	160.	89.	73.	0.	225.	205.	103.	191.	189.	160.	109.	152.	147.
7	276.	277.	280.	199.	199.	225.	0.	105.	173.	288.	286.	284.	183.	192.	218.
8	291.	294.	297.	206.	204.	205.	105.	0.	147.	312.	310.	297.	176.	199.	204.
9	203.	205.	208.	125.	121.	103.	173.	147.	0.	238.	235.	212.	65.	107.	146.
10	62.	69.	66.	193.	186.	191.	288.	312.	238.	0.	15.	57.	206.	213.	258.
11	53.	57.	54.	191.	184.	189.	286.	310.	235.	15.	0.	48.	200.	207.	257.
12	20.	30.	32.	179.	170.	160.	284.	297.	212.	57.	48.	0.	175.	190.	236.
13	166.	164.	167.	120.	119.	109.	183.	176.	65.	206.	200.	175.	0.	55.	134.
14	181.	175.	175.	140.	144.	152.	192.	199.	107.	213.	207.	190.	55.	0.	152.
15	230.	232.	231.	158.	153.	147.	218.	204.	146.	258.	257.	236.	134.	152.	0.

TABLE 5.4

A MATRIX SHOWING THE DISTANCE BETWEEN ANY TWO CLASSES.
ONLY THE PHASE DATA ARE USED TO CALCULATE THE N.N. DISTANCE.

CLASS	1	2	3	4	5	6	7	8	9	10	11	12	13	14	15
1	0.	150.	76.	202.	208.	250.	198.	235.	119.	156.	172.	153.	187.	165.	147.
2	150.	0.	145.	195.	206.	212.	89.	138.	52.	47.	63.	80.	69.	56.	85.
3	76.	145.	0.	186.	194.	213.	178.	216.	125.	146.	167.	143.	189.	167.	147.
4	202.	195.	186.	0.	18.	111.	227.	269.	197.	179.	201.	164.	229.	187.	212.
5	208.	206.	194.	18.	0.	123.	240.	284.	207.	188.	209.	171.	241.	196.	220.
6	250.	212.	213.	111.	123.	0.	212.	234.	229.	209.	236.	210.	226.	220.	254.
7	198.	89.	178.	227.	240.	212.	0.	64.	133.	100.	115.	132.	81.	101.	163.
8	235.	138.	216.	269.	284.	234.	64.	0.	176.	160.	175.	193.	104.	159.	210.
9	119.	52.	125.	197.	207.	229.	133.	176.	0.	77.	88.	91.	106.	88.	56.
10	156.	47.	146.	179.	188.	209.	100.	160.	77.	0.	30.	38.	103.	32.	91.
11	172.	63.	167.	201.	209.	236.	115.	175.	88.	30.	0.	45.	115.	38.	89.
12	153.	80.	143.	164.	171.	210.	132.	193.	91.	38.	45.	0.	138.	56.	92.
13	187.	69.	189.	229.	241.	226.	81.	104.	106.	103.	115.	138.	0.	94.	148.
14	165.	56.	167.	187.	196.	220.	101.	159.	88.	32.	38.	56.	94.	0.	106.
15	147.	85.	147.	212.	220.	254.	163.	210.	56.	91.	89.	92.	148.	106.	0.

TABLE 5.5

A MATRIX SHOWING THE DISTANCE BETWEEN ANY TWO CLASSES.
BOTH AMPLITUDE AND PHASE DATA ARE USED.

CLASS	1	2	3	4	5	6	7	8	9	10	11	12	13	14	15
1	0.	152.	79.	259.	260.	292.	339.	374.	235.	168.	180.	154.	251.	245.	273.
2	152.	0.	146.	255.	260.	264.	291.	325.	212.	83.	85.	85.	178.	183.	247.
3	79.	146.	0.	249.	252.	267.	332.	367.	243.	160.	176.	147.	252.	242.	274.
4	259.	255.	249.	0.	27.	142.	302.	339.	234.	263.	277.	243.	259.	234.	264.
5	260.	260.	252.	27.	0.	143.	312.	350.	240.	264.	279.	241.	269.	243.	268.
6	292.	264.	267.	142.	143.	0.	309.	311.	251.	283.	302.	264.	251.	267.	293.
7	339.	291.	332.	302.	312.	309.	0.	123.	218.	305.	309.	313.	200.	217.	273.
8	374.	325.	367.	339.	350.	311.	123.	0.	229.	351.	356.	354.	205.	255.	293.
9	235.	212.	243.	234.	240.	251.	218.	229.	0.	250.	251.	231.	125.	138.	157.
10	168.	83.	160.	263.	264.	283.	305.	351.	250.	0.	34.	68.	230.	215.	273.
11	180.	85.	176.	277.	279.	302.	309.	356.	251.	34.	0.	66.	231.	210.	272.
12	154.	85.	147.	243.	241.	264.	313.	354.	231.	68.	66.	0.	223.	198.	254.
13	251.	178.	252.	259.	269.	251.	200.	205.	125.	230.	231.	223.	0.	109.	200.
14	245.	183.	242.	234.	243.	267.	217.	255.	138.	215.	210.	198.	109.	0.	185.
15	273.	247.	274.	264.	268.	293.	273.	293.	157.	273.	272.	254.	200.	185.	0.

$\beta = 0$ (phase only), and $\beta = 1$ (amplitude and phase). Table 5.6 is a matrix which shows the cross-correlation coefficients of any two classes in the data base. Note that the N.N. distance and the cross-correlation coefficient between a class and itself are 0 and 1, respectively, as shown in the diagonal of the matrices. In the tables the nearest neighbor of a ship other than the ship itself is underlined once if the nearest neighbor comes from the same ship, and is underlined twice if it comes from different ships. The percentage of entries with double underlines in the matrices indicates the classification error introduced by an error of 15 degrees in the estimated target aspect angles. The percentage of double underlines is 13% in Table 5.3, and 20% in Tables 5.4, 5.5, and 5.6. This indicates the tolerable uncertainty of target aspect angles. If the misclassification probability is too high the target aspect angles should be determined more accurately.

The signal power of the data in the data base may vary depending on frequency, aspect angles, and geometries of the targets. The noise added to each data point was set to have the same variance so that data with higher signal powers would have higher signal-to-noise power ratios. The signal power of each class was estimated by taking the average over all data points of that class, i.e.,

$$p = \frac{1}{N} \sum_{i=1}^{N} A^2(f_i); \quad A \equiv \text{Amplitude} \tag{5.33}$$

Since additive zero-mean Gaussian noise is used, the noise power is equal to its variance α^2. The average signal-to-noise ratio

TABLE 5.6

A MATRIX SHOWING THE CROSS-CORRELATION COEFFICIENT FOR ANY TWO CLASSES

CLASS	1	2	3	4	5	6	7	8	9	10	11	12	13	14	15
1	1.00	0.81	0.75	0.58	0.59	0.44	0.61	0.51	0.49	0.68	0.75	0.88	0.51	0.71	0.57
2	0.81	1.00	0.90	0.66	0.58	0.52	0.76	0.54	0.63	0.70	0.77	0.87	0.79	0.54	0.55
3	0.75	0.90	1.00	0.83	0.78	0.55	0.66	0.47	0.51	0.86	0.80	0.78	0.63	0.59	0.56
4	0.58	0.66	0.83	1.00	0.98	0.55	0.54	0.42	0.50	0.69	0.66	0.58	0.55	0.55	0.55
5	0.59	0.58	0.78	0.98	1.00	0.61	0.47	0.48	0.57	0.67	0.65	0.57	0.56	0.57	0.57
6	0.44	0.52	0.55	0.55	0.61	1.00	0.61	0.72	0.73	0.55	0.53	0.48	0.67	0.50	0.49
7	0.61	0.76	0.66	0.54	0.47	0.61	1.00	0.70	0.77	0.50	0.57	0.62	0.88	0.68	0.66
8	0.51	0.54	0.47	0.42	0.48	0.72	0.70	1.00	0.91	0.45	0.41	0.61	0.70	0.50	0.63
9	0.49	0.63	0.51	0.50	0.57	0.73	0.77	0.91	1.00	0.50	0.52	0.44	0.82	0.65	0.70
10	0.68	0.70	0.86	0.69	0.67	0.55	0.50	0.45	0.50	1.00	0.98	0.79	0.61	0.61	0.53
11	0.75	0.77	0.80	0.66	0.65	0.53	0.57	0.41	0.52	0.98	1.00	0.89	0.65	0.62	0.48
12	0.88	0.87	0.78	0.58	0.57	0.48	0.62	0.61	0.44	0.79	0.89	1.00	0.66	0.67	0.42
13	0.51	0.79	0.63	0.55	0.56	0.67	0.88	0.70	0.82	0.61	0.65	0.66	1.00	0.62	0.72
14	0.71	0.54	0.59	0.55	0.57	0.50	0.68	0.50	0.65	0.61	0.62	0.67	0.62	1.00	0.81
15	0.57	0.55	0.56	0.55	0.57	0.49	0.66	0.63	0.70	0.53	0.48	0.42	0.72	0.81	1.00

is given by

$$SNR = \frac{1}{K} \sum_{j=1}^{N} (P_j/\alpha^2)$$

$$= \frac{1}{\alpha^2} \left(\frac{1}{k} \sum_{j=1}^{k} P_j\right) \qquad (5.34)$$

where p_j is the average power of class j, and K is the number of classes, which is equal to 15 here. The term in the parenthesis in Eq. (5.34) is the average power over all classes in the data base, and was calculated to be approximately 44 dB-square-meters. The probability of misclassification was calculated based on Equation (5.24) with the number of experiments = 15.

Let's use Equation (5.25) to calculate a 90 percent confidence interval for the probability of misclassification P_E. Let the probability of misclassification be about 30 percent, i.e., $\tilde{p}_o \sim .3$ With M=15, n=15, α=0.1, and ξ_α satisfying

$$\Phi(\xi_\alpha) = 1 - \frac{\alpha}{2} = 0.95 \quad .$$

or

$$\xi_\alpha = 1.65 \quad .$$

the confidence interval for P_E is given as

$$\hat{P}_E \pm \xi_\alpha \sqrt{\frac{\hat{P}_o(1-\hat{P}_o)}{Mn}}$$

$$= \hat{P}_E \pm 1.65 \sqrt{\frac{0.3(1-0.3)}{15x15}}$$

$$= \hat{P}_E \pm 5 \text{ percent} \quad . \tag{5.35}$$

Therefore a 90 percent confidence interval for $\hat{P}_E \approx 30$ percent is ± 5 percent.

In the following we will present plots of misclassification percentages as a function of signal-to-noise power ratio (S/N) under the following conditions:

1. As a function of the number of frequencies utilized,
2. For different classification algorithms,
3. With or without a priori knowledge of target aspect angles.

Figures 5.4-5.7 are plots of error probabilities with the number of frequencies N as a parameter. In all four figures we assume that target aspect angles are known a priori, and the number of frequencies N is set to 2, 4 and 8. Figures 5.4, 5.5, and 5.6 are results of frequency-domain classifications using, respectively, amplitude returns only, phase returns only, and both amplitude and phase returns. Figure 5.7 shows the result for time-domain algorithms. It can be seen that the error probabilities can be improved significantly by increasing the number of frequencies. This is especially true for time-domain classifications.

Figures 5.8-5.10 show the effects of employing different types of classification algorithms. For convenience let A stand for "use only amplitude", W for "use only phase", A and W for "use both amplitude and phase", and TIME for "use time-domain algorithms". In all three figures

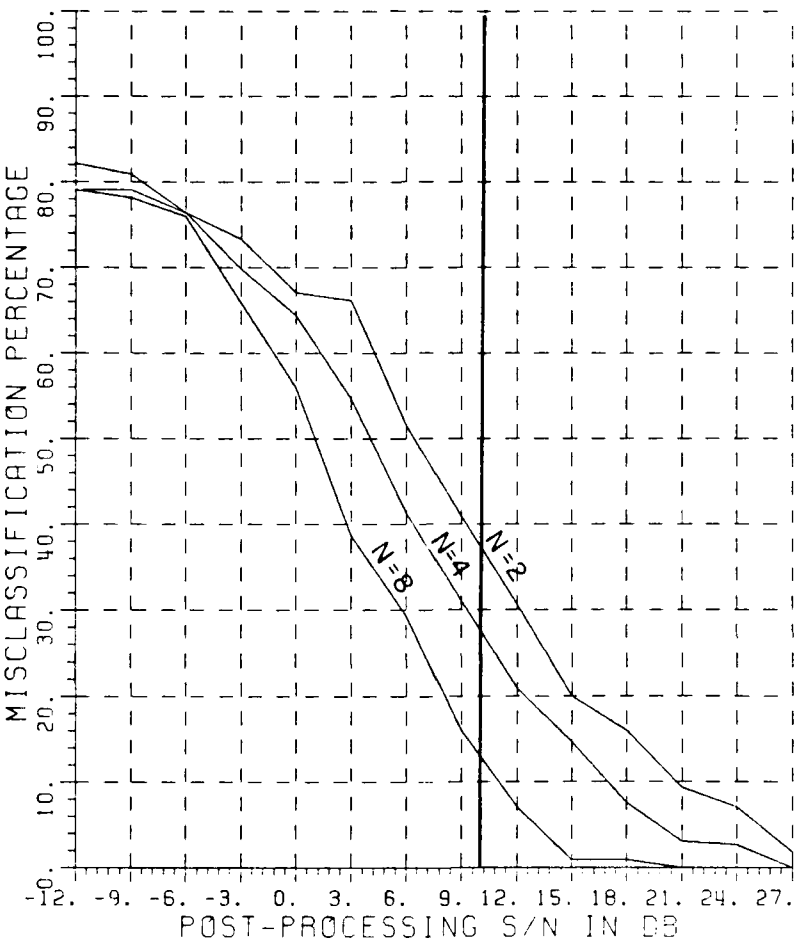

Figure 5.4. Plots of error probabilities with the number of frequencies N as a parameters. Only amplitude is used. Aspect angles are assumed known. A 90% confidence interval for a classification error of 30% is approximately ± 5% .

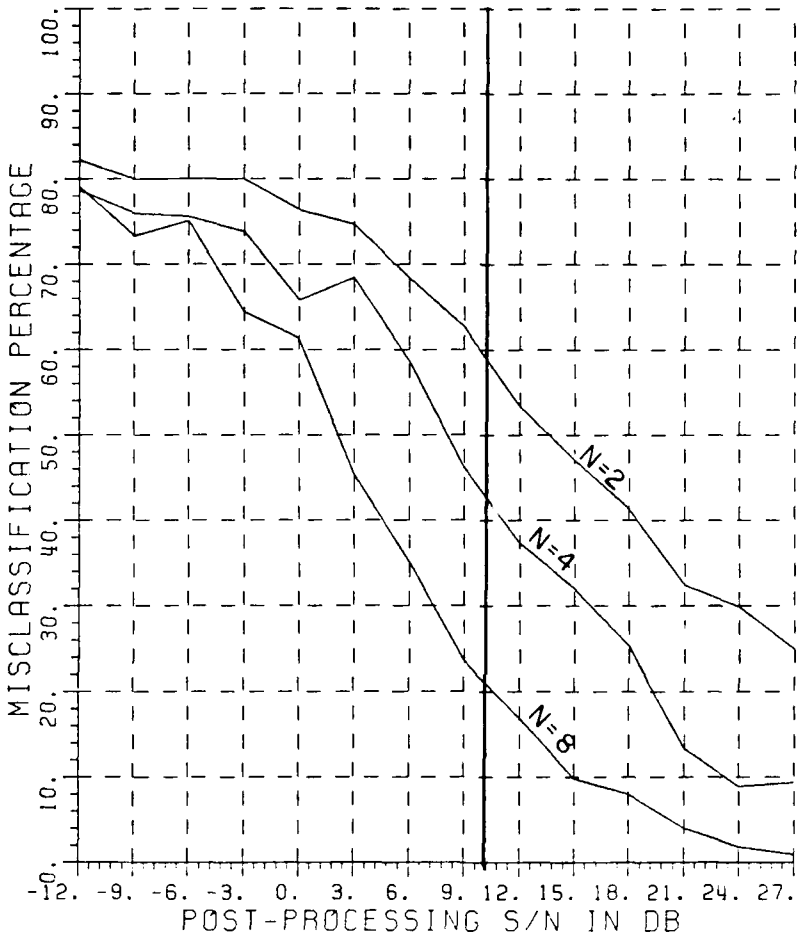

Figure 5.5. Plots of error probabilities with the number of frequencies N as a parameters. Only phase is used. Aspect angles are assumed known. A 90% confidence interval for a classification error of 30% is approximately ± 5% .

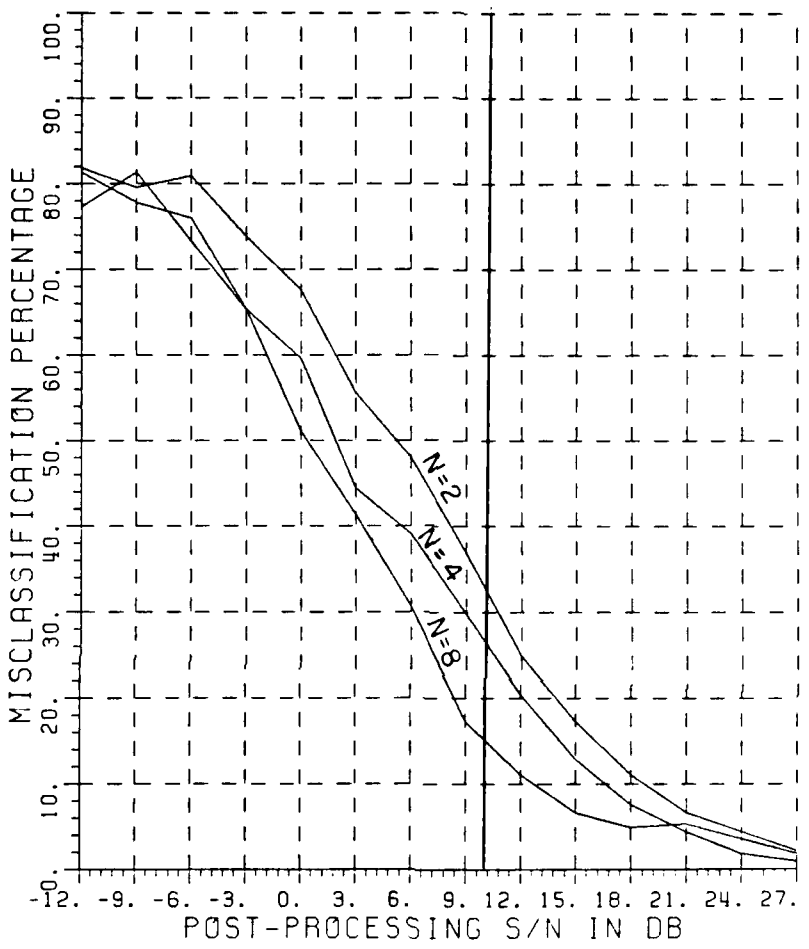

Figure 5.6. Plots of error probabilities with the number of frequencies N as a parameters. Both amplitude and phase are used. Aspect angles are known a priori. A 90% confidence interval for a classification error of 30% is approximately ± 5% .

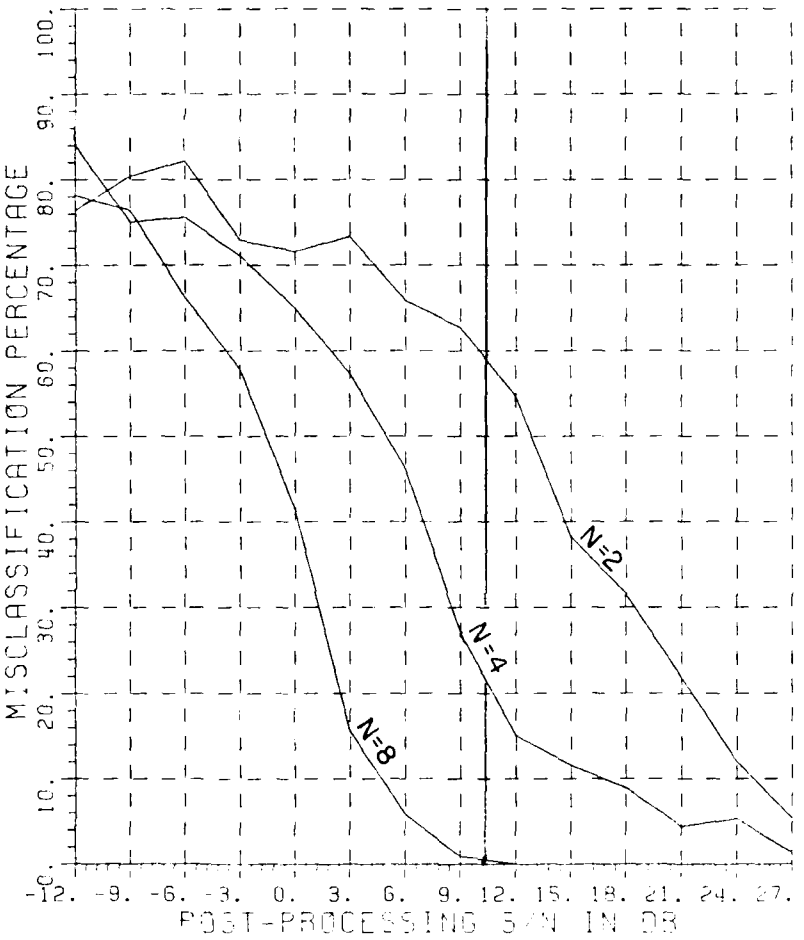

Figure 5.7. Error probabilities for N=2,4,8 frequencies. Time-domain algorithm is used, and the aspect angles are assumed a priori. A 90% confidence interval for a classification error of 30% is approximately ± 5% .

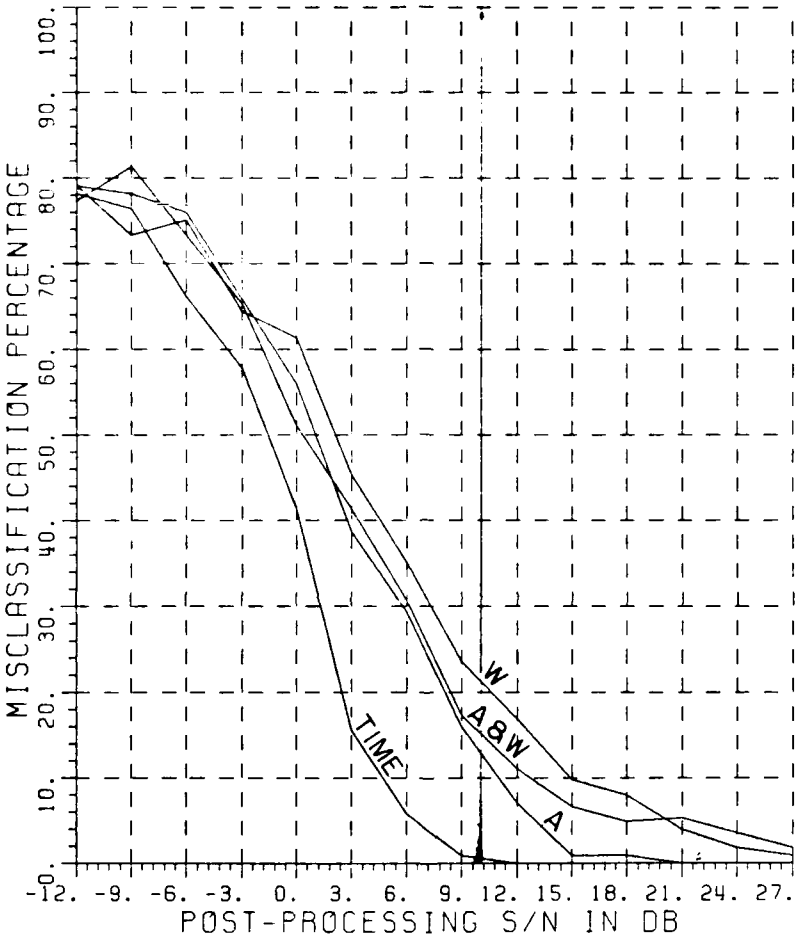

Figure 5.8. Error probabilities for four algorithms. Number of frequency = 8. Aspect angles are known a priori. A 90% confidence interval for a classification error of 30% is approximately ± 5% .

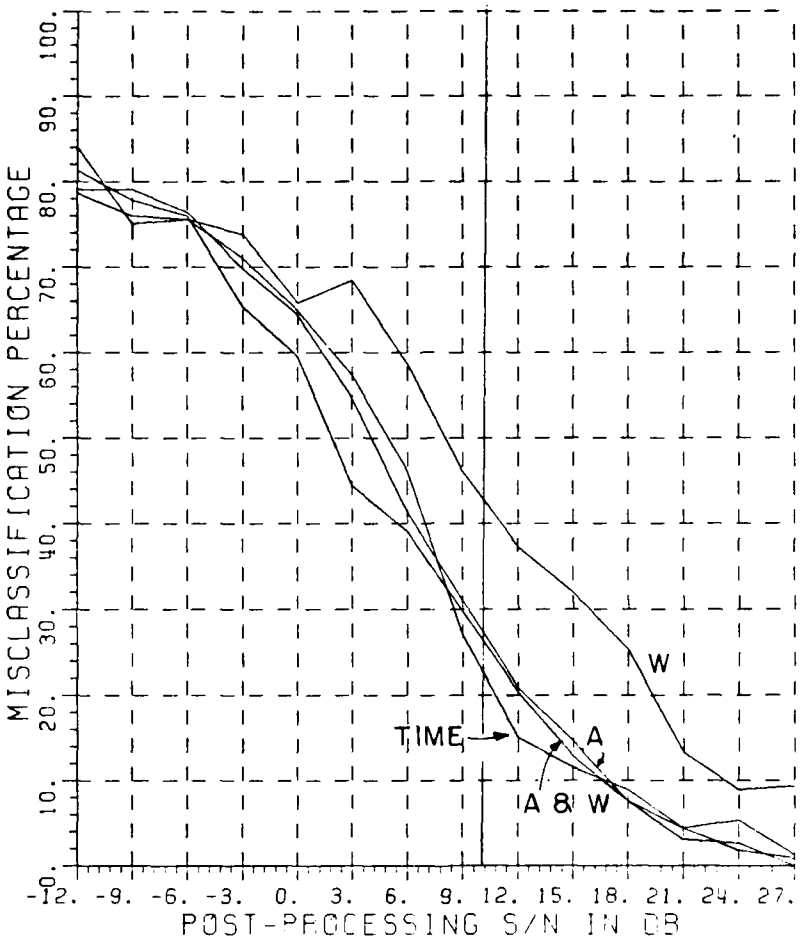

Figure 5.9. Error probabilities for four algorithms. Number of frequencies = 4. Known aspect angles. A 90% confidence interval for a classification error of 30% is approximately ± 5% .

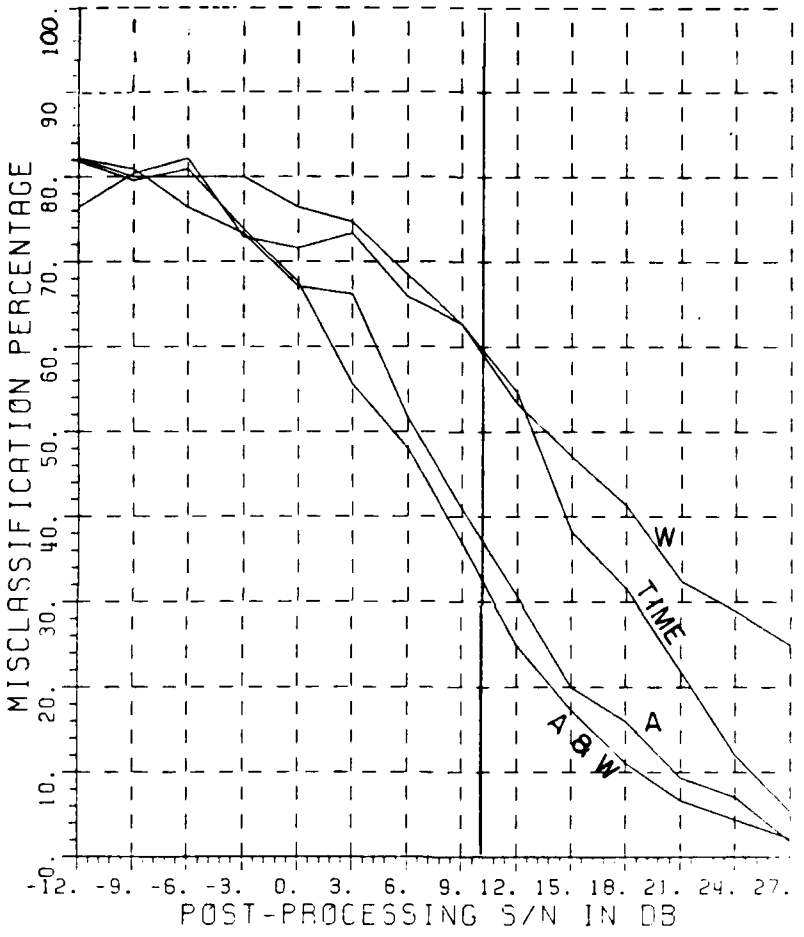

Figure 5.10. Error probabilities for four algorithms. Number of frequencies = 2. Aspect angles are known a priori. A 90% confidence interval for a classification error of 30% is approximately ± 5% .

we assume that target aspect angles are known a priori. The number of frequencies used is N = 8 in Figure 5.8, N = 4 in Figure 5.9, and N = 2 in Figure 5.10. It can be seen that the time-domain algorithms produce the best results in Figure 5.8 and Figure 5.9. In Figure 5.10 where N = 2, the time-domain results are worse than those of 'A' or 'A or W'.

It can be seen from the definition of the noise model that certain amounts of noise introduced in the I and Q components may cause large errors in W due, in part, to branch-cut effects. As a result, the error in the phase features dominates the decision. The error becomes larger if the number of frequencies is increased. Due to this effect, it can be seen in Figure 5.8, where N = 8, the 'A' curve is better than 'A and W' or 'W' curves. In Figure 5.10 where the number of frequencies becomes smaller (N = 2) and the 'A and W' curve becomes better than the 'A' curve.

Figure 5.11 shows the error probabilities, in which relative amplitudes, $\overline{A}$, as defined in Equation (5.30), are employed. As is the case for the W's, the relative amplitudes may also be distorted significantly when certain amounts of noise are introduced into the I and Q components, resulting in the same effects as discussed above. In

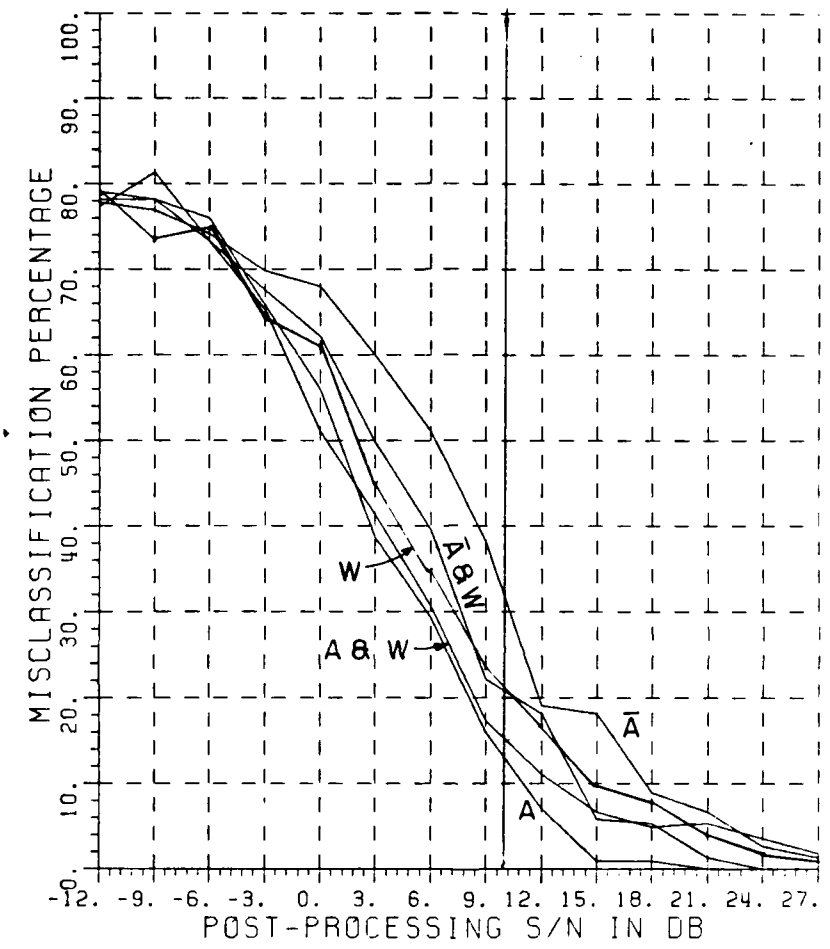

Figure 5.11. Error probabilities for relative amplitudes. Numbers of frequencies = 8. Aspect angles are known. A 90% confidence interval for a classification error of 30% is approximately ± 5% .

Figure 5.11 we can see that the 'W' curve is better than the 'A and W' curve which indicates that errors in the $\bar{A}$'s are even larger than those in the W's. A conclusion we can draw here is that, when using incompatible features such as the $\bar{A}$'s and W's, we must carefully select the parameters so that the features have equal effects in making the N.N. decision.

Figures 5.12-5.15 are comparisons of error probabilities between cases where target aspect angles are either known or unknown. Figures 5.12-5.15 show, respectively, the results of using amplitude returns only, phase returns only, both amplitude and phase returns, and the time-domain algorithms. Note that if the aspect angles are known the maximum error is 4/5 = 80 percent, and if the aspect angle are unknown the maximum error is 14/15 = 93 percent. It is seen that knowledge of target aspect angles will decrease the errors.

Based on the above figures we can derive a list of minimum S/N values required for 10 percent or less error probabilities as shown in Table 5.7. This gives us a quantitative indication of the performance of each algorithm. From the table we note that, for N = 2, the 'A and W' algorithm requires the least S/N, followed by 'A' , 'TIME', and 'W', in increasing order. For N = 4, the required SNR are about the same for the 'A and W', 'A', and 'TIME' algorithms, while 'W' algorithms requires higher S/N. For N = 8, the minimum SNR required for each algorithm has the following order:

'TIME' < 'A' < 'A and W' < '$\bar{A}$ & W' ≈ 'W' < '$\bar{A}$'.

TABLE 5.7

MINIMUM S/N REQUIRED (in dB) FOR 10 PERCENT OR LESS CLASSIFICATION ERRORS. FOR EACH ALGORITHM (e.g., A&W) THERE ARE FOUR S/N VALUES (e.g., 19, 17, 13, 15) CORRESPONDING TO FOUR DIFFERENT CONDITIONS REGARDING ASPECT ANGLES AND THE NUMBER OF FREQUENCIES USED N.

	A	W	A&W	$\overline{A}$	$\overline{A}$&W	TIME
KNOWN ASP, N = 2	21	33	19	/	/	25
KNOWN ASP, N = 4	17	23	17	/	/	17
KNOWN ASP, N = 8	11	15	13	18	13	5
UNKNOWN ASP, N = 8	12	18	15	/	/	6

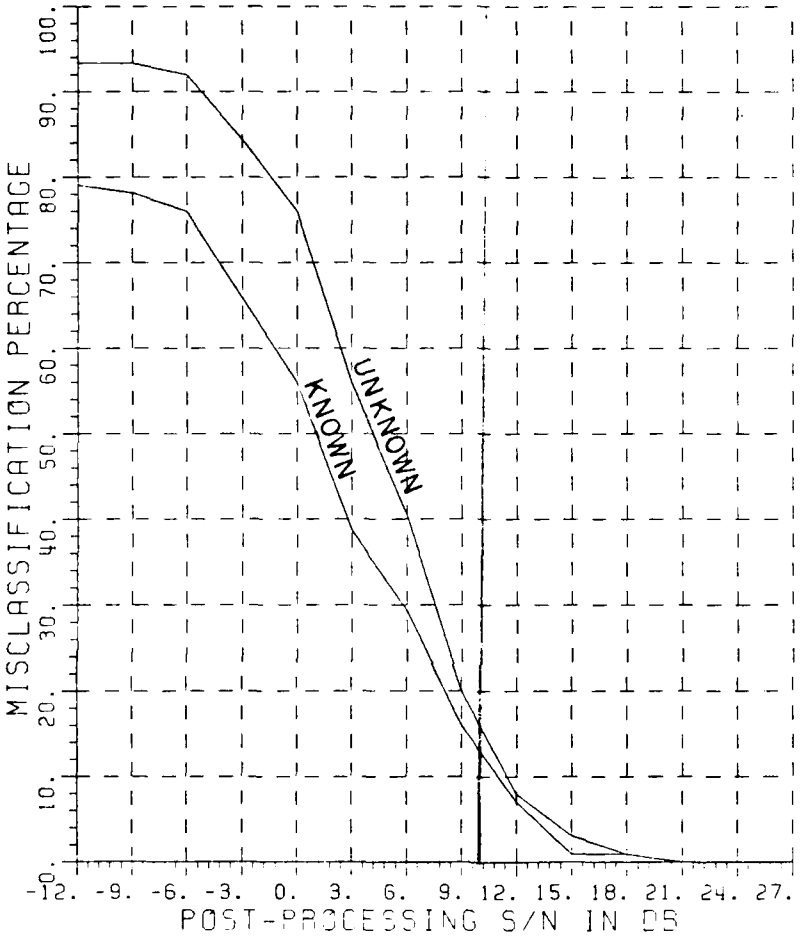

Figure 5.12. Comparison of error probability between the cases where aspect angles are either known or unknown. Only amplitude is used. N = 8 frequencies. A 90% confidence interval for a classification error of 30% is approximately ± 5% .

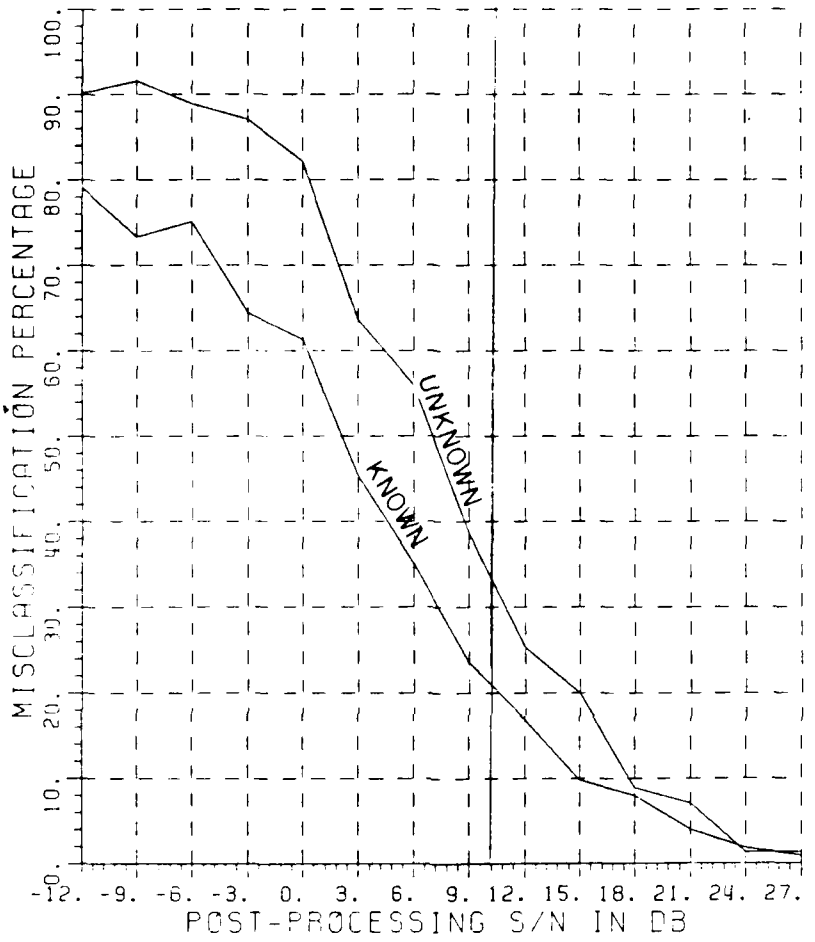

Figure 5.13. Comparison of error probabilities between the cases for known aspect angles and unknown aspect angles. Only phase is used. N = 8 frequencies. A 90% confidence interval for a classification error of 30% is approximately ± 5% .

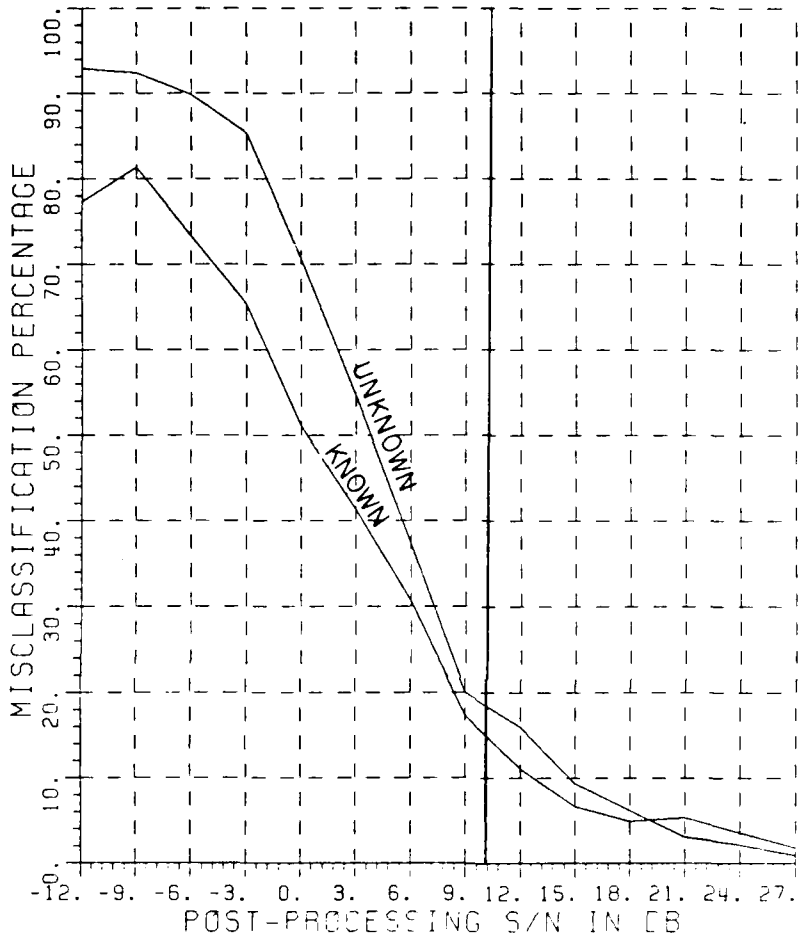

Figure 5.14. Error probabilities for "known aspect angles" and "unknown aspect angles". Both amplitude and phase are used. Number of frequencies = 8.
A 90% confidence interval for a classification error of 30% is approximately ± 5% .

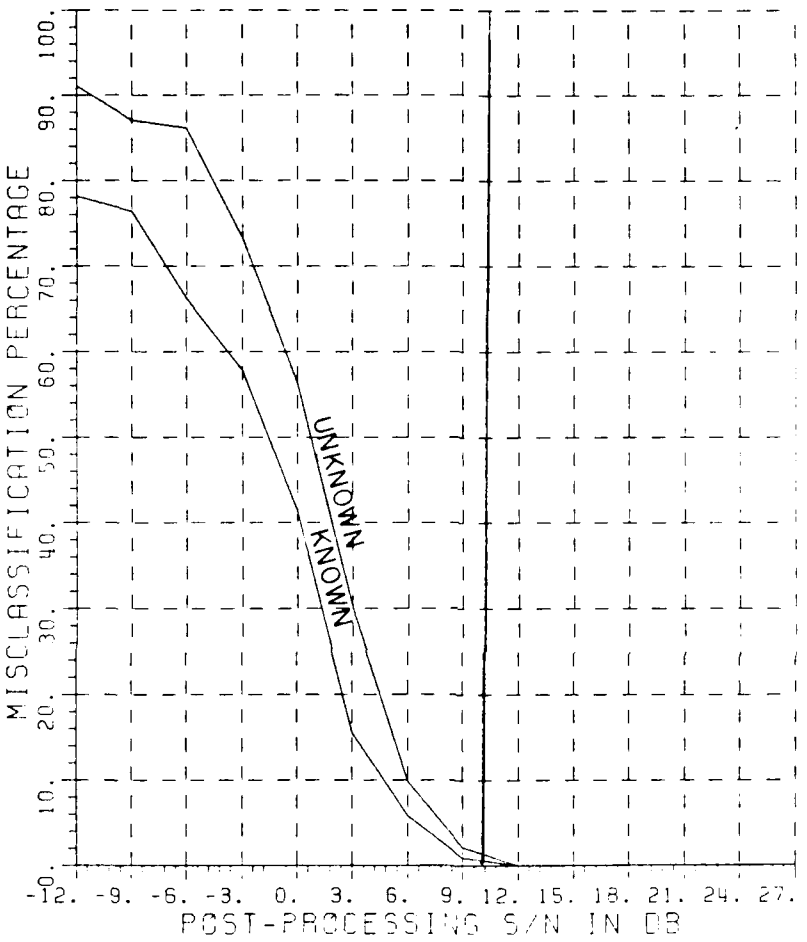

Figure 5.15. Error probabilities for the cases where the aspect angles are either known or unknown. Time-domain algorithm is used. Number of frequencies = 8. A 90% confidence interval for a classification error of 30% is approximately ± 5% .

The table also shows that increasing the number of frequencies will significantly decrease the required S/N. In particular there is a decrease of 20 dB for the 'TIME' algorithm if N is increased from 2 to 8. It can also be seen from the table that knowledge of the target aspect angle can reduce the required S/N by about 2 dB.

E. CLASSIFICATION OF AIRCRAFT

The type of experiments discussed in section D were applied to an aircraft data base consisting of 12 classes, as shown in Table 5.8 The aspect angles of the aircraft were chosen to be 0, 90, and 180 degrees so that classes in the data base are independent of each other. The aircraft have dimensions of the order of 50 meters, which, from Equation (5.27), implies that the frequency-sampling interval for the radar returns should satisfy

$$\Delta f < \frac{3 \times 10^8}{6 \times 50} = 1 \text{ MHz} \quad . \tag{5.32}$$

Based on the criterion in Equation (5.32) we choose the frequency-sampling interval Δf as 1 MHz. The frequency ranges were chosen as $7 \text{ MHZ} < f < 8 \text{ MHZ}$ for N = 2 frequencies, $7 \text{ MHZ} < f < 10 \text{ MHZ}$ for N = 4, and $7 \text{ MHZ} < f < 14 \text{ MHZ}$ for N = 8. The corresponding range of wavelengths for $7 \text{ MHZ} < f < 14 \text{ MHZ}$ is $21 \text{ m} < \lambda < 42 \text{ m}$, and the ratio of the aircraft dimensions versus the wavelength is of the order of

TABLE 5.8

A LIST OF AIRCRAFT USED IN THE CLASSIFICATION EXPERIMENT

CLASS	TARGET	ASPECT ANGLE
1	F	0
2	F	90
3	F	180
4	G	0
5	G	90
6	G	180
7	H	0
8	H	90
9	H	180
10	I	0
11	I	90
12	I	180

Elevation angle = 0

Polarization: Vertical

$$\frac{D}{\lambda} \approx 1$$

which means the radar returns are in the lower resonance region. The signal power of the radar returns may vary over a wide range. For the data base, the average signal power was estimated to be approximately equal to 28 dB-square-meters.

In this case the number of classes is 12, therefore the 90 percent confidence interval for the probability of misclassification P_E is slightly different from that of the ship classification where there were 15 classes. From Equation (5.25), with M = 12, n = 15, α = 0.1, ξ_α = 1.65, $\hat{P}_o \sim 0.3$, a 90 percent confidence interval for P_E is given by

$$\hat{P}_E \pm \xi_\alpha \sqrt{\frac{\hat{p}_o(1-\hat{p}_o)}{Mn}}$$

$$= \hat{P}_E \pm 1.65 \sqrt{\frac{0.3(1-0.3)}{12x15}}$$

$$= \hat{P}_E \pm 5.6 \text{ percent}$$

Figures 5.16-5.19 are plots of error probabilities for various classification algorithms with the number of frequencies N as a parameter. In all four figures we assume that target aspect angles are known a priori, and the number of frequencies N is set to 2, 4, and 8. It can be seen that the error probabilities can be improved significantly by increasing the number of frequencies. This is especially true for the time-domain algorithms.

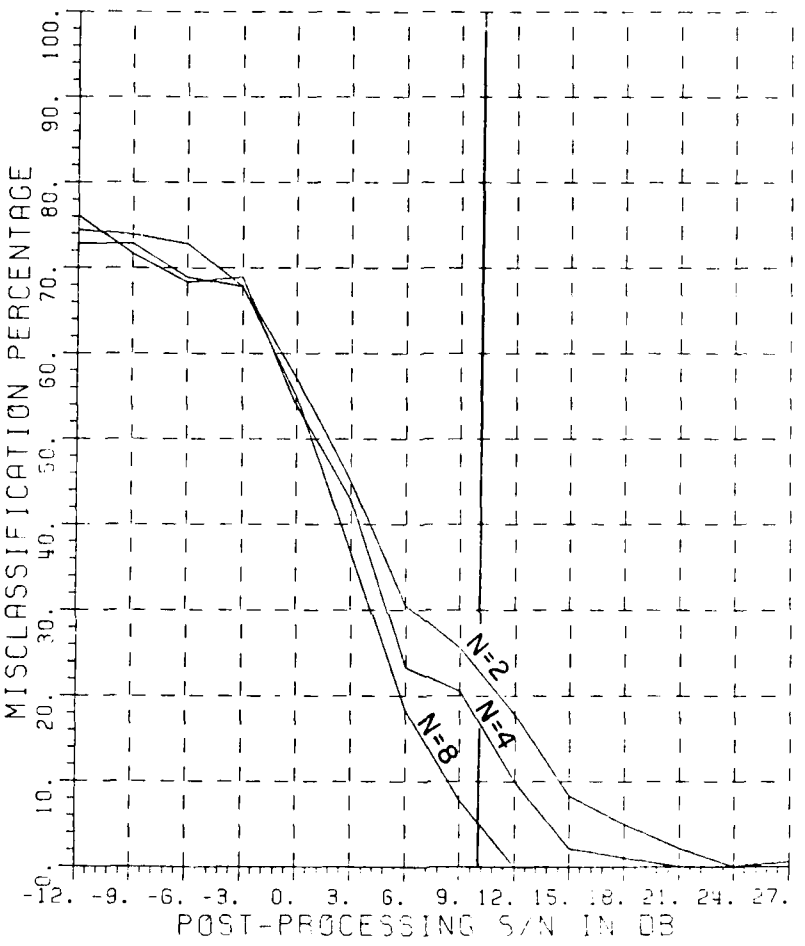

Figure 5.16. Error probabilities for N=2,4,8 frequencies. Only amplitude data are used. The aspect angles are assumed known. A 90% confidence interval for 30% classification error is approximately ± 5.6% .

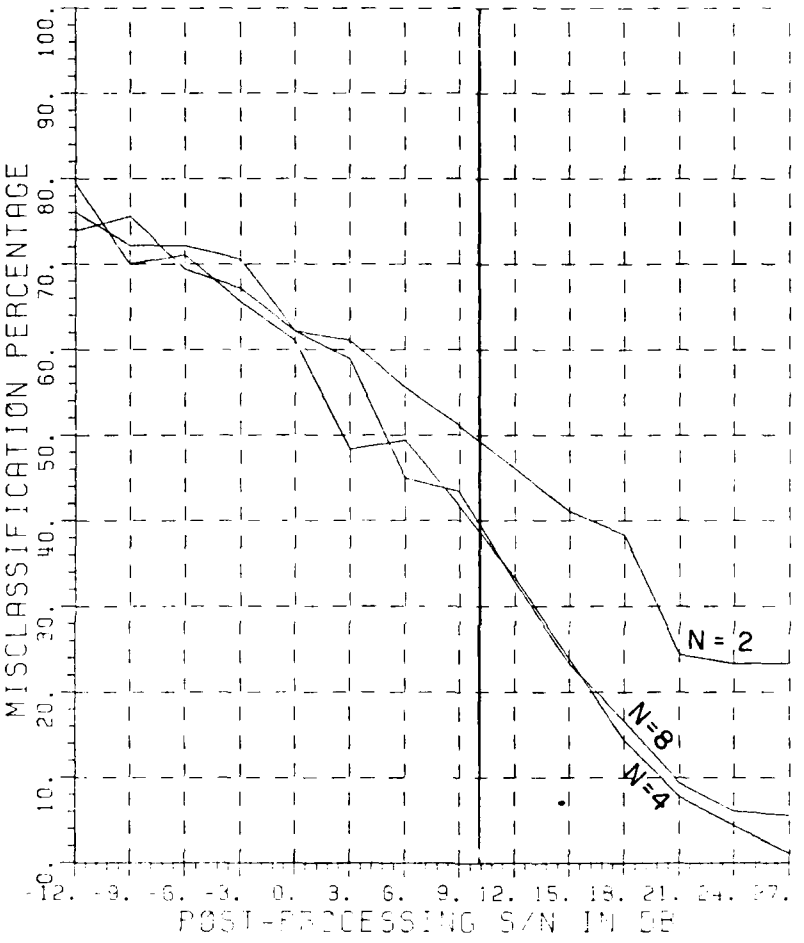

Figure 5.17. Error probabilities for N=2,4,8 frequencies. Only phase data are used. The aspect angles are assumed known. A 90% confidence interval for 30% classification error is approximately ± 5.6% .

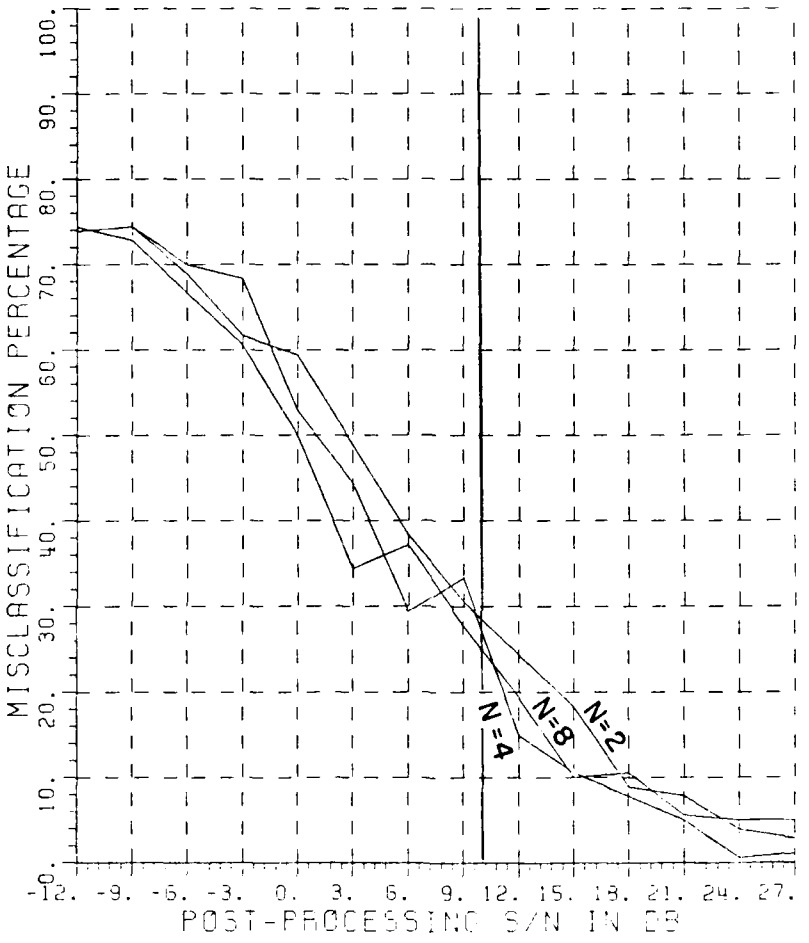

Figure 5.18. Error probabilities for N=2,4,8 frequencies. Both amplitude and phase data are used. The aspect angles are assumed known. A 90% confidence interval for 30% classification error is approximately ± 5.6% .

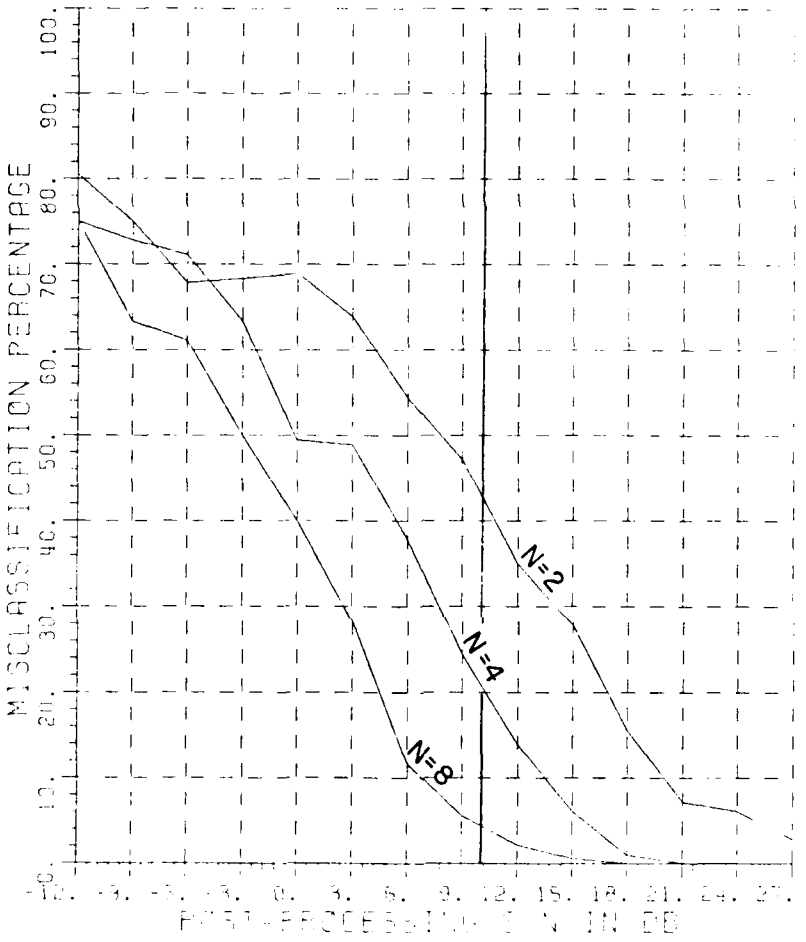

Figure 5.19. Error probabilities for N=2,4,8 frequencies. The time-domain algorithm is used. The aspect angles are assumed known. A 90% confidence interval for 30% classification error is approximately ± 5.6% .

Figures 5.20-5.22 show the effects of employing different types of classification algorithms. In all three figures we assume that target aspect angles are known. The number of frequencies N used in each figures are N = 8 in Figure 5.20, N = 4 in Figure 5.21, and N = 2 in Figure 5.22. It can be seen that the performance of the 'TIME' algorithms becomes better than the others as the number of frequencies N is increased. As is the case in ship classifications, the error in the phase feature, W, dominates the N.N. decision.

Figure 5.23 shows the error probabilities when relative amplitudes, $\overline{A}$, are employed. As is the case for the W's, the error in the relative amplitudes dominates the decisions.

Figures 5.24-5.27 are comparisons of error probabilities between the cases where target aspect angles are either known or unknown. Figures 5.24-5.27 show, respectively, the results of using amplitude returns only, phase returns only, both amplitude and phase returns, and the time-domain algorithms. Note if the aspect angle of the unknown target is known a priori, the maximum error is 4/5 = 80 percent, and if the aspect angle is unknown the maximum error is 11/12 = 92 percent. It is seen that knowledge of the target aspect angle will improve the results.

Based on the above figures we can derive a list of minimum signal-to-noise power ratios (S/N) required for less than 10 percent error probabilities as shown in Table 5.9. This gives us a quantitative indication of the performance of each algorithm. From the table we note

that, for N = 2, the minimum S/N required for each algorithm has the following order.

'A' < 'A&W' < 'TIME' < 'W'

For N = 4, the order is given as follows.

'A' < 'TIME' < 'A&W' < 'W'

And for N = 8 the order is given as follows.

'TIME' < 'A' < 'A&W' < 'W' ≈ '$\overline{A}$&W' ≈ '$\overline{A}$'

The table also shows that increasing the number of frequencies will significantly decrease the required S/N. It can also be seen from the table that knowledge of target aspect angles can reduce the required S/N by about 4 dB.

TABLE 5.9

MINIMUM S/N REQUIRED (in dB) FOR 10 PERCENT OR LESS CLASSIFICATION ERRORS. FOR EACH ALGORITHM (e.g., 'A&W') THERE ARE FOUR S/N VALUES (e.g., 18, 16, 15, 21) CORRESPONDING TO FOUR DIFFERENT CONDITIONS REGARDING TARGET ASPECT ANGLES AND THE NUMBER OF FREQUENCIES USED N.

	A	W	A&W	$\overline{A}$	$\overline{A}$&W	TIME
KNOWN ASP, N = 2	14	40	18	/	/	20
KNOWN ASP, N = 4	12	20	16	/	/	14
KNOWN ASP, N = 8	8	21	15	21	21	7
UNKNOWN ASP, N = 8	11	23	21	/	/	11

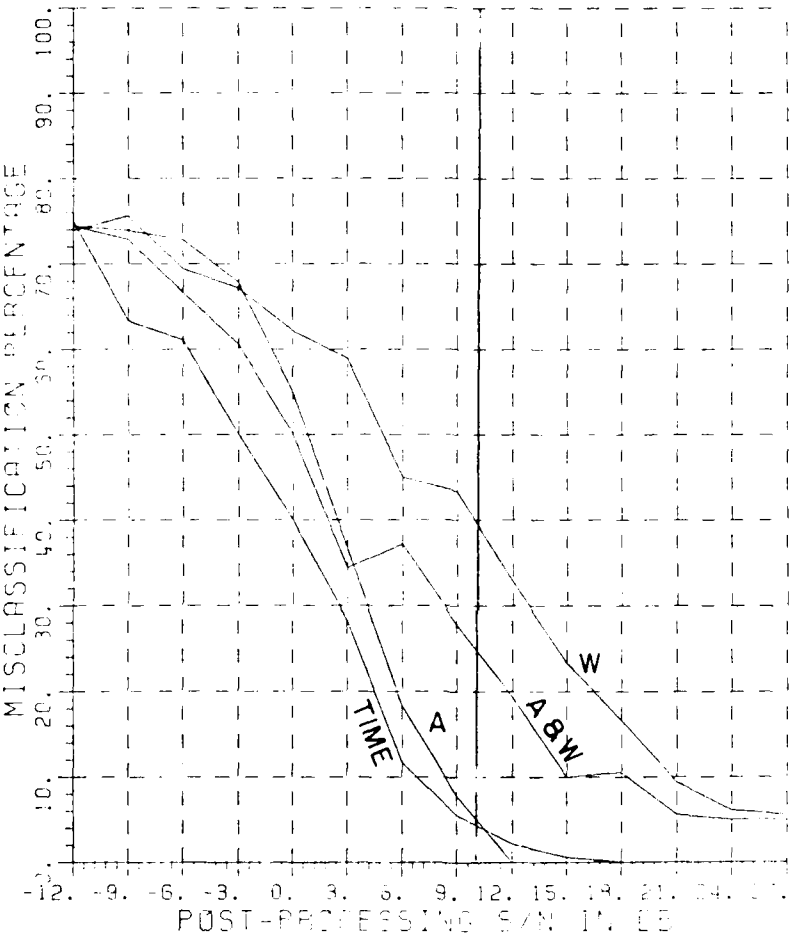

Figure 5.20. Error probabilities for four algorithms. Number of frequencies = 8, and the aspect angles are known. A 90% confidence interval for 30% classification error is approximately ± 5.6% .

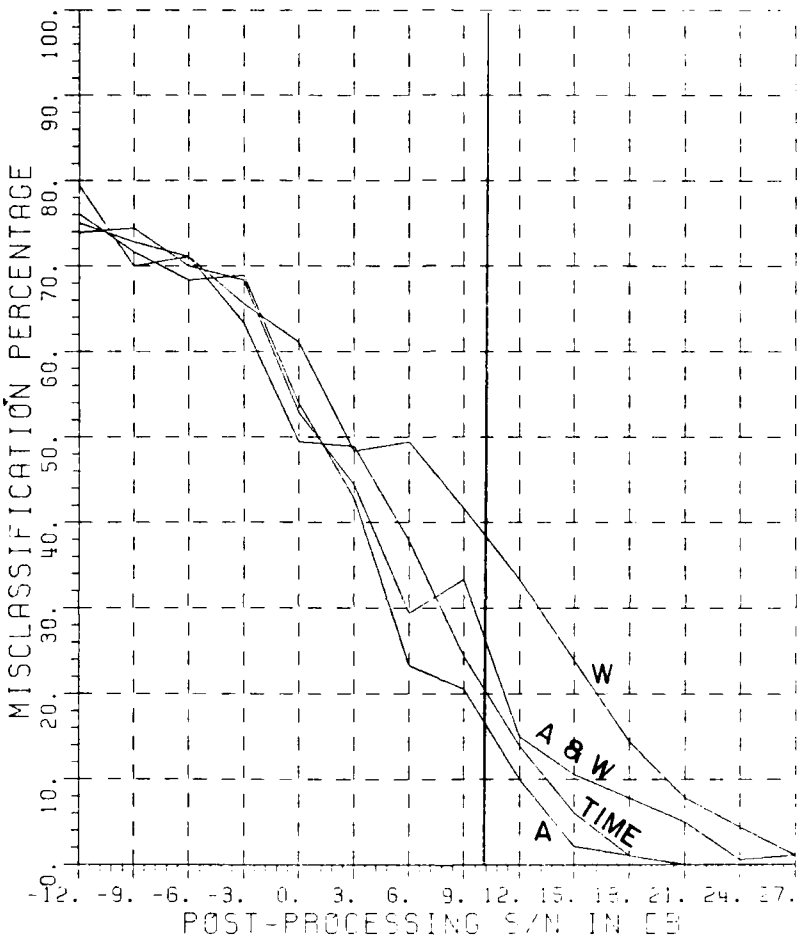

Figure 5.21. Error probabilities for four algorithms. Number of frequencies = 4, and the aspect angles are known. A 90% confidence interval for 30% classification error is approximately ± 5.6% .

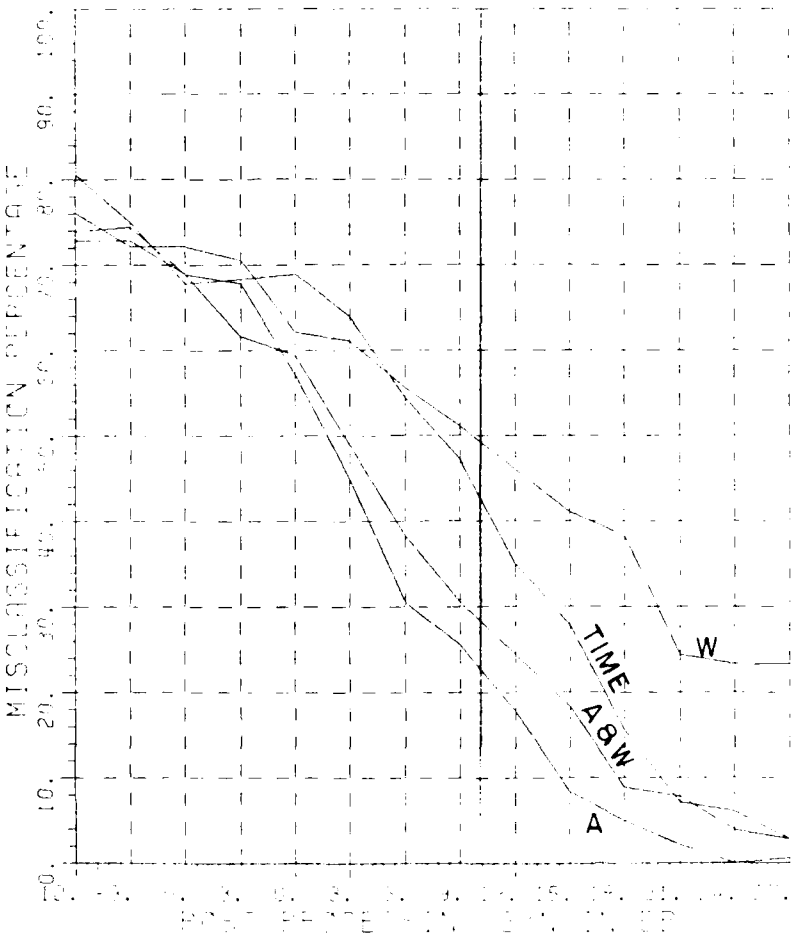

Figure 5.22. Error probabilities for four algorithms. Number of frequencies = 2, and the aspect angles are known. A 90% confidence interval for 30% classification error is approximately ± 5.6% .

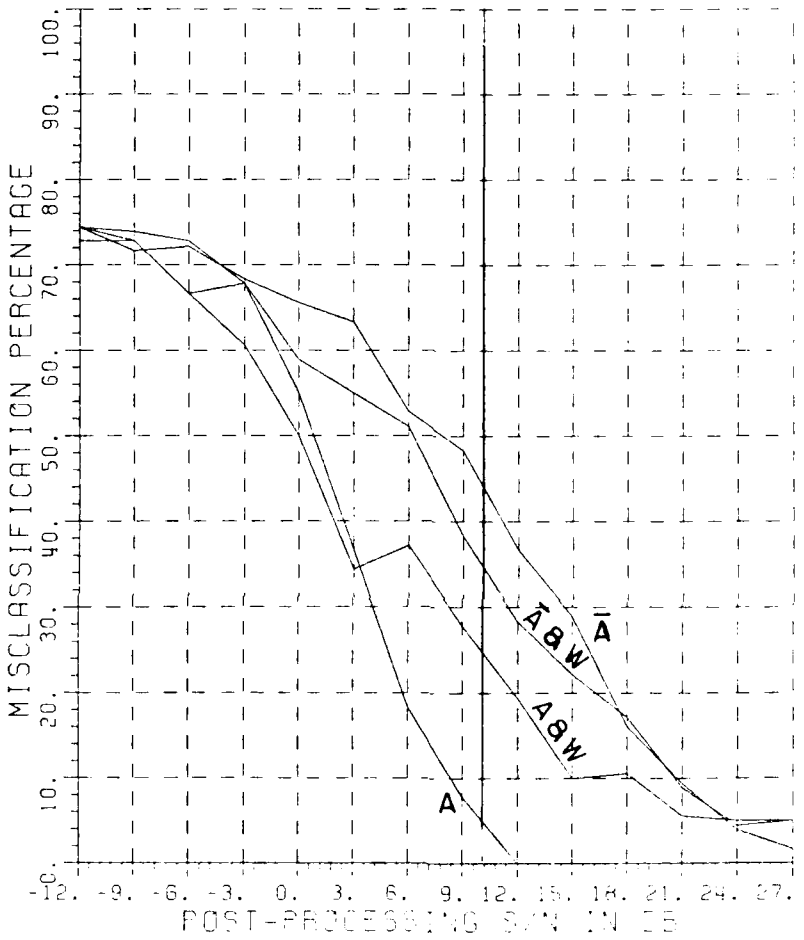

Figure 5.23. Error probabilities for four algorithms. Number of frequencies = 8, and the aspect angles are known. A 90% confidence interval for 30% classification error is approximately ± 5.6% .

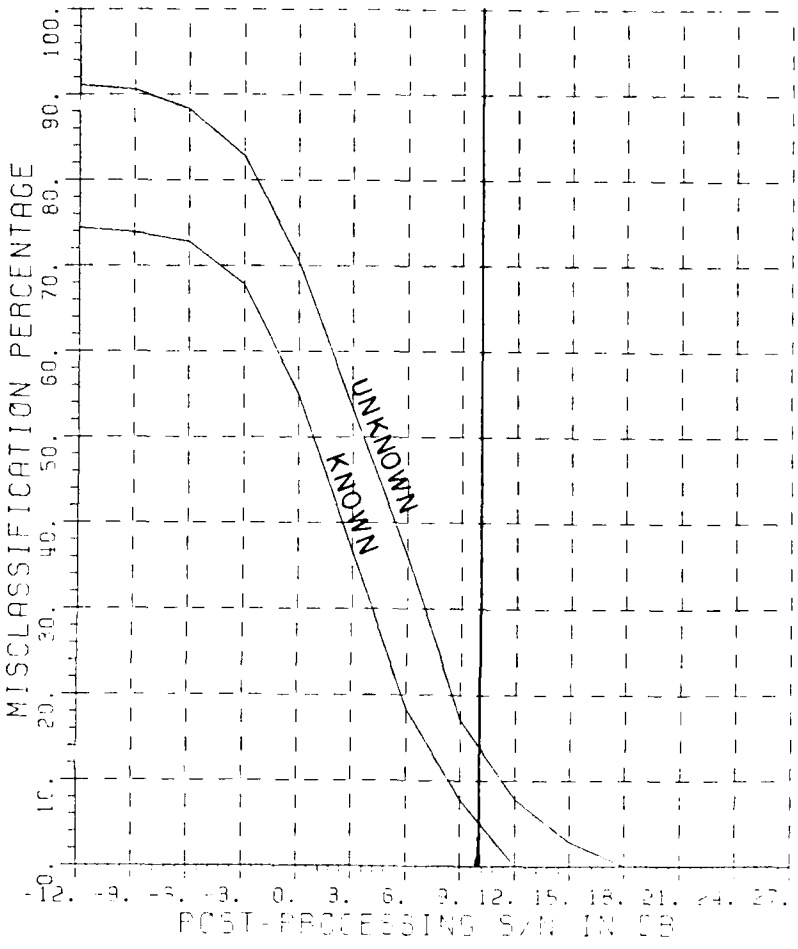

Figure 5.24. Comparison of error probabilities between the cases where aspect angles are known or unknown. Only amplitude data are used, and number of frequencies = 8. A 90% confidence interval for 30% classification error is approximately ± 5.6% .

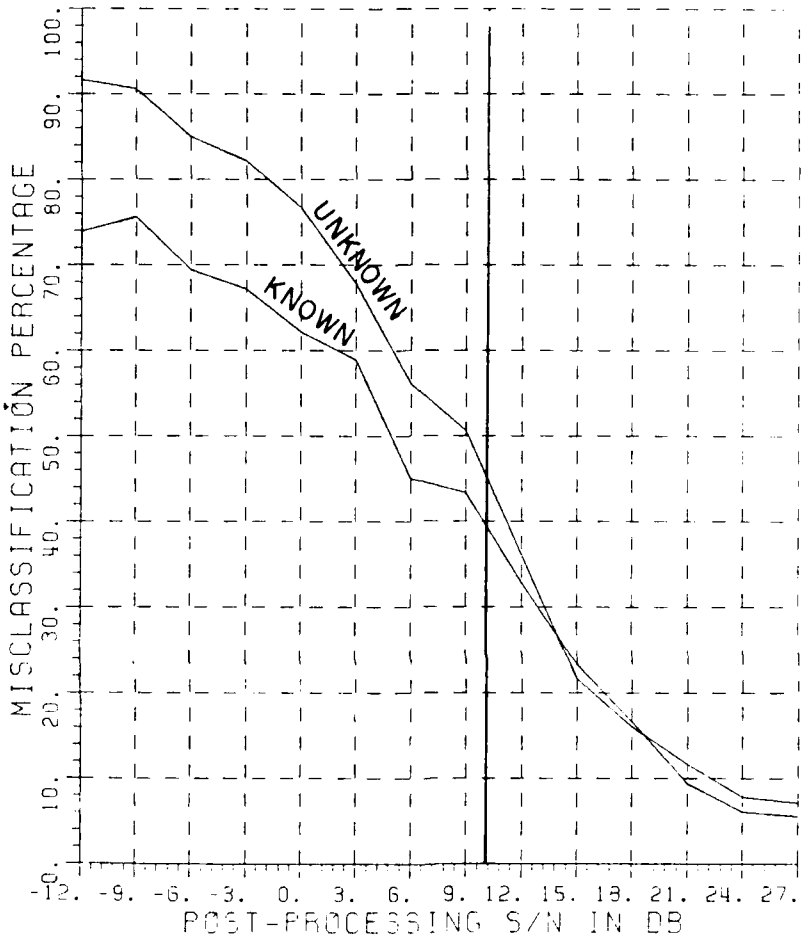

Figure 5.25. Comparison of error probabilities between the cases where aspect angles are known or unknown. Only phase data are used, and number of frequencies = 8. A 90% confidence interval for 30% classification error is approximately ± 5.6% .

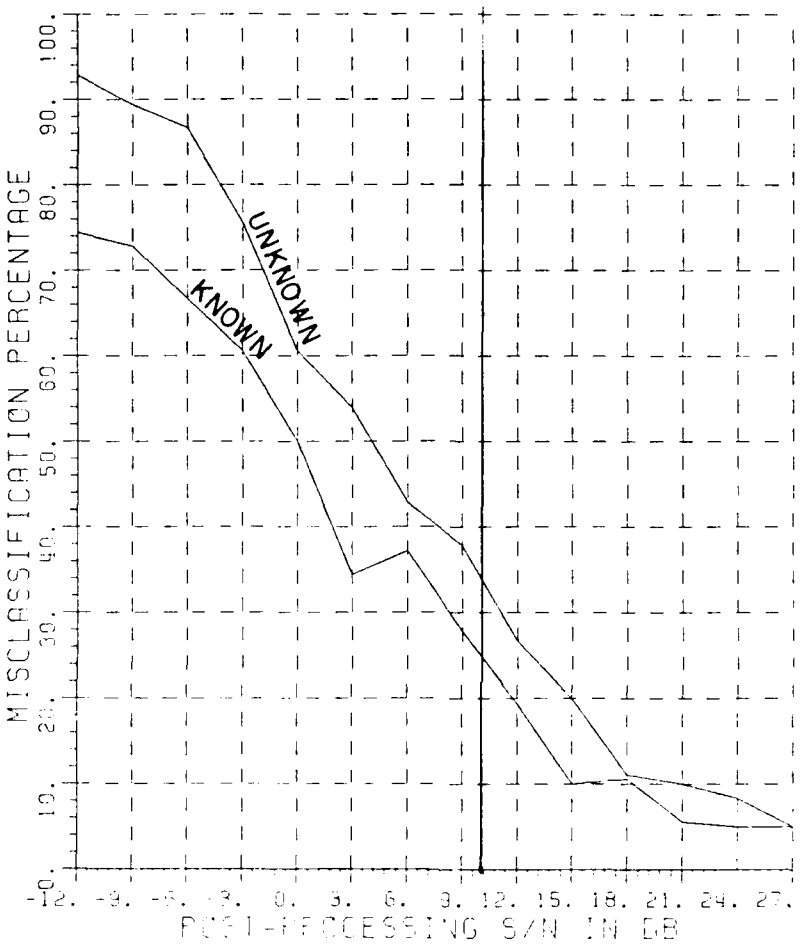

Figure 5.26. Comparison of error probabilities between the cases where aspect angles are known or unknown. Both amplitude and phase data are used, and number of frequencies = 8. A 90% confidence interval for 30% classification error is approximately ± 5.6% .

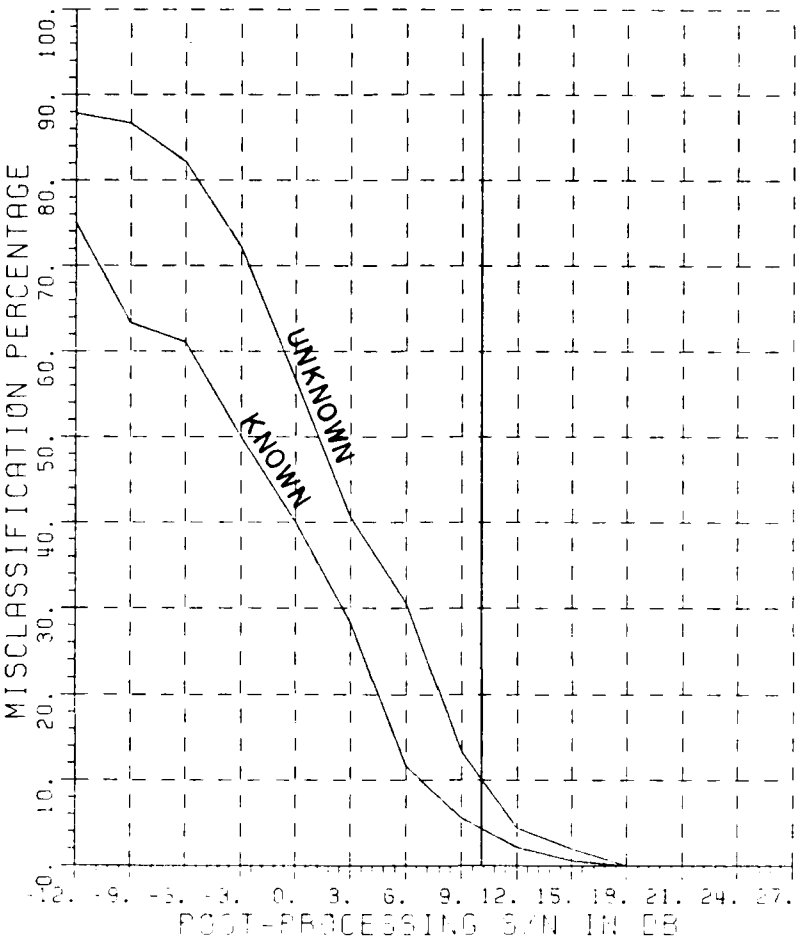

Figure 5.27. Comparison of error probabilities between the cases where aspect angles are known or unknown. The time-domain algorithm are used, and number of frequencies = 8. A 90% confidence interval for 30% classification error is approximately ± 5.6% .

CHAPTER VI

CONCLUSIONS AND RECOMMENDATIONS

H.F. radars can detect targets at over-the-horizon distances, but their performance is dominated by ionospheric conditions and sea states. As a result, H.F. radar returns are usually accompanied by a large amount of variability, and must be extensively processed. One reliable processing technique is to calibrate the radar return with respect to a reference. For the calibration of amplitude returns, we can choose sea scatter as a reference whose radar cross section can either be predicted or measured by other means. We derived an equation which approximately described the relation between the coherent observation time and the post-processing signal-to-noise power ratio (SNR). This equation showed that we can obtain an SNR of 10 dB for a coherent observation time of 16 minutes. Higher SNR can be obtained for longer coherent observation time. The measurement of the phase of the target returns requires an elaborate processing scheme because the phase path length may vary over a wide range, resulting in ramp-type phase errors as a function of frequency.

Because of the errors, the phase of the measured target returns in most cases cannot be directly chosen as a set of features for classification. Instead we derived a variable W from the phase, and showed that

the W's were independent of wave path length and therefore, did not require a phase reference. The amplitude of the RCS and a set of normalized W's formed a feature set for the frequency-domain Nearest-Neighbor classification. The Nearest-Neighbor decision rule assigned a target to a class whose distance from the target was the smallest among all classes in the data base. Time-domain data were obtained by taking the Discrete Inverse Fourier Transform (DIFT) of the multi-frequency measurements of the target returns. The DIFT converted the ramp-type phase errors to shifts of waveforms along the time axis. By choosing the maximum value of a cross-correlation function of two waveforms, we essentially eliminated the difference in time-shifts between the waveforms. The time-domain decision rule assigned a target to a class whose maximum cross-correlation with the target was the largest among all classes in the data base.

A set of radar backscatter measurements of scale models of ships and aircraft was used to generate a data base for testing the target classification algorithms. The measurements were conducted in an anechoic chamber at certain scaled frequency ranges, e.g., 1-2GHZ, 2-4GHZ, 4-8GHZ, or 8-12GHZ. Connecting some of these frequency bands, and removing possible phase offsets, we obtained a number of data files of wider frequency ranges. The resulting data files were convolved with a Hamming window to remove clutter present in the waveforms, and, at the same time, estimate the values of the data at selected frequencies. The Hamming window was equivalent to a time-domain low-pass filter with

a properly-designed time-width, and its center coincided with the target's center so that it effectively removed clutter returns located outside the target zone. The filtered results were scaled according to scale factors for each target and a full-scale data base was generated.

The testings of the classification algorithms made use of the computed full-scale data base, and were conducted using FORTRAN programs on a DEC VAX computer. By adding Gaussian noise to each class in the data base, we created a set of test target data upon which the classification algorithms were applied. The classification experiments were repeated several times, and, based on the results, a Maximum Likelihood Estimator (MLE) was applied to estimate the probabilities of misclassification. We constructed two data bases for testings of both ship and aircraft classification techniques. The former consisted of 15 independent classes, corresponding to 5 ships at 0, 90, and 180 degrees aspect angles, and the latter consisted of 12 classes corresponding to 4 aircraft at 0, 90 and 180 degrees aspect angles. The frequency ranges were chosen as 1.7 MHz $<$ f $<$ 4.5 MHz for the ships, and 7 MHz $<$ f $<$ 14 MHz aircraft so that the ratios of the target dimensions to the wavelengths were of the order of 1, which implied that the radar frequencies were located in the lower Resonance region. Based on the Shannon's sampling theorem, the frequency increments were selected as 1 MHz for the ships and 0.5 MHZ for the aircraft. The aspect angles were assumed known for most experiments in order to obtain lower errors. We compared the mis-

classification percentages as a function of post-processing signal-to-noise power ratio (SNR) with respect to the following cases.

1. Use of 2, 4, or 8 frequencies.
2. Use of different classification algorithms including the frequency-domain and the time-domain algorithms.
3. Target aspect angles are known or unknown a priori.

From the results of case 1 we found that increasing the number of frequencies would significantly decrease the error probabilities, especially for the time-domain curves. From the results of case 2, we found that for, a small number of frequencies the ' amplitude only ' algorithm had the lowest error probabilities, while, for high number of frequencies, the 'time-domain' algorithm had the lowest error probabilities. The results showed that for an SNR of greater than 10 dB, which means that the noise power is about 10% of the signal power, it would be possible to obtain a misclassification error of less than 10%. The 'W' and the 'relative amplitude' algorithms had the highest misclassification errors. It was noted that, when two incompatible features such as 'amplitude and W' or 'relative amplitude and W' were to be used together, they should be properly weighted in order to get better results. From the results of case 3 we found that a priori knowledge of the aspect angle would decrease the error probabilities, and not by as much as an increase in the number of frequencies.

This study shows that classifications of targets at over-the-horizon distances by processing H.F. radar returns is feasible. For a reasonable coherent observation time such as 16 minutes or longer, we can obtain an SNR of about 10 dB or higher, which, according to our experimental results, supports the possibility that we can classify the targets with less than 10 percent errors. We conclude that classification of targets using HF radars is feasible.

It is recommended that future work be focused on five areas. First of all, in order to minimize the probability of misclassification it is recommended that optimum normalization constants for both the phase features W and the relative-amplitude features $\overline{A}$ be found. An optimum range of frequencies which minimizes the probabilities of misclassification should also be found. Secondly, a larger data base should be established. Even though the above data base served to indicate classifiability, it was not large enough to draw adequate statistical conclusions on the expected probabilities of misclassification. Thirdly, uncataloged targets should be considered. Fourthly, since previous efforts to classify targets were based upon a set of data obtained from measurements of scaled model targets. It is recommended that data obtained from full-scale OTH radar systems be used to test the classification algorithms developed here, and to provide insight into new approaches for classification. And lastly, methods for measuring more accurately the phase and amplitude of the target returns

should be developed since the accuracy is directly related to the probability of misclassification.

REFERENCES

[1] M.I. Skolnik, Introduction to Radar Systems, McGraw-Hill, New York, 1980.

[2] J.M. Headrick and M.I. Skolnik, "Over-the-Horizon Radar in the HF Band," PROC. IEEE, Vol. 62, pp. 664-673, No. 6, June 1974.

[3] E.M. Kennaugh and D.L. Moffatt, "Transient and Impulse Response Approximations," PROC. IEEE, Vol. 53, pp. 893-901, Aug. 1965.

[4] D.L. Moffatt, "Interpretation and Application of Transient and Impulse Response Approximations in Electromagnetic Scattering Problems," Report 2415-1, Dept. of Electrical Engineering, The Ohio State University, ElectroScience Lab., Columbus, Ohio, March 1968.

[5] A.A. Ksienski, Y.T. Lin, and L.J. White, "Low-Frequency Approach to Target Identification," Proc. IEEE, Vol. 63, pp. 1651-1660, December, 1975.

[6] D.L. Moffatt and R.K. Mains, "Detection and Discrimination of Radar Targets," IEEE Trans. Antennas Propagat., Vol. AP-23, pp. 358-367, May 1975.

[7] C.W. Chuang and D.L. Moffatt, "Natural Resonances of Radar Targets Via Prony's Method and Target Discrimination," IEEE Trans., Vol. AES-12, pp. 583-589, November, 1976.

[8] Y.T. Lin and A.A. Ksienski, "Identificatin of Complex Geometrical Shapes by Means of Low-Frequency Radar Returns," The Radio and Electronic Engineer, Vol. 46, No. 10, pp. 472-486, October 1976.

[9] D.L. Moffatt, J.D. Young, A.A. Ksienski, H.C. Lin, and C.M. Rhoads, "Transient Response Characteristics in Identification and Imaging," IEEE Trans. Antennas Propagat., Vol. AP-29, No. 2, March, 1981.

[10] H. Lin and A.A. Ksienski, "Optimum Frequencies for Aircraft Classification," IEEE Trans. Aerospace and Electron. Sys., Vol. AES-17, No. 5, September, 1981.

[11] J.D. Young, "Radar Imaging from Ramp Response Signatures," IEEE Trans. Antennas Propagat., Vol. AP-24, No. 3, May, 1976.

[12] K.A. Shubert, J.D. Young, and D.L. Moffatt, "Synthetic Radar Imagery," IEEE Trans. Antennas Propagat., Vol. AP-25, No. 4, July, 1977.

[13] E.K. Walton and J.D. Young, "Surface Ship Target Classification Using HF Multifrequency Radar," Final Report 712352-1, The Ohio State University ElectroScience Lab., Columbus, Ohio, May, 1980.

[14] G.H. Millman and G.R. Nelson, "Surface Wave HF Radar for Over-the-Horizon Detection," IEEE International Radar Conference, CH1493-6/80/0000-0106, 1980.

[15] K. Davis, Ionospheric Radio Propagation, National Bureau of Standards Monograph 80, Washington, D.C., 1965.

[16] E. Navon and H. Cory, "The Determination of Sky-Wave Received Signal Level," IEEE Trans. Antennas Propagat., Vol. AP-26, No. 5, September, 1978.

[17] D.E. Barrick, "Theory of HF and VHF Propagation Across the Rough Sea, 2, Application to HF and VHF Propagation Above the Sea," Radio Science, Vol. 6, pp. 527-533, May, 1971.

[18] D.B. Trizna, "Estimation of the Sea Surface Radar Cross Section at HF from Second-Order Doppler Spectrum Characteristics," Naval Research Laboratory, Report 8579, May, 1982.

[19] W.B. Goggins, P. Blacksmith, and G.J. Sletten, "Phase Signature Radars," IEEE Trans. Antennas Propagat., Vol. AP-22, No. 6, November, 1974.

[20] D.E. Barrick and J.B. Snider, "The Statistics of HF Sea-Echo Doppler Spectra," IEEE Trans. Antennas Propagat., Vol. AP-25, January, 1977.

[21] R.O. Duda and P.E. Hart, Pattern Classification and Scene Analysis, John Wiley and Sons, New York, 1973.

[22] H.L. Van Trees, Detection, Estimation, and Modulation Theory, Part I, John Wiley & Sons, New York, 1968.

[23] H.C. Lin, "Identification of Catalogued and Uncatalogued Classes," Ph.D. Dissertation, The Ohio State University, December, 1978.

[24] P.G. Hoel, S.C. Port, and C.J. Stone, Introduction to Statistical Theory, Houghton Mifflin, Boston, 1981.

[25] D.D. Crombie, "Doppler Spectrum at Sea Echo at 13.56 Mc./s," Nature, No. 4459, Vol. 175, pp. 681-682, April, 1955.

[26]. M.I. Skolnik, Radar Handbook, McGraw-Hill, New York, 1970.

[27] D.E. Barrick, "First-Order Theory and Analysis of MF/HF/VHF Scatter from the Sea," IEEE Trans. Antennas Propagat., Vol. AP-20, pp. 2-10, January, 1972.

[28] D.B. Trizna, J.C. Moore, J.M. Headrick, R.W. Bogle, "Directional Sea Spectrum Determination Using HF Doppler Radar Techniques," IEEE Trans. Antennas Propagat., Vol. AP-25, No. 1, January, 1977.

[29] C.C. Teague, G.L. Tyler, and R.H. Stewart, "Studies of the Sea Using HF Radio Scatter," IEEE Trans. Antennas Propagat., Vol. AP-25, No. 1, January, 1977.

[30] J.W. Maresca, Jr., and J.R. Barnum, "Theoretical Limitation of the Sea on the Detection of Low Doppler Targets by Over-the-Horizon Radar," IEEE Trans. on Antennas Propagat., Vol. AP-30, No. 5, September, 1982.

[31] A. Papoulis, Probability, Random Variables, and Stochastic Processes, McGraw-Hill , New York, 1965.

[32] L.R. Rabiner and B. Gold, Theory and Application of Digital Signal Processing, Prentice-Hall, Englewood Cliffs, New Jersey, 1975.

[33] D.A.S. Fraser, Non-Parametric Methods in Statistics, John Wiley and Sons, New York, 1957.

[34] A.V. Oppenheim and R.W. Schafer, Digital Signal Processing, Prentice-Hall, Englewood Cliffs, New Jersey, 1975.

[35] A. Papoulis, Signal Analysis, McGraw-Hill, New York, 1977.

[36] P.L. Meyer, Introductory Probability and Statistical Applications, Addison-Wesley, Reading, Mass., 1970.

APPENDIX A

This appendix contains plots of amplitude and phase of the processed radar returns of five ships and four aircrafts. The aspect angles are 0, 90, and 180 degrees.

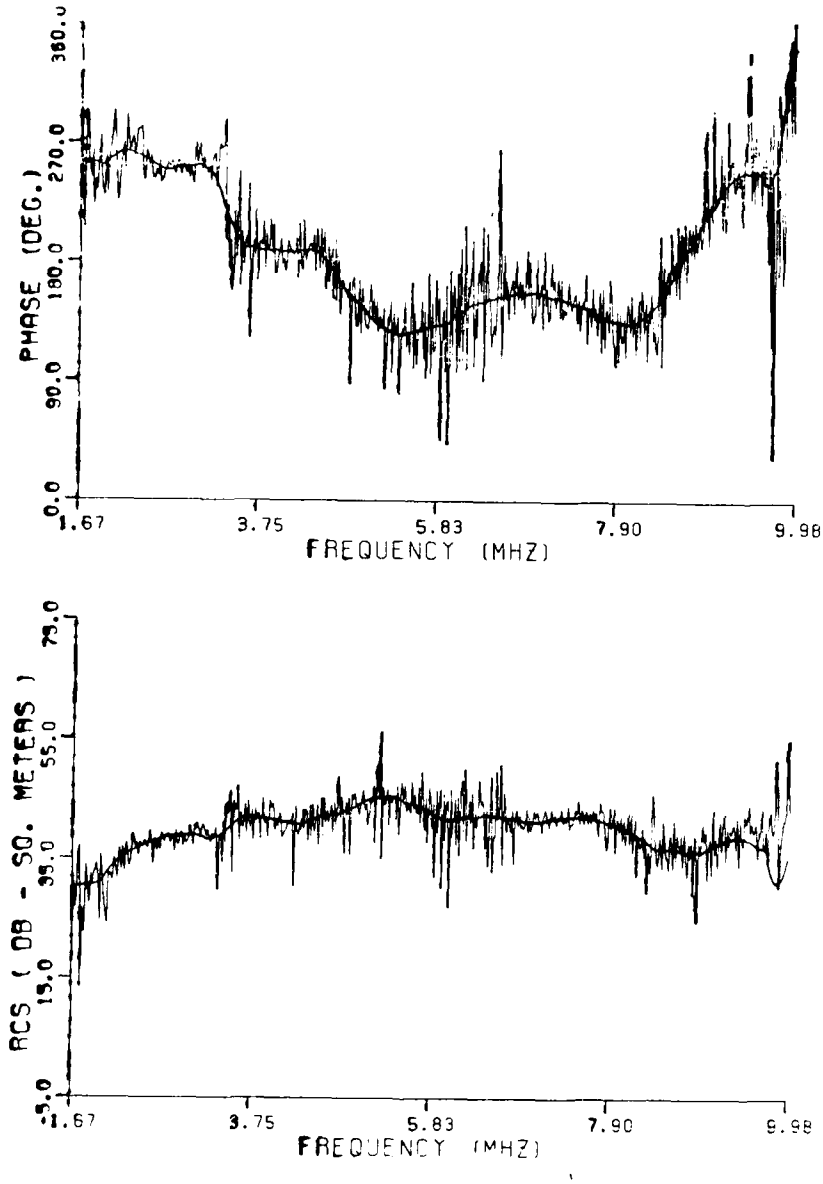

Figure A.1. Ship A at 0 degrees.

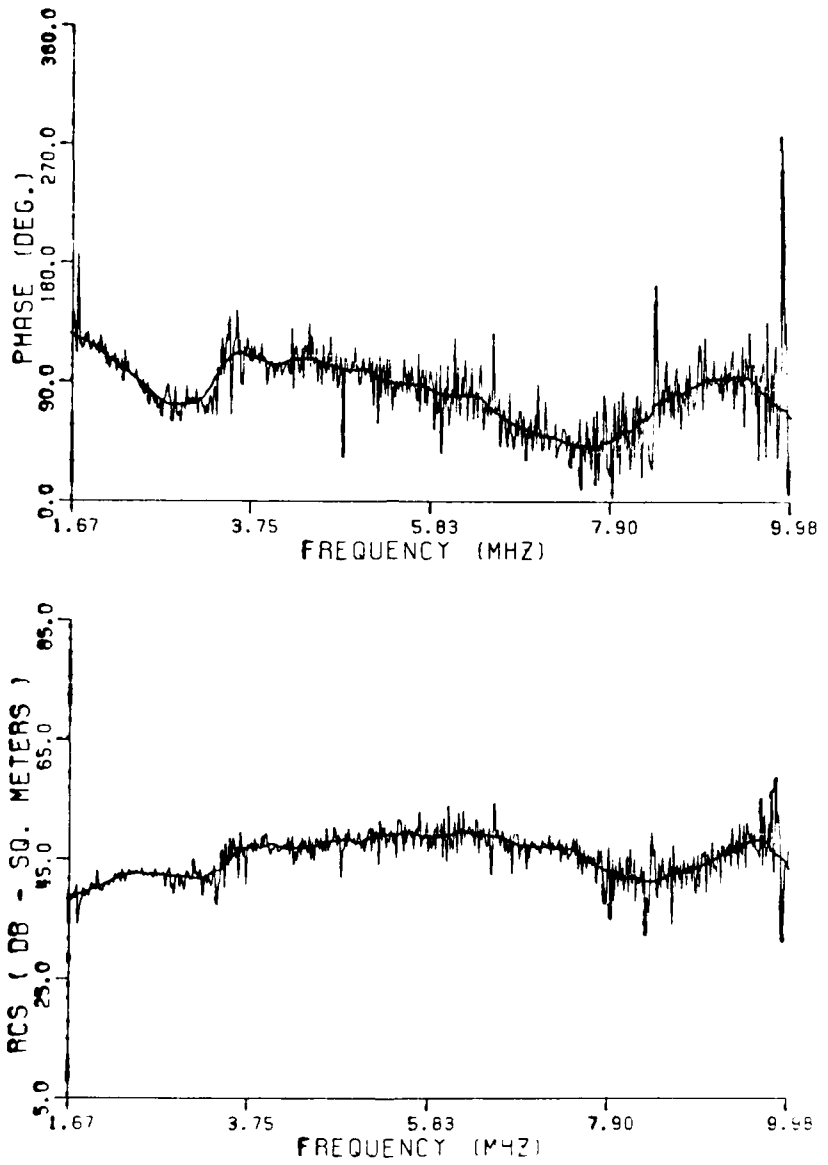

Figure A.2. Ship A at 90 degrees.

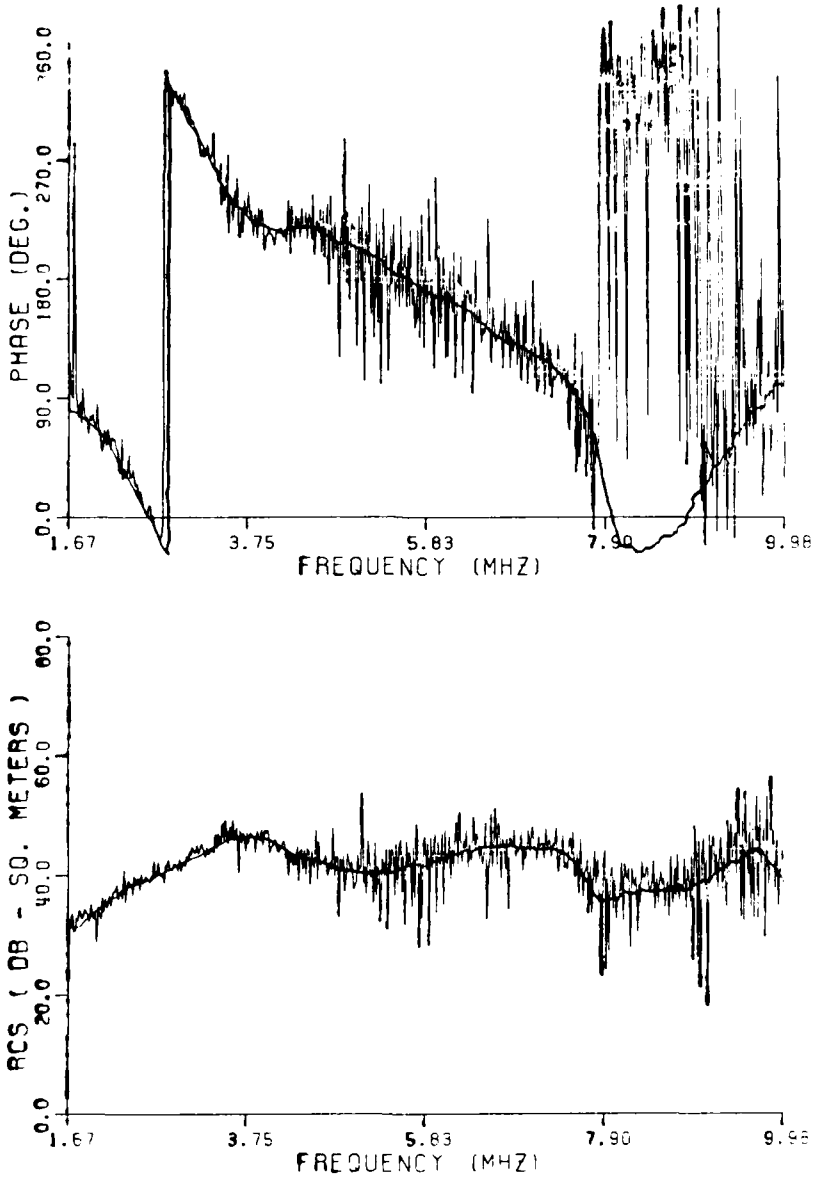

Figure A.3. Ship A at 180 degrees.

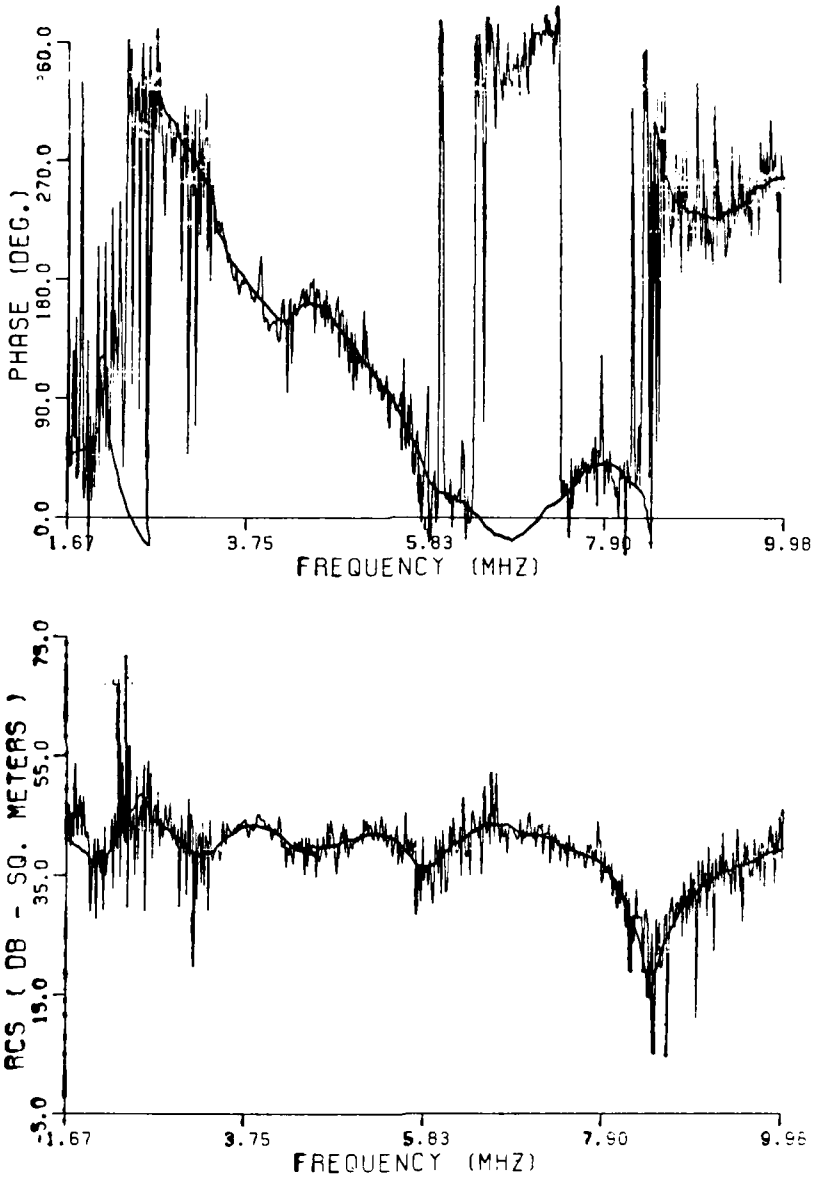

Figure A.4. Ship B at 0 degrees.

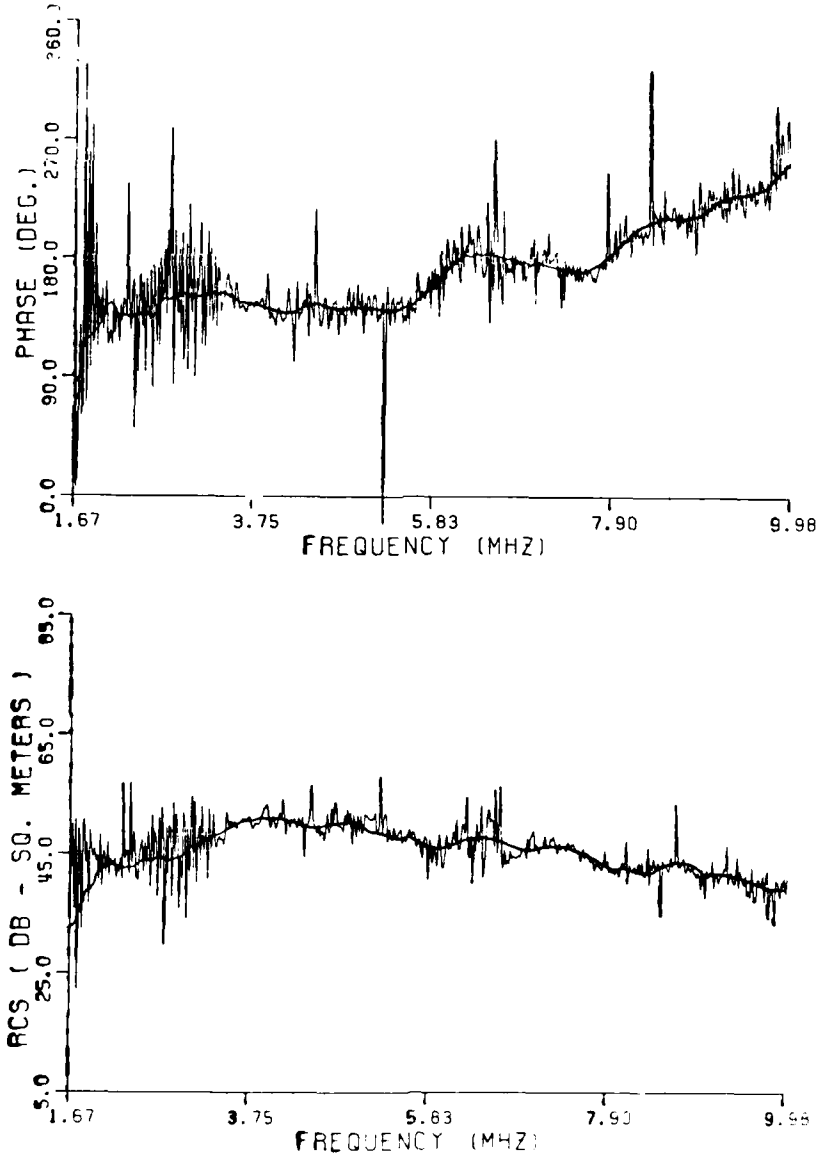

Figure A.5. Ship B at 90 degrees.

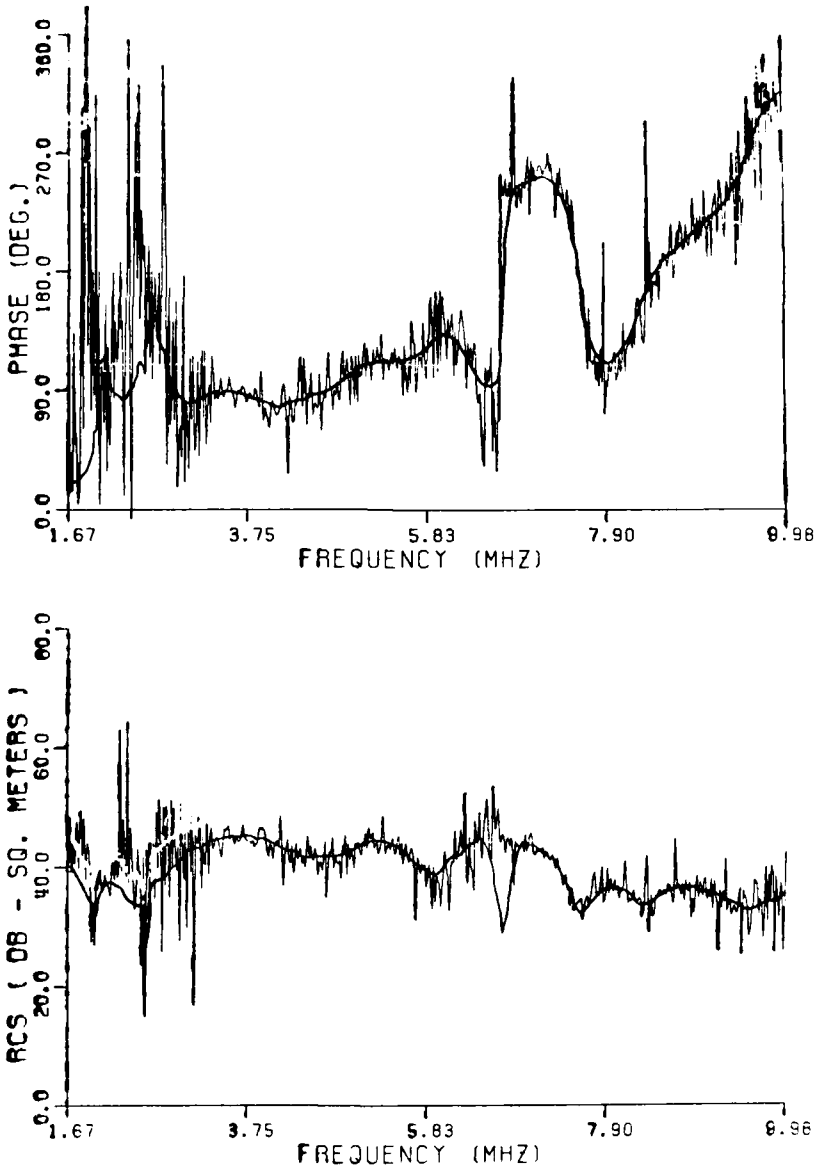

Figure A.6. Ship B at 180 degrees.

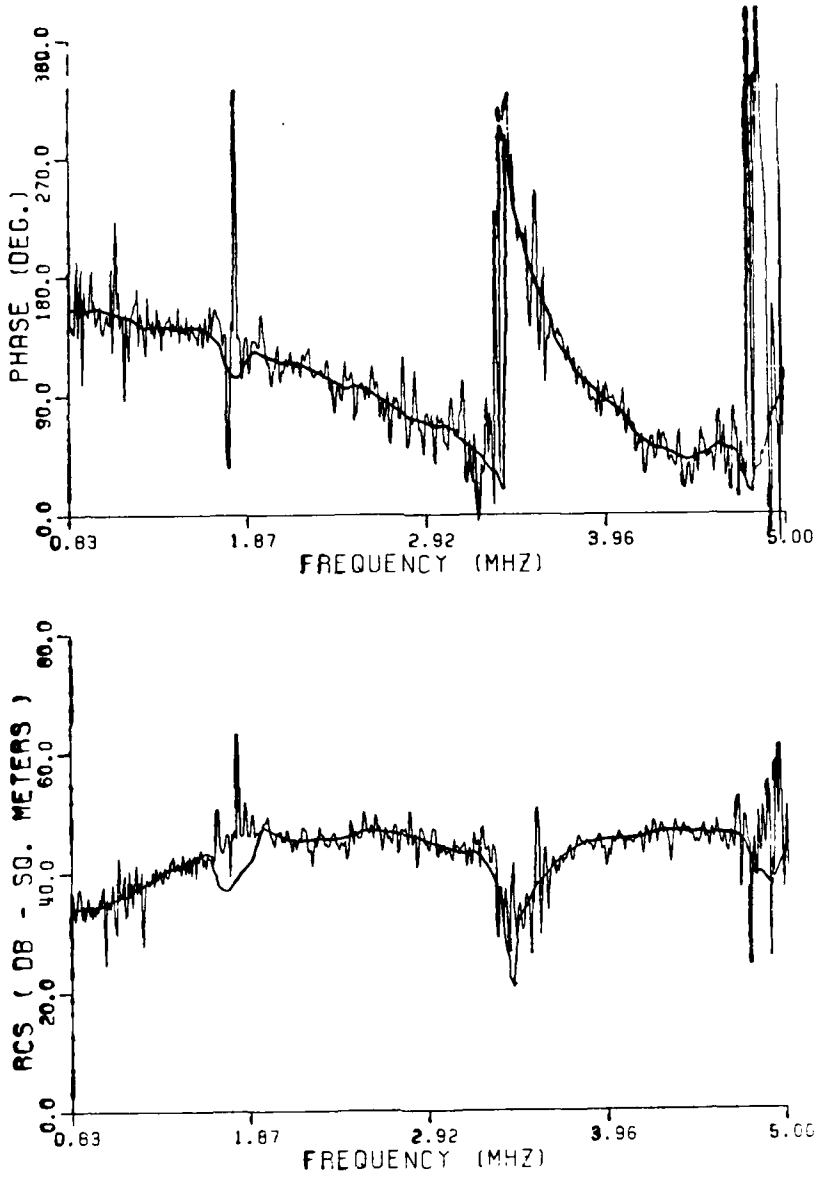

Figure A.7. Ship C at 0 degrees.

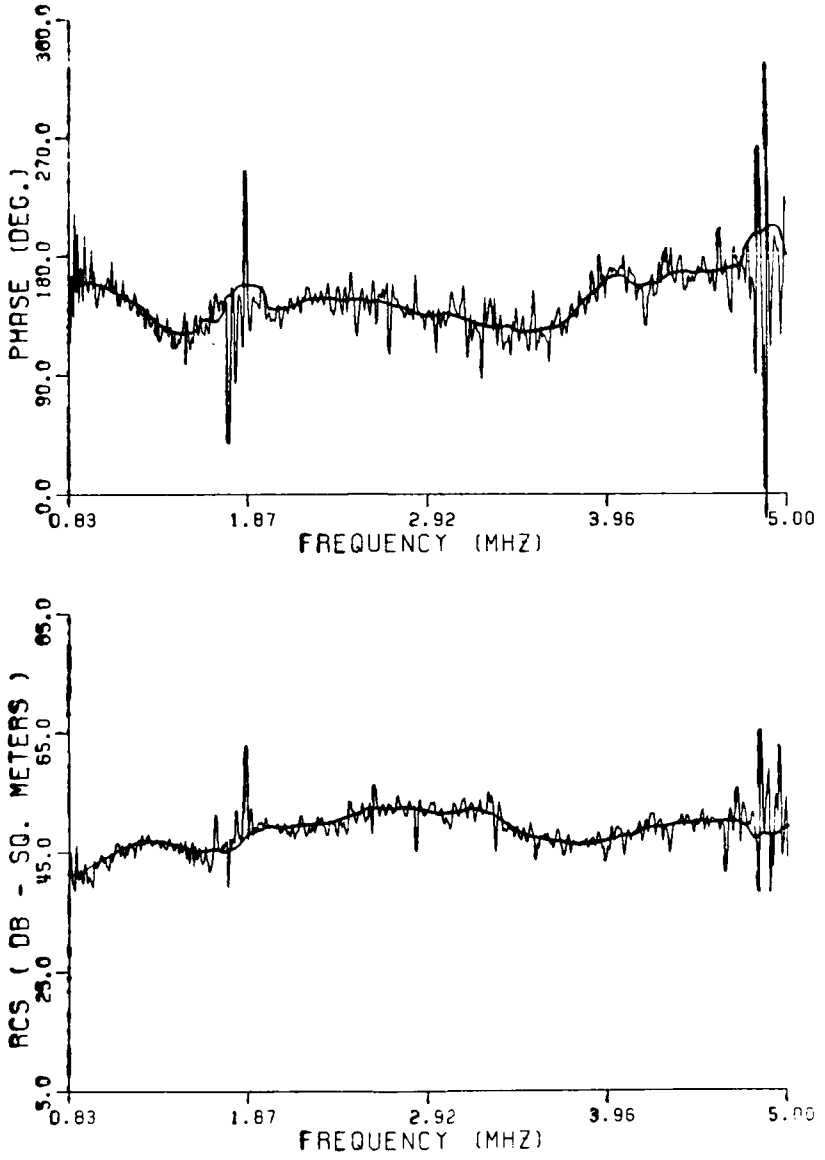

Figure A.8. Ship C at 90 degrees.

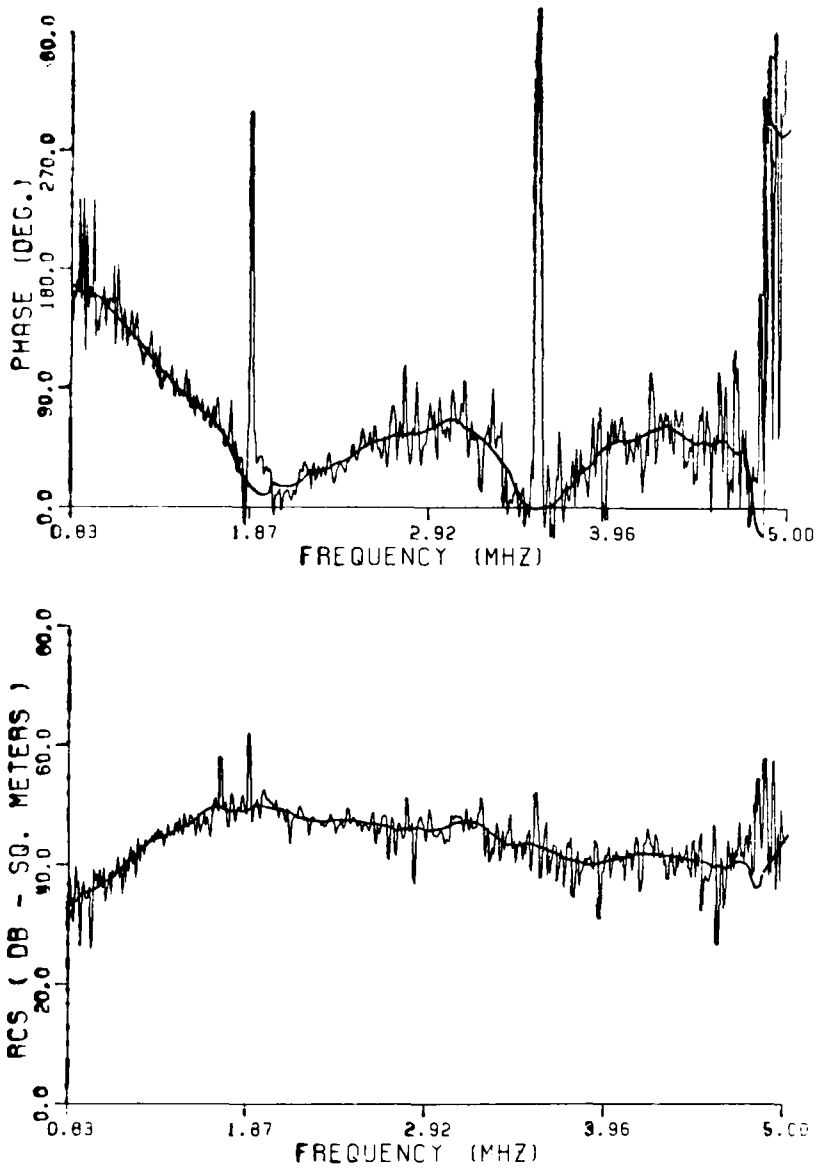

Figure A.9. Ship C at 180 degrees.

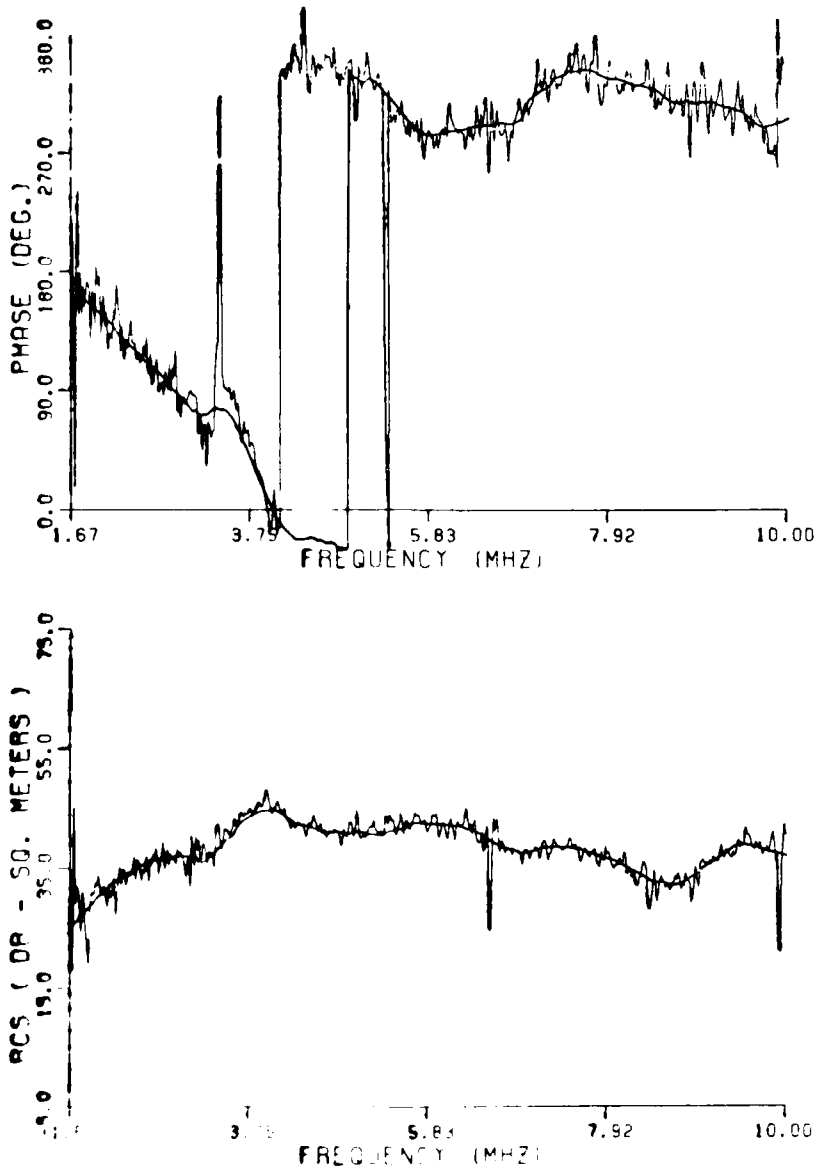

Figure A.10. Ship D at 0 degrees.

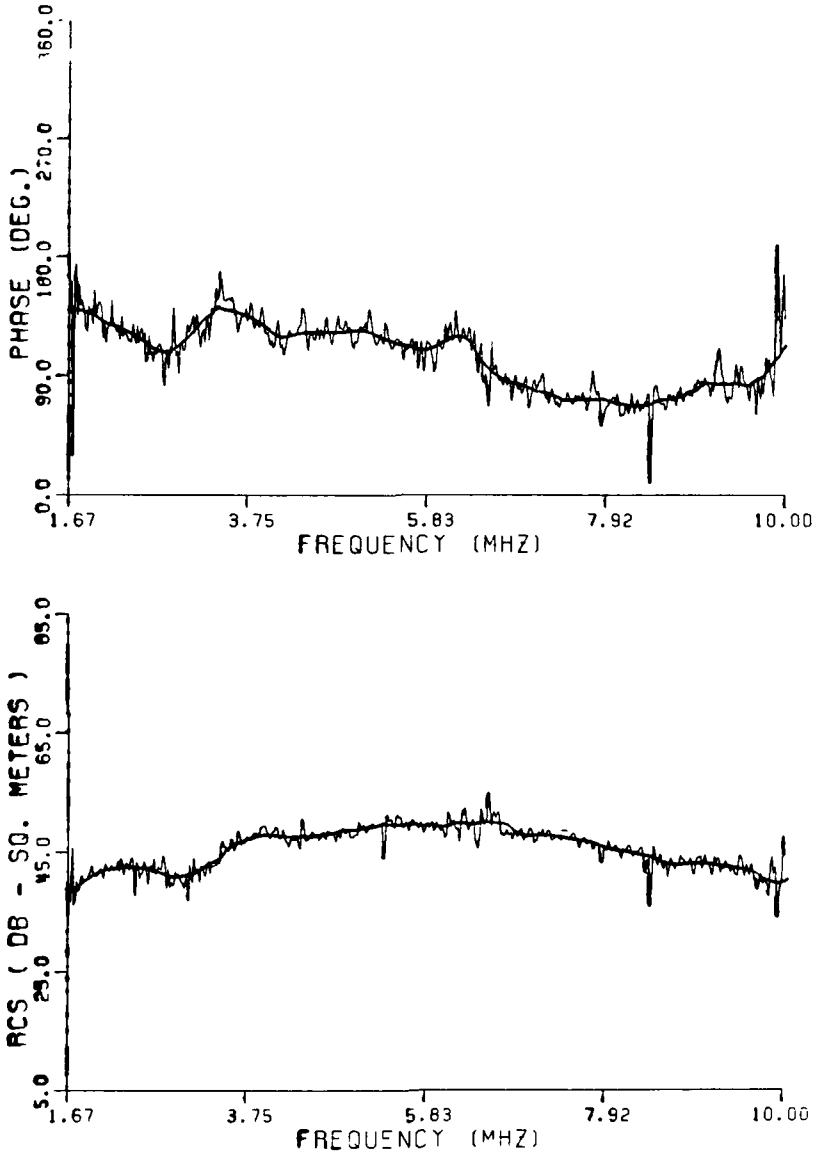

Figure A.11. Ship D at 90 degrees.

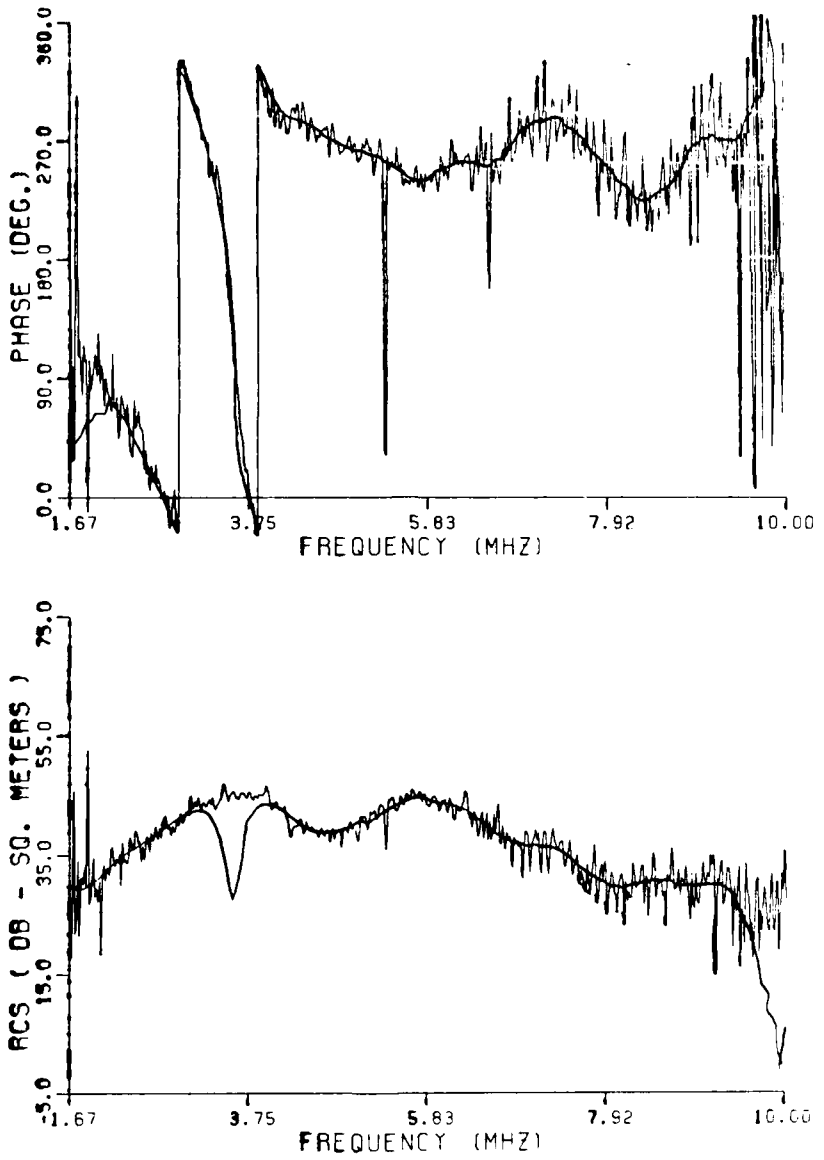

Figure A.12. Ship D at 180 degrees.

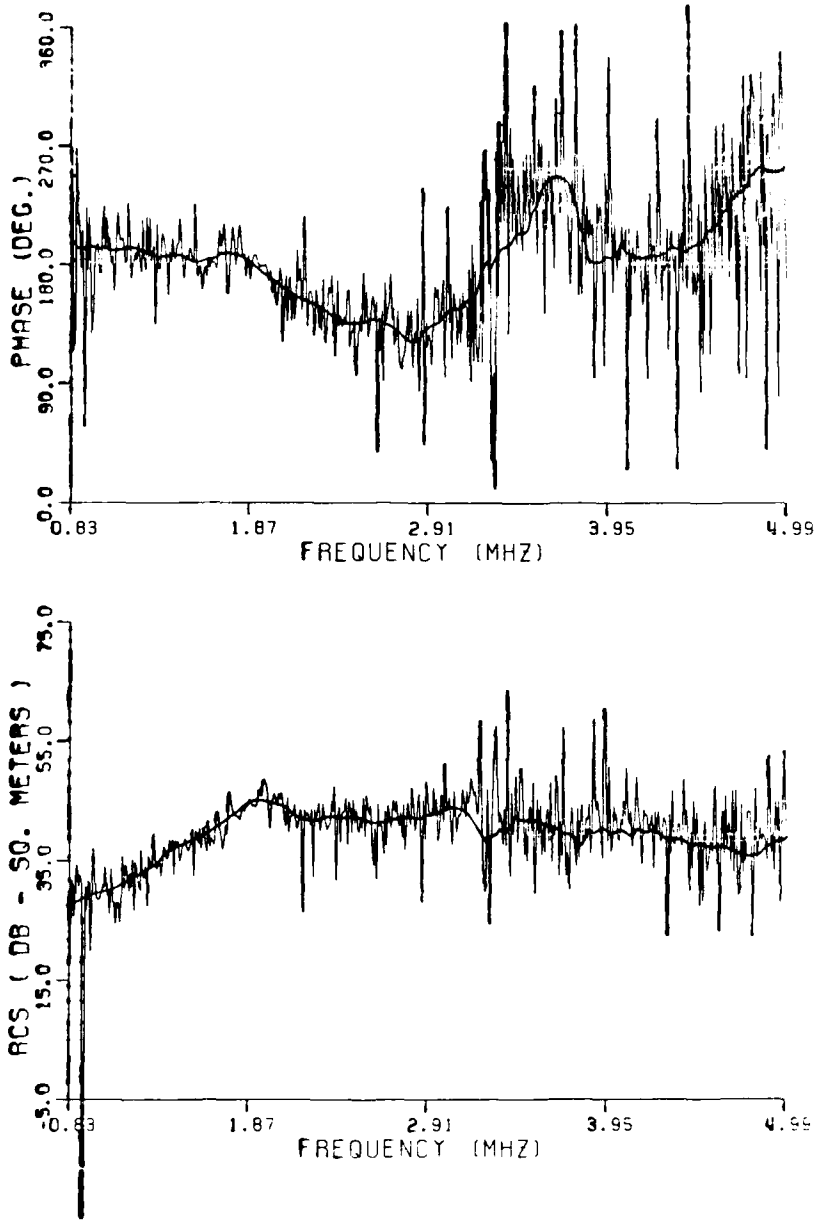

Figure A.13. Ship E at 0 degrees.

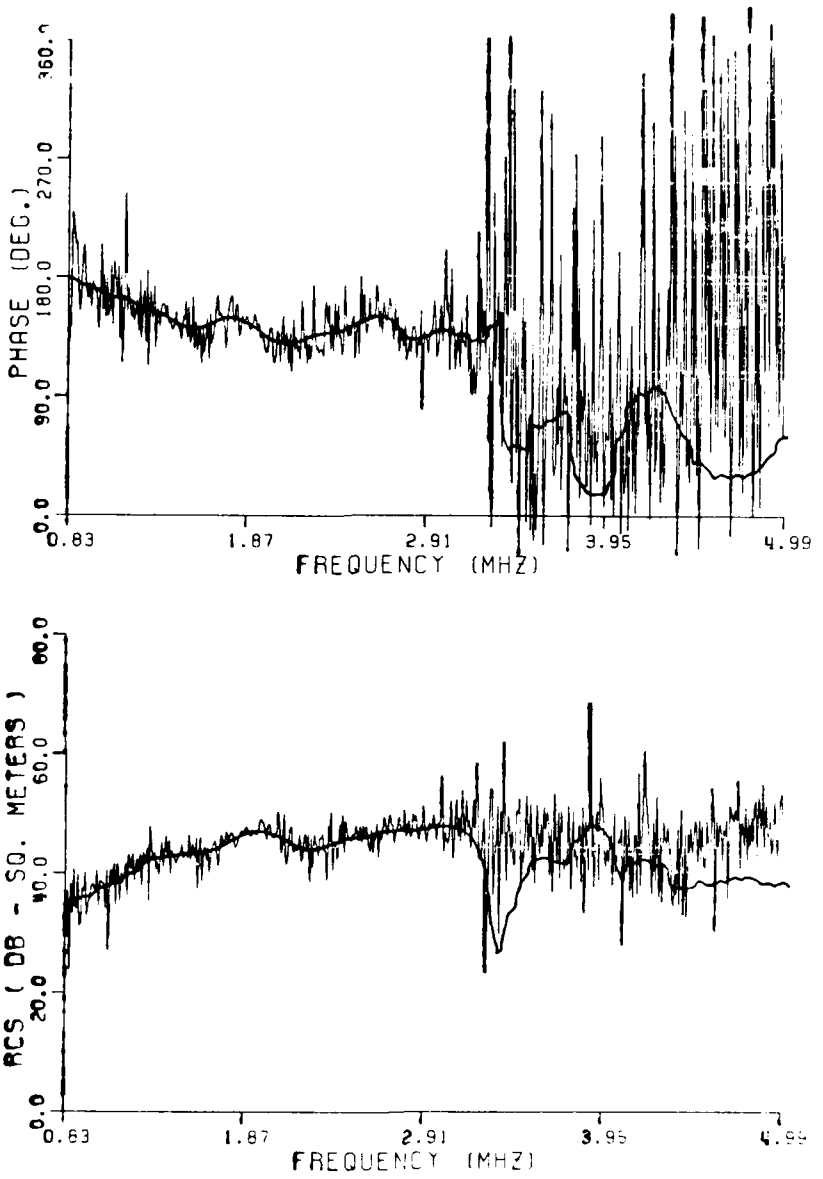

Figure A.14. Ship E at 90 degrees.

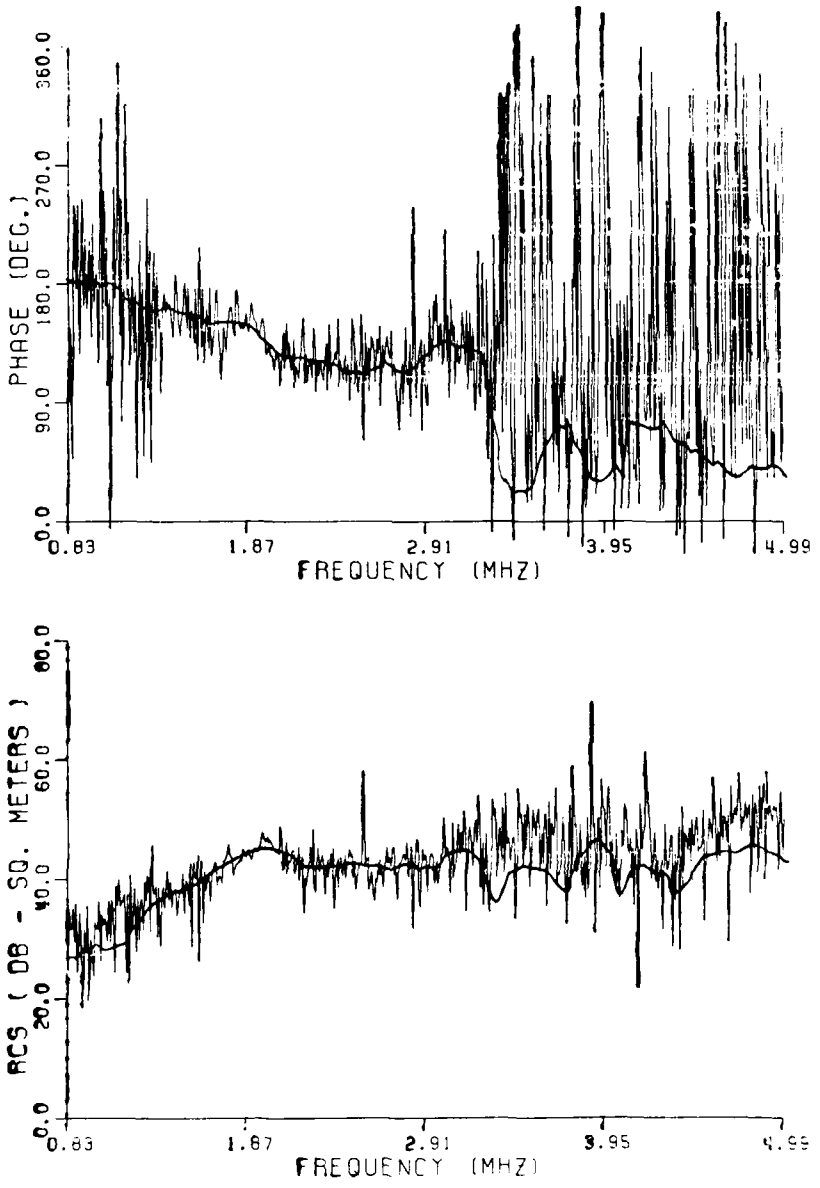

Figure A.15. Ship E at 180 degrees.

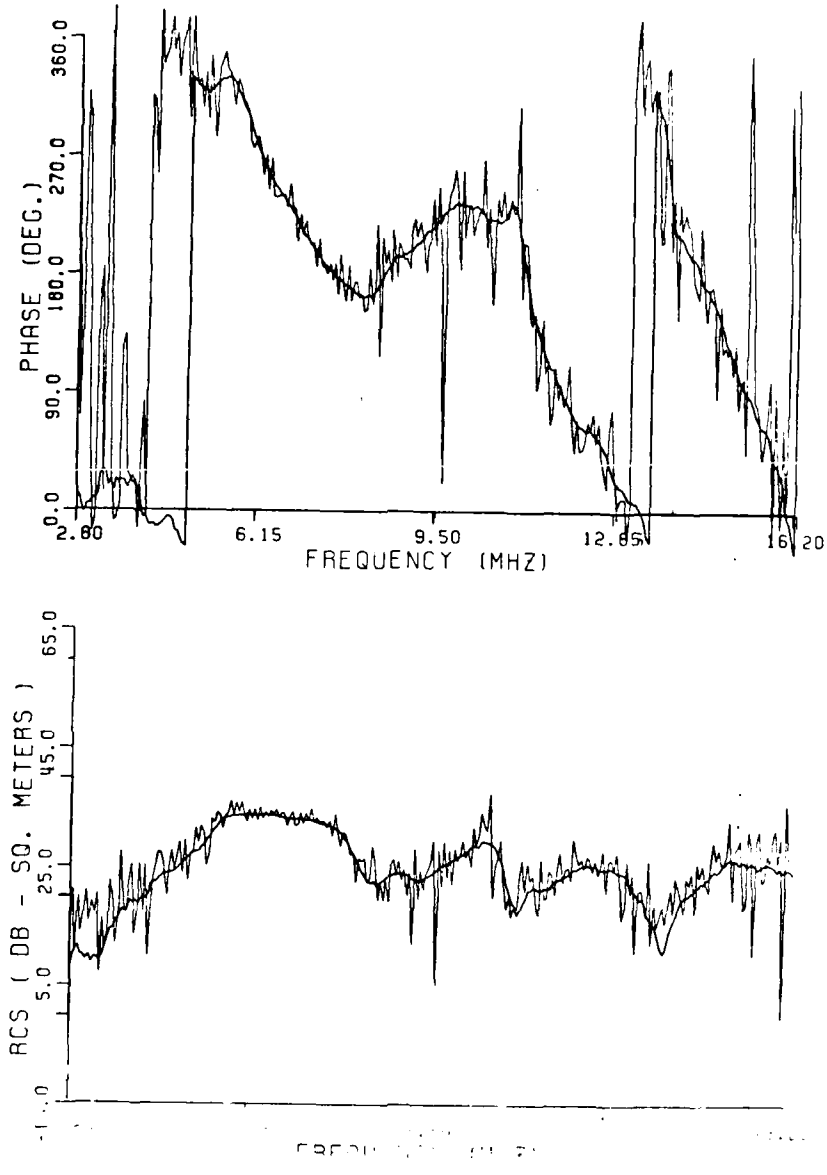

Figure A.16. Aircraft F at 0 degrees.

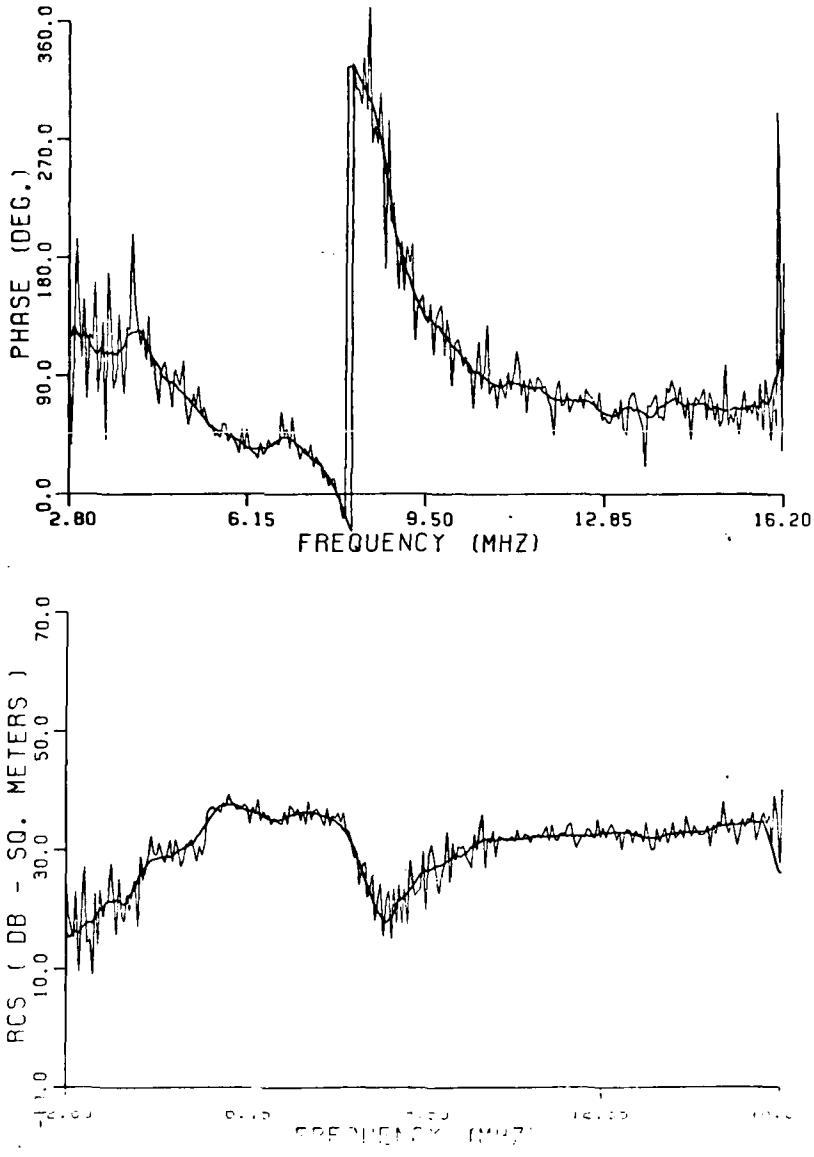

Figure A.17. Aircraft F at 90 degrees.

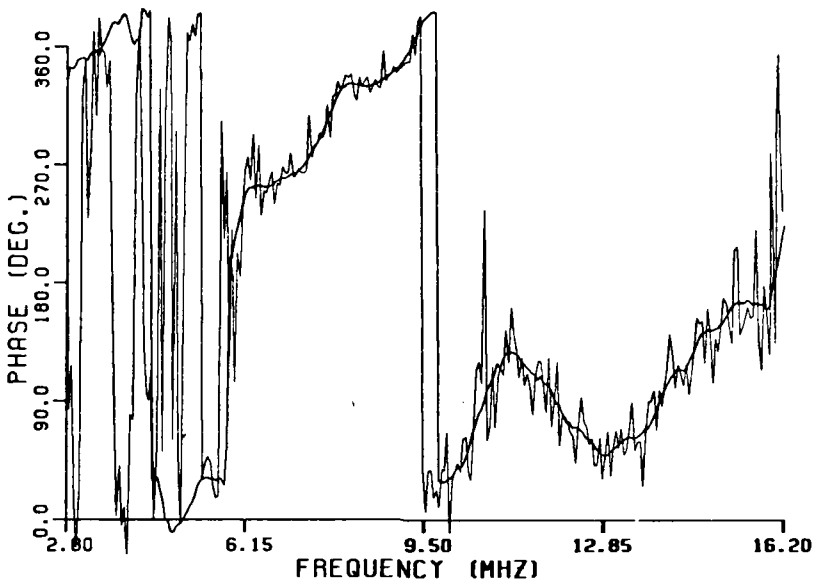

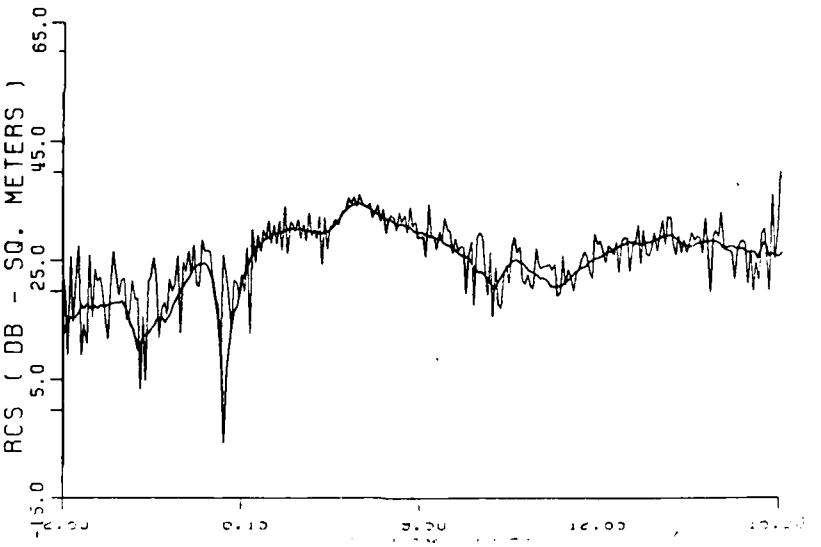

Figure A.18. Aircraft F at 180 degrees.

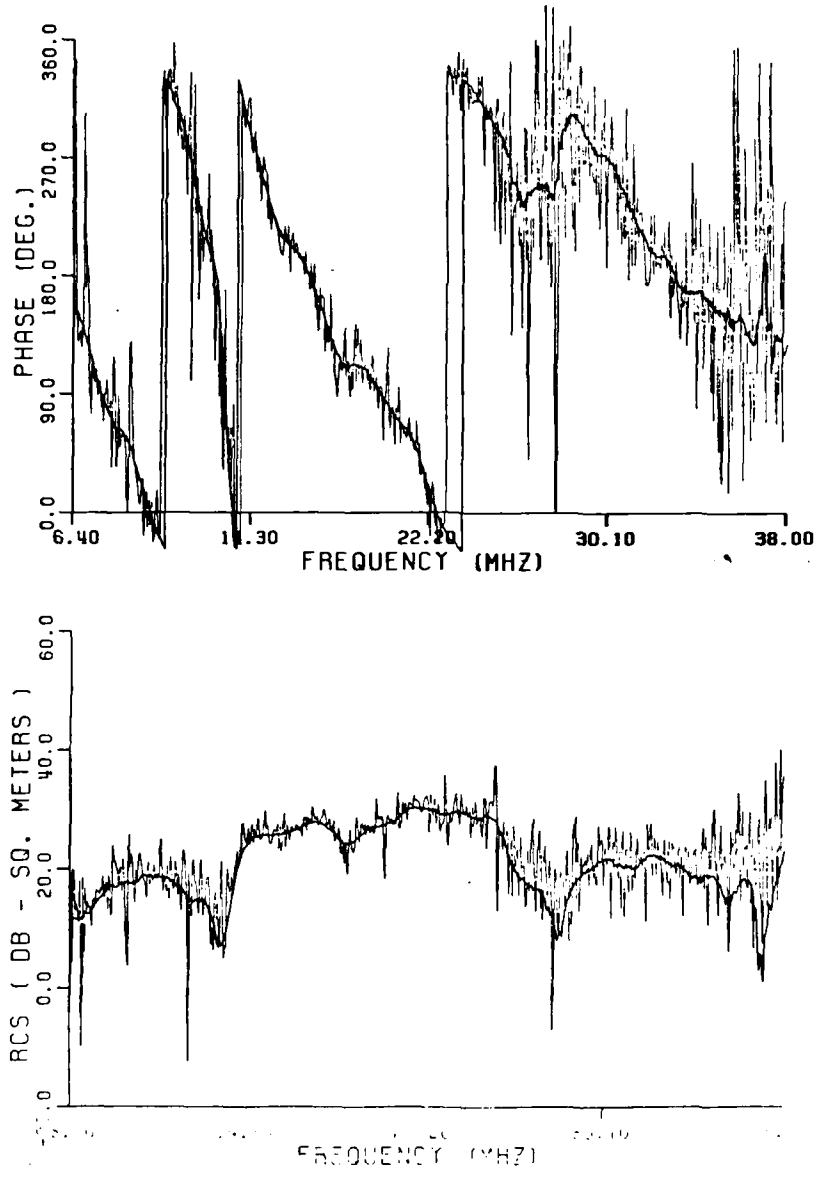

Figure A.19. Aircraft G at 0 degrees.

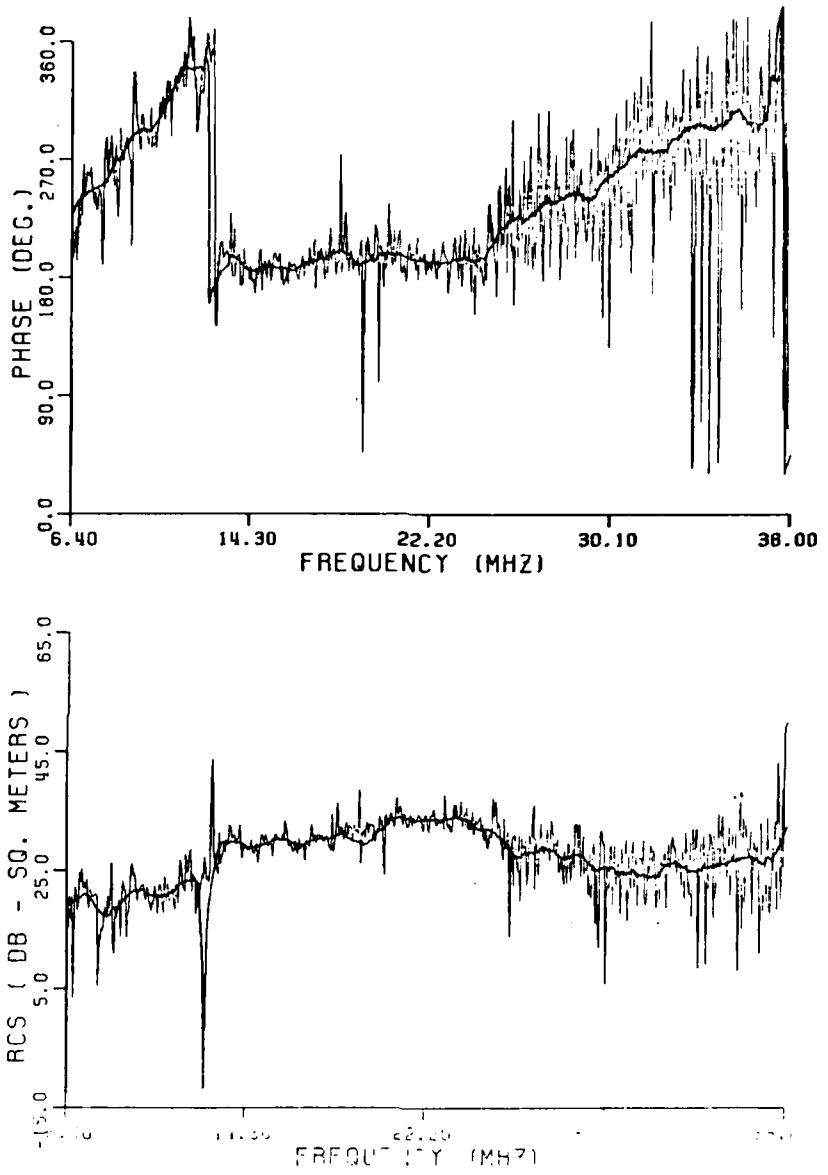

Figure A.20. Aircraft G at 90 degrees.

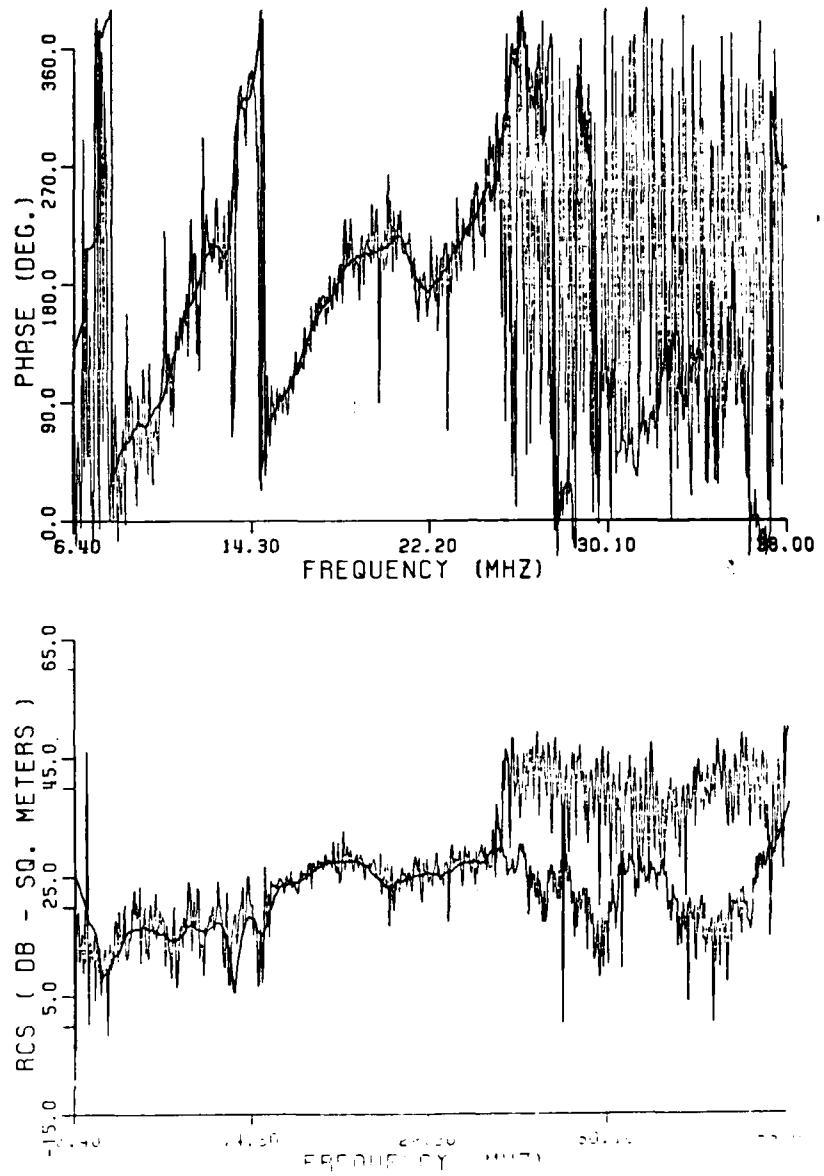

Figure A.21. Aircraft G at 180 degrees.

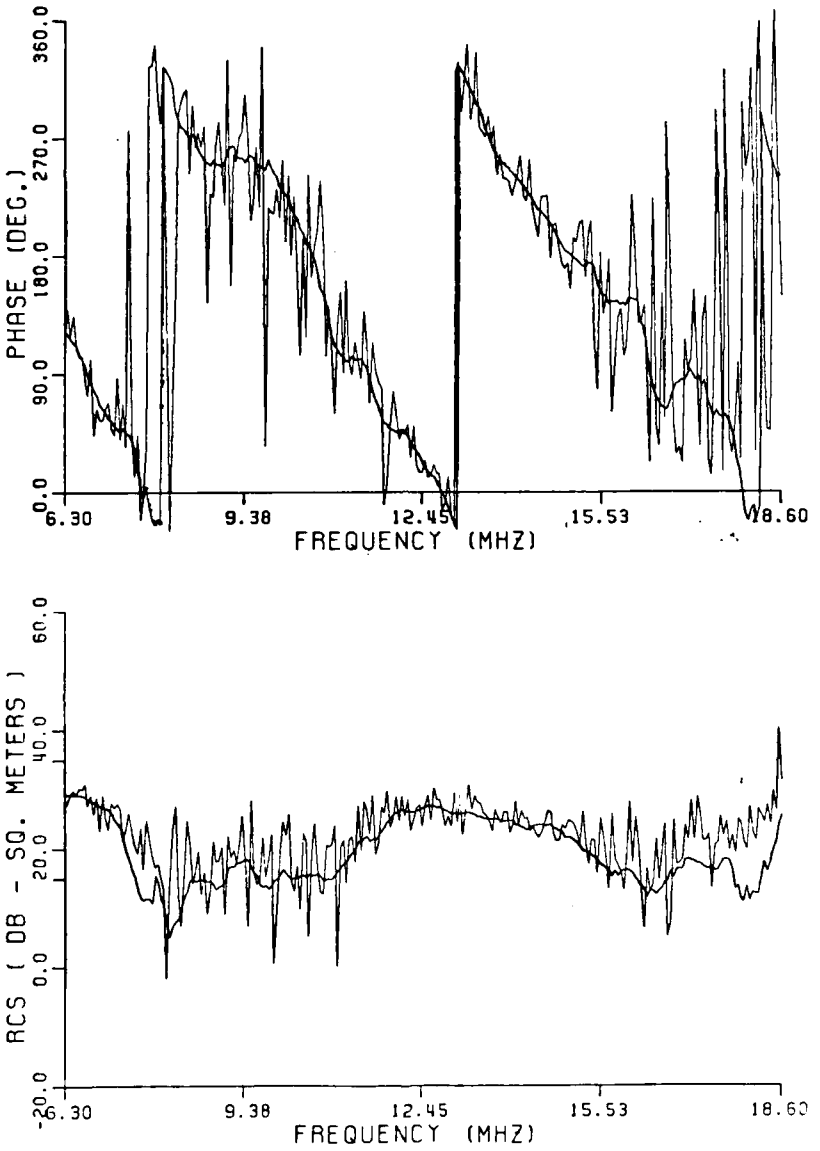

Figure A.22. Aircraft H at 0 degrees.

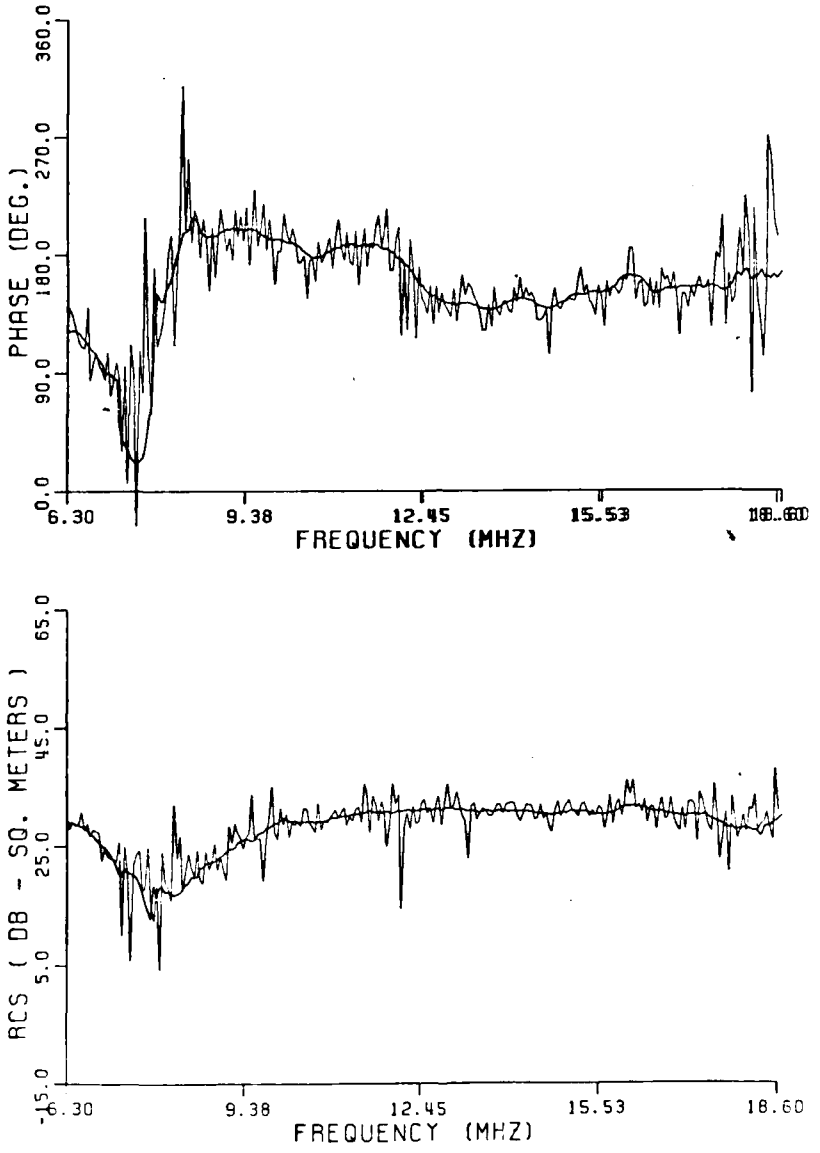

Figure A.23. Aircraft H at 90 degrees.

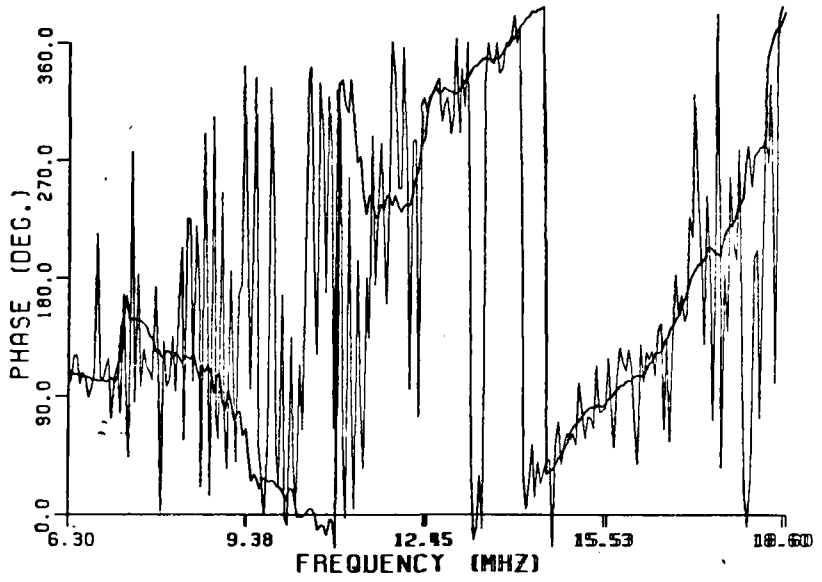

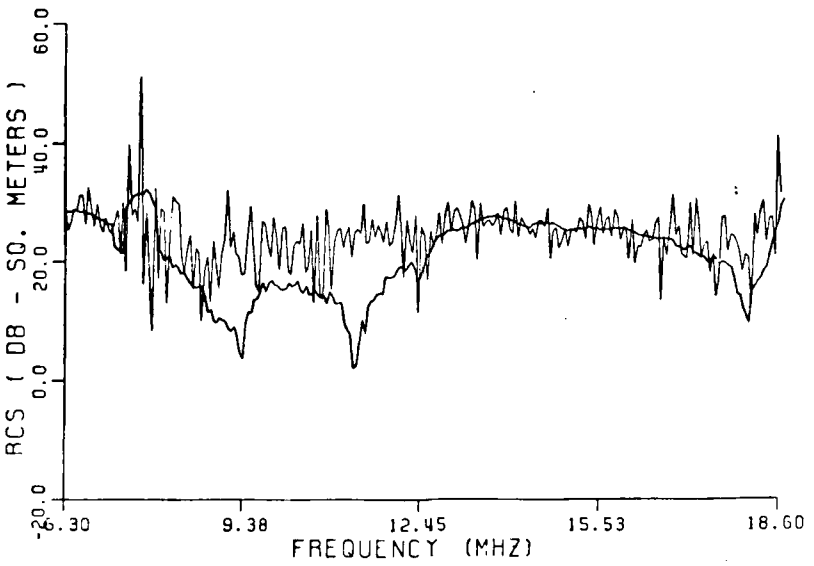

Figure A.24. Aircraft H at 180 degrees.

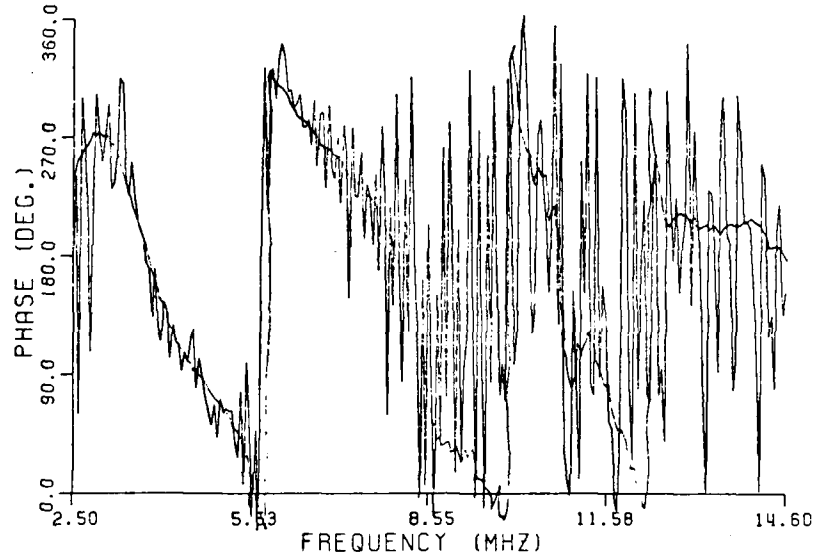

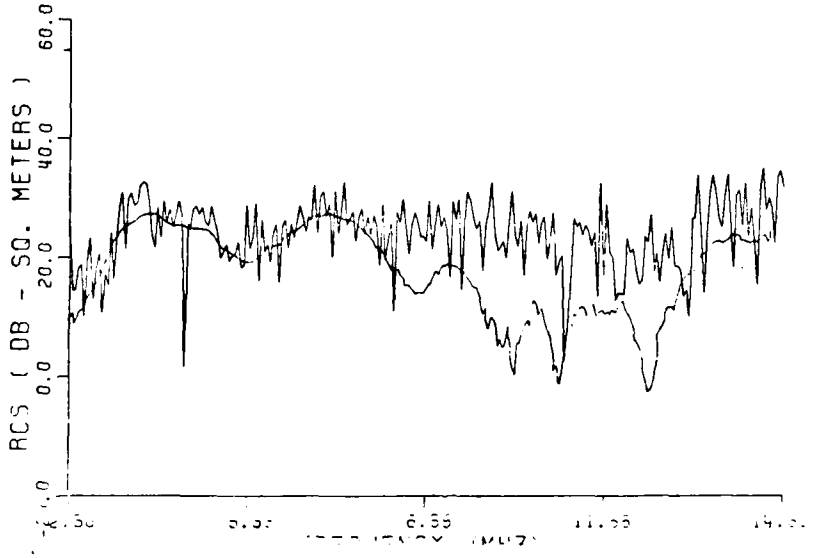

Figure A.25. Aircraft I at 0 degrees.

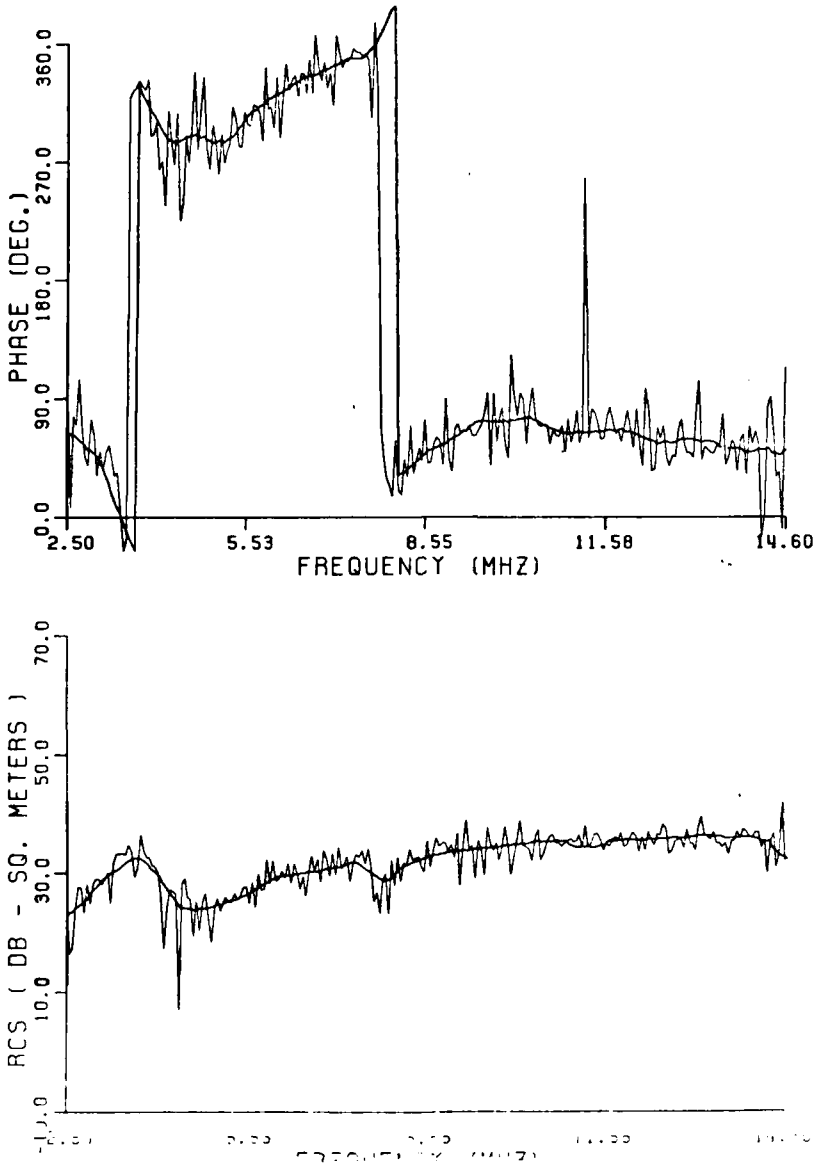

Figure A.26. Aircraft I at 90 degrees.

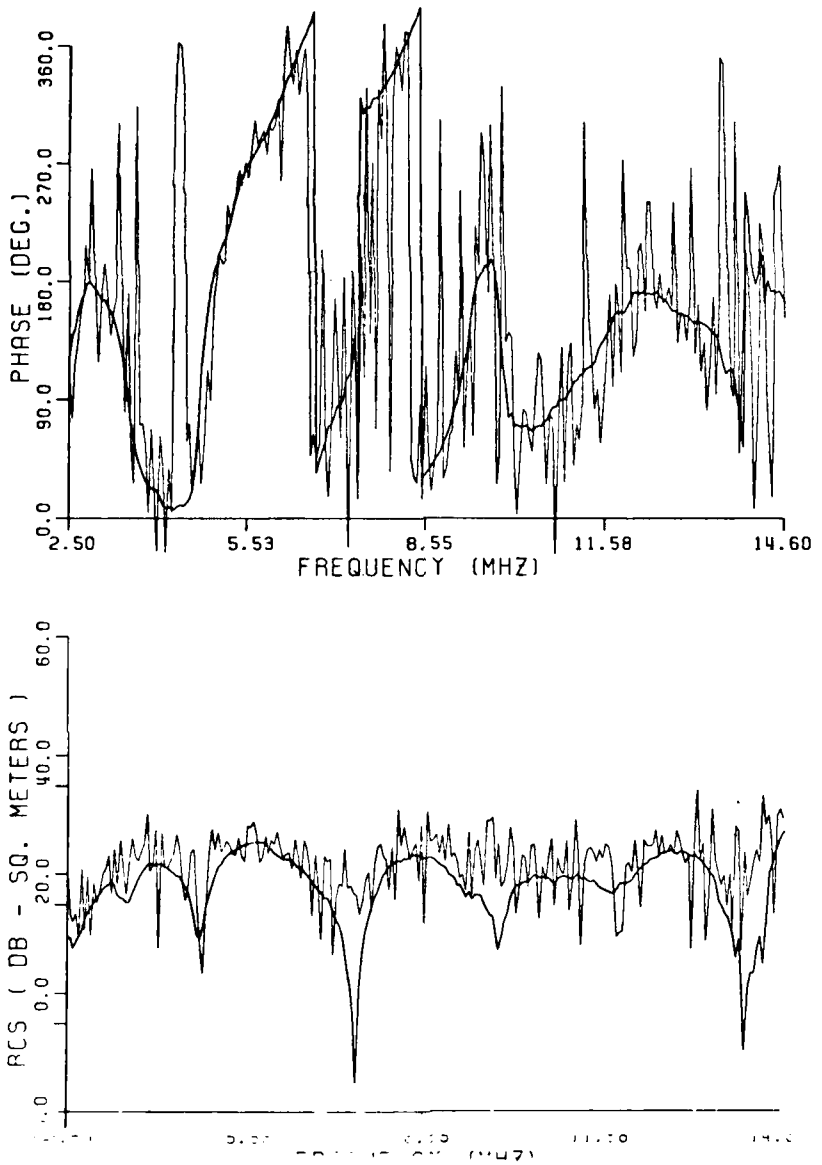

Figure A.27. Aircraft I at 180 degrees.

APPENDIX B

The computer programs developed for this research are listed in this appendix with comments. The program names are DOC.FOR, B3.FOR, FREQ.FOR, and TIME.FOR.

AD-A162 449 AUTOMATIC TARGET CLASSIFICATION USING HF MULTIFREQUENCY RADARS(U) OHIO STATE UNIV COLUMBUS ELECTROSCIENCE LAB J CHEN OCT 83 ESL-714190-3 N00014-82-K-0037 3/3

UNCLASSIFIED F/G 17/9 NL

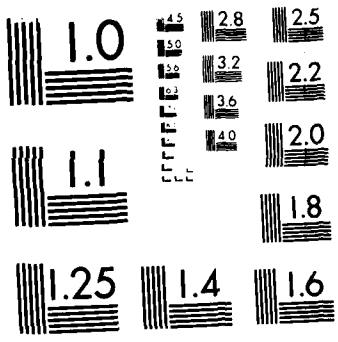

```
C
C       PROGRAM NAME : DOC.FOR
C
C       THIS PROGRAM CALIBRATES MEASURED TARGET RETURNS
C
C
        REAL*4 AM(201),PH(201)
        INTEGER*2 TFILE(6),BFILE(6),CFILE(6),EFILE(6),RFILE(6)
        INTEGER*2 BUFF(1024)
        CHARACTER*12 RSFILE
        COMPLEX*8 TA(201),BA(201),CAS(201),EXS(201),RS(201)
        DATA N/201/
C
C       SET UP AN OUTPUT BUFFER
C
        COMMON /BLK1/BUFF
C
C       FILE NAMES ARE STORED IN INTEGER ARRAYS AND
C       ARE INITIALLY SET TO 0.
C
288     DO 147 I=1,6
        TFILE(I)=0
        BFILE(I)=0
        CFILE(I)=0
        EFILE(I)=0
147     RFILE(I)=0
10      FORMAT(1X,/,' INPUT THE TARGET')
C
C       READ A TARGET FILE FROM A STORAGE UNIT
C       ( IN MOST CASES FROM A FLOPPY DISK )
C
        TYPE 10
        ACCEPT 120,TFILE
120     FORMAT(6A2)
        CALL TDATA(RSFILE,TFILE,TA,0)
C
C       READ A BACKGROUND FILE
C
        TYPE 20
20      FORMAT(1X,/,' INPUT THE BACKGROUND')
        ACCEPT 120,BFILE
        CALL TDATA(RSFILE,BFILE,BA,0)
C
C       READ A CALIBRATION-SPHERE FILE
C
        TYPE 40
40      FORMAT(1X,/,' INPUT THE CALIBRATE SPHERE')
        ACCEPT 120,CFILE
        CALL TDATA(RSFILE,CFILE,CAS,0)
C
C       READ A THEORETICAL CALIBRATION-SPHERE FILE
C
        TYPE 50
50      FORMAT(1X,/,' INPUT THE EXACT SPHERE')
        ACCEPT 120,EFILE
```

```
      CALL TDATA(RSFILE,EFILE,EXS,0)
C
C     CALIBRATE THE TARGET FILE
C
C     IF THE CALIBRATED RESULTS ARE IDENTICAL
C     TO ZERO SET THEM TO 1.E-15
C
      DO 260 I=1,N
      RS(I)=(TA(I)-BA(I))*EXS(I)/(CAS(I)-BA(I))
      IF(AIMAG(RS(I)).EQ.0.AND.REAL(RS(I)).EQ.0.)
     1 RS(I)=CMPLX(1.E-15,1.E-15)
260   CONTINUE
C
C     STORE THE FILE NAMES IN THE OUTPUT BUFFER
C
      DO 478 I=1,6
      BUFF(24+I)=TFILE(I)
      BUFF(24+6+I)=BFILE(I)
      BUFF(24+12+I)=CFILE(I)
      BUFF(24+18+I)=EFILE(I)
478   CONTINUE
C
C     STORE THE CALIBRATED TARGET FILE ON A STORAGE UNIT
C
      CALL TDATA(RSFILE,RFILE,RS,1)
C
      TYPE *,' DO YOU WANT TO PROCEED? Y=1 N=0'
      ACCEPT *,IYN
      IF(IYN.EQ.1)GO TO 288
      CALL EXIT
      END
C
C
      SUBROUTINE TDATA(RFILE,INFILE,CA,IRW)
C
C     THIS SUBROUTINE HANDLES DATA I/O
C     SET IRW = 0 FOR INPUT
C     SET IRW = 1 FOR OUTPUT
C
      COMPLEX*8 CA(201)
      INTEGER*2 BUFF(1024),ID(48),ICODE(4)
      REAL*4 AM(201),PH(201)
      INTEGER*2 INFILE(6)
      CHARACTER*12 RFILE
      EQUIVALENCE (ID(1),BUFF(1)),(ICODE(1),BUFF(49)),
     1 (AM(1),BUFF(53)),(PH(1),BUFF(455))
      COMMON /BLK1/BUFF
      IF(IRW.EQ.1)GO TO 10
C
C     THIS SECTION READS A FILE
C
C     THE FILES TO BE READ WERE ORIGINALLY
C     WRITTEN ON DISKS IN R-T FORMATS ON A PDP-11/03
C     COMPUTER, WHICH MONITORED THE MEASUREMENTS.
C     THE FILE FORMATS WERE TRANSFORMED
```

```
C       TO VAX FORMATS, AND CAN BE READ BY
C       A VAX COMPUTERS.
C       THE TRANSFOMATION CONVERTS THE DATA
C       INTO ASCII CODES, AND STORED THE
C       THE CODES IN A 256-INTEGER BUFFER,
C       WHERE EACH INTEGER CAN HOLD TWO ASCII BYTES.
C
C
C       OPEN A FILE WHOSE FILE NAME IS STORED IN
C       THE ARRAY INFILE
C
        OPEN(UNIT=19,NAME=INFILE,TYPE='OLD')
        DO 20 I=1,1024,256
        J=I+255
20      READ(19,30)(BUFF(K),K=I,J)
30      FORMAT(256A2)
C
C       THE UNITS OF THE AMPLITUDE RETURNS STORED IN THE
C       ORIGINAL FILES ARE DB-SQUARE-CM, AND THE UNITS OF
C       THE PHASE RETURNS ARE RADIANS.
C       THE FOLLOWING CONVERTS THE DATA INTO COMPLEX FORM
C
        DO 70 I=1,201
        AM(I)=10**(AM(I)/20.)
70      CA(I)=CMPLX(AM(I)*COS(PH(I)),AM(I)*SIN(PH(I)))
        GO TO 80
C
C       THIS SECTION WRITES A CALIBRATED TARGET
C       RETURNS ON A STORAGE UNIT
C
C       CONVERTS THE COMPLEX DATA INTO
C       AMPLITUDE-PHASE FORMAT
C
10      DO 210 I=1,201
        AM(I)=20.*ALOG10(CABS(CA(I)))
210     PH(I)=ATAN2(AIMAG(CA(I)),REAL(CA(I)))
C
C       SPECIFY A NAME FOR THE OUTPUT FILE
C
        TYPE 92
        ACCEPT 94,RFILE
C
C       WRITE A 48-CHARACTER SENTENCE EXPLAINING THE OUTPUT FILE
C
        TYPE 112
112     FORMAT(1X,/,' INPUT THE ID FOR THE RESULTS')
        ACCEPT 128,(ID(I),I=1,24)
128     FORMAT(24A2)
92      FORMAT(1X,/,' INPUT A FILE NAME FOR THE RESULTS')
94      FORMAT(A12)
C
C       OPEN AN OUTPUT FILE
C
        OPEN(UNIT=19,NAME=RFILE,TYPE='NEW',RECORDSIZE=512)
C
```

```
C       SOTRE THE OUTPUT BUFFER
C
        WRITE(19,30)BUFF
80      CLOSE(UNIT=19,DISP='SAVE')
        RETURN
        END
```

```
C
C       PROGRAM NAME : B3.FOR
C
C
C       THIS PROGRAM MAKES USE OF THE 2-4GHZ, 4-8GHZ, AND 8-12GHZ
C       CALIBRATED DATA FILES GENERATED BY THE PROGRAM
C       DOC.FOR, AND GENERATE A FULL-SCALE DATA FILE.
C
C
        REAL*4 FA(801),SA(801),A24(201),A48(201),A82(201)
     1,P24(201),P48(201),P82(201),FA24(201),FA48(201),FA82(201)
        INTEGER*4 ID(12)
        INTEGER*2 F12(6),F24(6),F48(6),F82(6),RFILE(6),LINE2(24)
        COMPLEX*8 TA(201),CA(801),R(801)
C
C       INPUT THE SCALE FACTOR OF A TARGET, A DESIRED
C       FREQUENCY INCREMENT FOR THE OUTPUT FILE, AND
C       THE WIDTH OF THE HAMMING WINDOW.
C
3542    TYPE *,'INPUT THE SCALE FACTOR, FREQ INC AND WINDOW SIZE (MHZ)'
        ACCEPT *,SF,FINC,WD
C
C       READ THE NAME OF A 2-4GHZ CALIBRATED DATA FILE
C
        TYPE 20
20      FORMAT(1X,/,' INPUT THE 2-4G FILE ')
        ACCEPT 120,F24
120     FORMAT(6A2)
C
C       READ THE NAME OF A 4-8GHZ CALIBRATED RETURNS
C
        TYPE 40
40      FORMAT(1X,/,' INPUT THE 4-8G FILE')
        ACCEPT 120,F48
C
C       READ THE NAME OF A 8-12GHZ CALIBRATED RETURNS
C
        TYPE 50
50      FORMAT(1X,/,' INPUT THE 8-12G FILE')
        ACCEPT 120,F82
C
C       SPECIFY A NAME FOR THE OUTPUT FILE
C
        TYPE *,' INPUT A FILE NAME FOR THE RESULT'
C
C       INPUT A FILE-HEADER WHICH EXPLAINS THE OUTPUT
C       FILE
C
        ACCEPT 120,RFILE
        TYPE *,' INPUT A HEADER (48 CHARACTERS)'
        ACCEPT 732,(ID(IZ),IZ=1,12)
732     FORMAT(12A4)
C
C       INITIALIZE THE FILE-NAME ARRAYS
C
```

```
      F24(6)=0
      F24(5)=0
      F48(6)=0
      F48(5)=0
      F82(6)=0
      F82(5)=0
      RFILE(6)=0
      RFILE(5)=0
C
C     CALCULATE FULL-SCALE FREQUENCIES
C     ACCORDING TO THE SCALED FACTOR
C
      DO 46 I=1,201
      FA24(I)=(2.+(I-1)/100.)/SF*1000.
      FA48(I)=(4.+(I-1)/50.)/SF*1000.
46    FA82(I)=(8.+(I-1)/50.)/SF*1000.
C
C     READ THE 2-4GHZ, 4-8GHZ, AND 8-12 GHZ FILES
C
      CALL TDATA(F24,A24,P24,P24A,P24Z)
      CALL TDATA(F48,A48,P48,P48A,P48Z)
      CALL TDATA(F82,A82,P82,P82A,P82Z)
C
C     CALCULATE PHASE OFFSETS AT
C     THE JUNCTIONS OF THE FILES, NAMELY, AT 4 GHZ,
C     AND 8 GHZ.
C
      DPL=P24Z-P48A
      DPR=P82A-P48Z
C
C     CORRECT THE PHASE OFFSETS IN THE
C     2-4GHZ, AND 8-12 GHZ FILES,
C     AND USE THE 4-8GHZ FILE AS REFERENCE
C
      CALL PHCR(DPL,FA24,201,P24)
      CALL PHCR(DPR,FA82,1,P82)
C
C     CONNECT THE CORRECTED FILES ( 2-4GHZ, 4-8GHZ, AND 8-12 GHZ )
C     AND CREATE A FULL-SCALE COMPLEX TARGET
C     RETURNS ACCORDING TO THE SCALE FACTOR
C
      DO 3540 I=1,201
      CA(I)=CMPLX(SF*A24(I)*COS(P24(I)),SF*A24(I)*SIN(P24(I)))
      CA(I+200)=CMPLX(SF*A48(I)*COS(P48(I)),SF*A48(I)*SIN(P48(I)))
      CA(I+400)=CMPLX(SF*A82(I)*COS(P82(I)),SF*A82(I)*SIN(P82(I)))
      SA(I)=2.
      SA(I+200.)=4.
      SA(I+400.)=4.
      FA(I)=FA24(I)
      FA(I+200)=FA48(I)
3540  FA(I+400)=FA82(I)
C
C     STORE THE INPUT-FILE NAMES IN A BUFFER
C
      DO 997 I=1,24
```

```
997     LINE2(I)='  '
        DO 999 I=1,4
        LINE2(I+6)=F24(I)
        LINE2(I+12)=F48(I)
        LINE2(I+18)=F82(I)
999     CONTINUE
C
C       SMOOTH THE FULL-SCALE DATA FILE BY CONVOLVING
C       THE FILE WITH A HAMMING WINDOW
C
C       CALCULATE PARAMETERS FOR THE CONVOLUTIONS, WHERE,
C       FLOW IS THE LOWEST FULL-SCALE FREQUENCY
C       FHIGH IS THE HIGHEST FULL-SCALE FREQUENCY
C       FINC IS THE FULL-SCALE FREQUENCY INCREMENT
C
        FLOW=2./SF*1000.
        FHIGH=12./SF*1000.
        FLOW=INT(FLOW*10.)/10.+.1
        FHIGH=INT(FHIGH*10.)/10.
        I=1
        K=0
        ICNT=601
        TYPE *,'FA(1)=',FA(1),' FA(ICNT)=',FA(ICNT)
        TYPE *,'SF=',SF,' ICNT=',ICNT,' FLOW=',FLOW,' FHIGH=',FHIGH
C
C       PICK UP THE DESIRED FREQUENCY AND POSITION THE
C       CENTER OF THE HAMMING WINDOW AT THAT FREQUENCY.
C       ESTIMATE THE DATA VALUE OF THE DESIRED FREQUENCY BY
C       TAKING THE WEIGHTED AVERAGE OF THE NEIGHBORING DATA POINTS
C       COVERED BY THE HAMMING WINDOW, WITH THE WEIGHTINGS DETERMINED
C       THE HAMMING WINDOW.
C
        DO 7720 RF=FLOW,FHIGH,FINC
7740    IF(RF.GE.FA(I).AND.RF.LE.FA(I+1))GO TO 7730
        I=I+1
        IF(I.GT.ICNT)GO TO 4912
        GO TO 7740
7730    K=K+1
        CALL INTER(R,CA,FA,SA,ICNT,NS,I,K,WD,RF)
7720    CONTINUE
C
C       OUTPUT THE SMOOTHED FULL-SCALE DATA FILES
C
4912    CALL PDATA(RFILE,R,K,FLOW,FINC,SF,ID,LINE2)
C
C
        TYPE *,' NPT=',K,' FLOW=',FLOW,' FINC=',FINC
        TYPE *,'DO YOU WANT TO PROCEED ? Y=1,N=0'
        ACCEPT *,IYN
        IF(IYN.EQ.1)GO TO 3542
        CALL EXIT
        END
C
C
        SUBROUTINE TDATA(INFILE,AMT,PHT,PHA,PHZ)
```

```
C
C       THIS SUBROUTINE READS A DATA FILE
C
        INTEGER*2 BUFF(1024),INFILE(6)
        REAL*4 AM(201),PH(201),AMT(201),PHT(201)
        EQUIVALENCE (AM(1),BUFF(53)),(PH(1),BUFF(455))
        OPEN(UNIT=19,NAME=INFILE,TYPE='OLD')
        PI=4.*ATAN(1.)
        TPI=PI*2.
        DO 20 I=1,1024,256
        J=I+255
20      READ(19,30)(BUFF(K),K=I,J)
30      FORMAT(256A2)
        DO 10 I=1,201
        IF(AM(I).GT.40.)AM(I)=40.
        AMT(I)=10**(AM(I)/20.)
        PHT(I)=PH(I)*180./PI
10      CONTINUE
C
C       ELIMINATE BRANCH CUTS IN THE PHASE RETURNS
C
        CALL LPV(PHT,185.,30.,180.,-180.,201)
C
        DO 55 I=1,201
55      PHT(I)=PHT(I)*PI/180.
        CLOSE(UNIT=19,DISP='SAVE')
C
C       ESTIMATE THE PHASE VALUES AT THE ENDS OF THE FILE
C
        CALL EPH(PHA,PHT,2,7,1)
        CALL EPH(PHZ,PHT,200,195,-1)
C
        RETURN
        END
C
        SUBROUTINE PDATA(RFILE,CA,NPT,FLOW,FINC,SF,ID,LINE2)
C
C       THIS SUBROUTINE WRITES A FILE ON A STORAGE UNIT
C
        INTEGER*2 RFILE(6),LINE2(24)
        INTEGER*4 ID(12)
        REAL*4 AM(801),PH(801)
        COMPLEX*8 CA(801)
10      DO 210 I=1,NPT
        IF(CABS(CA(I)).EQ.0.)CA(I)=(1.E-15,1.E-15)
        AM(I)=20.*ALOG10(CABS(CA(I)))
210     PH(I)=ATAN2(AIMAG(CA(I)),REAL(CA(I)))
        OPEN(UNIT=19,NAME=RFILE,TYPE='NEW',RECORDSIZE=512)
        WRITE(19,30)(ID(I),I=1,12),LINE2,NPT,FLOW,FINC,SF
30      FORMAT(12A4,24A2,4A4)
        WRITE(19,40)(AM(I),I=1,NPT),(PH(I),I=1,NPT)
40      FORMAT(128A4)
80      CLOSE(UNIT=19,DISP='SAVE')
        RETURN
        END
```

```
C
C       THIS SUBROUTINE CALCULATES THE WEIGHTED AVERAGE
C       OF THE DATA POINTS, USING A HAMMING WINDOW TO DECIDE
C       THE WEIGHTINGS
C
        SUBROUTINE INTER(R,CA,FA,SA,ICNT,NS,I,K,WD,RF)
        COMPLEX*8 R(801),CA(801)
        REAL*4 FA(801),SA(801)
        WEI=0
        IS=I
        XTMP=0.
        YTMP=0.
        RFL=RF-WD/2.
        RFH=RF+WD/2.
20      IF(IS.GT.ICNT)GO TO 10
        IF(FA(IS).GT.RFH)GO TO 10
        T=FA(IS)-RF
        HAMM=.54+.46*COS(3.1415926*T/WD)
        XTMP=XTMP+HAMM*SA(IS)*REAL(CA(IS))
        YTMP=YTMP+HAMM*SA(IS)*AIMAG(CA(IS))
        WEI=WEI+HAMM*SA(IS)
        IS=IS+1
        GO TO 20
10      IS=I-1
15      IF(IS.LT.1)GO TO 30
        IF(FA(IS).LT.RFL)GO TO 30
        T=FA(IS)-RF
        HAMM=.54+.46*COS(3.1415926*T/WD)
        XTMP=XTMP+HAMM*SA(IS)*REAL(CA(IS))
        YTMP=YTMP+HAMM*SA(IS)*AIMAG(CA(IS))
        WEI=WEI+HAMM*SA(IS)
        IS=IS-1
        GO TO 15
30      R(K)=CMPLX(XTMP/WEI,YTMP/WEI)
        RETURN
        END
C
C       THIS SUBROUTINE CORRECTS THE PHASE OFFSETS
C
        SUBROUTINE PHCR(DPH,FA,IBASE,PH)
        REAL*4 PH(201),FA(201)
        TWOPI=8.*ATAN(1.)
        PI=TWOPI/2.
30      IF(DPH.LT.PI)GO TO 20
        DPH=DPH-TWOPI
        GO TO 30
20      IF(DPH.GT.-PI)GO TO 40
        DPH=DPH+TWOPI
        GO TO 20
40      FBASE=FA(IBASE)
        DO 10 I=1,201
10      PH(I)=PH(I)-(DPH*FA(I)/FBASE)
        RETURN
        END
C
```

```
C       THIS SUBROUTINE ESTIMATES THE VALUES OF
C       PHASE RETURNS AT THE ENDS OF A DATA FILE,
C       USING A LINEAR INTERPOLATION
C
        SUBROUTINE EPH(PHM,PH,NS,NF,NI)
        REAL*4 PH(201)
        X=0
        Y=0
        XY=0
        X2=0
        DO 10 I=NS,NF,NI
        X=X+FLOAT(I)
        Y=Y+PH(I)
        XY=XY+FLOAT(I)*PH(I)
10      X2=X2+FLOAT(I)*FLOAT(I)
        XN=(NF-NS)*NI+1
        DELTA=XN*X2-X*X
        A=(XN*XY-X*Y)/DELTA
        B=(X2*Y-X*XY)/DELTA
        PHM=A*NS+B
        RETURN
        END
```

```
C
C       THIS SUBROUTINE ELIMINATES BRACH-CUTS
C       IN PHASE RETURNS
C
        SUBROUTINE LPV(P,VR,DV,PMAX,PMIN,NP)
        REAL*4 P(801)
        DO 100 I=1,NP
        IF(P(I).GT.PMAX)P(I)=P(I)-360.
100     IF(P(I).LT.PMIN)P(I)=P(I)+360.
        PMED=(PMAX+PMIN)/2.
        DO 10 I=1,NP-1
        IF(ABS(P(I+1)-P(I)).LT.VR)GO TO 10
        IF(P(I).LT.PMED)P(I+1)=P(I+1)-360.
        IF(P(I).GT.PMED)P(I+1)=P(I+1)+360.
        IF(P(I+1).GT.PMAX+DV)P(I+1)=P(I+1)-360.
        IF(P(I+1).LT.PMIN-DV)P(I+1)=P(I+1)+360.
10      CONTINUE
        RETURN
        END
```

```
C
C       PROGRAM NAME : FREQ.FOR
C
C
C       THIS PROGRAM CLASSIFIES TARGETS IN THE
C       FREQUENCY DOMAIN.
C
C
      COMPLEX C(18,50),NC(18,50)
      REAL D(18,18),A(18,50),P(18,50),W(18,50),AN(18,50),
     1PN(18,50),WN(18,50)
      REAL WL(50),PX(30),PY(10,30),PYT(30),SAP(18)
      TYPE *,' ***** YOU MUST ASSIGN DATA DIRECTORY TO R *****'
      TYPE *,' WANT TO PRINT DISTANCES IN CLASSIFICATION ? Y=1 N=0'
      ACCEPT *,IDIS
C
C       INPUT TWO ARBITRARY LARGE ODD INTEGERS
C       WHICH WILL SERVE AS SEEDS FOR GENERATEING RANDOM NUMBERS
C
      TYPE *,'INPUT 2 ARBITRARY LARGE ODD INTEGERS'
      ACCEPT *,IS3,IS4
C
C       SPECIFY THE MINIMUM, MAXIMUM, AND INCREMENT OF
C       ADDITIVE GAUSSIAN NOISE POWERS
C
      TYPE *,'INPUT MIN,MAX,INC OF THE NOISE POWER (DB)'
      ACCEPT *,IV1,IV2,IVT
C
C       SPECIFY TARGET ASPECT ANGLES
C
      TYPE *,'INPUT MIN,MAX,INC OF ASP'
      ACCEPT *,MINASP,MAXASP,INCASP
C
C       SPECIFY FREQUENCIES
C
      TYPE *,'INPUT FMIN,FINC,NO OF FREQ'
      ACCEPT *,FMIN,FINC,NF
C
      TYPE *,'DO YOU WANT TO USE RELATIVE AMPLITUDE ? Y=1 N=0'
      ACCEPT *,IRA
      TYPE *,'INPUT NO OF EXPERIMENTS'
      ACCEPT *,NEX
      TYPE *,' ASP KNOWN ---> TYPE 1'
      TYPE *,' ASP UNKNOWN ---> TYPE 0'
      ACCEPT *,IAK
      FMAX=FMIN+(NF-1)*FINC
      PRINT *,' LARGE INTEGERS : ',IS3,IS4
      PRINT *,' AMPLITUDE AND PHASE'
      IF(IRA.EQ.1)PRINT *,' RELATIVE AMPLITUDE USED'
      IF(IAK.EQ.1)PRINT *,' ASP ASSUMED KNOWN'
      IF(IAK.EQ.0)PRINT *,' ASP ASSUNED UNKNOWN'
      PRINT *,' ADDITIVE NOISE ADDED'
      PRINT *,' CLASSIFICATION IN FREQUENCY DOMAIN'
      PRINT *,' NO OF EXPERIMENTS ',NEX
      PRINT 2839,FMIN,FMAX,FINC,NF
```

```
2839    FORMAT(' FMIN = ',F8.3,' FMAX = ',F8.3,' FINC = ',
     1F8.3,/,' NO OF FREQ = ',I3)
        PRINT 2849,MINASP,MAXASP,INCASP
2849    FORMAT(' MIN,MAX,AND INC OF THE ASPECTS : ',3I5)
C
C       READ DATA FILES
C
        CALL DATA(MINASP,MAXASP,INCASP,FMIN,FMAX,FINC,
     1NF,NS,C,A,P,IRA)
C
C       COMPUTE WAVELENGTHS
C
6664    DO 99237 I=1,NF
99237   WL(I)=300./(FMIN+(I-1)*FINC)
        PRINT *,'NO OF TARGETS ',NS
C
C       COMPUTE W(J) AND RELATIVE AMPLITUDES
C
        PI=4.*ATAN(1.)
        TWOPI=2.*PI
        NF1=NF-1
        DO 1434 I=1,NS
        DO 1434 J=1,NF-1
        IF(IRA.EQ.1)A(I,J)=A(I,J)/A(I,J+1)
C
C       ELIMINATE BRANCH-CUTS
C
        PC=P(I,J)
        DP=P(I,J)-P(I,J+1)
        IF(DP.GT.PI)PC=PC-TWOPI
        IF(DP.LT.-PI)PC=PC+TWOPI
C
1434    W(I,J)=WL(J)*PC-WL(J+1)*P(I,J+1)
C
C       ESTIMATE VARIANCES OF THE AMPLITUDES
C
        IF(IRA.EQ.0)CALL VARN(A,NF,NS,VA,1)
        IF(IRA.EQ.1)CALL VARN(A,NF1,NS,VA,1)
C
C       ESTIMATE VARIANCES OF THE W'S
C
        CALL VARN(W,NF1,NS,VW,1)
C
        PRINT *,'VAR(AMP)=',VA
        PRINT *,'VAR(W)=',VW
C
C       ESTIMATE SIGNAL POWERS
C
2880    PAVE=0.
        DO 910 I=1,NS
        DO 910 J=1,NF
        PAVE=PAVE+A(I,J)*A(I,J)
910     CONTINUE
        PAVE=PAVE/(FLOAT(NF)*FLOAT(NS))
        PAVE=10.*ALOG10(PAVE)
```

```
      PRINT *,' AVE SIGNAL POWER (DB) = ',PAVE
C
C     DEFINE THE VARIANCE RATIO
C
555   TYPE *,'INPUT R=VAR(A)/VAR(KW)'
      ACCEPT *,RR
C
C     SPECIFY THE FEATURES AS FOLLOWS
C     IYW = 1 ---> USE THE W'S
C     IYW = 0 ---> DO NOT USE THE W'S
C     IYA = 1 ---> USE THE AMPLITUDES
C     IYA = 0 ---> DO NOT USE THE AMPLITUDES
C
      TYPE *,'INPUT IYW AND IYA'
      ACCEPT *,IYW,IYA
C
C     CALCULATE THE NORMALIZATION CONSTANT RK
C
      RK=SQRT(VA/(RR*VW))
C
      PRINT 18220
18220 FORMAT(1X,'****************************************')
      PRINT *,'IYW=',IYW,'IYA=',IYA
      PRINT 18221,RR
18221 FORMAT(1X,'VAR(A)/VAR(KW)=',E12.5)
C
C     VARY THE NOISE POWER FROM IV1 TO IV2 DB
C     AT AN INCREMENT OF IVT DB
C
      DO 80 IV=IV1,IV2,IVT
C
C     INITIALIZE THE NUMBER OF FALSE ALARMS
C
      RMIS=0
C
C     PERFORM CLASSIFICATIONS NEX TIMES
C
      DO 888 IEX=1,NEX
      IF(IDIS.EQ.1)PRINT *,'************************************'
C
C     ADD NOISE TO THE ORIGINAL DATA FILES TO GENERATE
C     TEST TARGETS
C
      VM=10.**(FLOAT(IV)/10.)
      CALL MN(VM,IS3,IS4,C,NC,NF,NS,IYA,IYW,IEX,SAP)
C
C     CALCULATE NOISY AMPLITUDE AND PHASE RETURNS
C
      DO 921 I=1,NS
      DO 921 J=1,NF
      AN(I,J)=ABS(NC(I,J))
921   PN(I,J)=ATAN2(AIMAG(NC(I,J)),REAL(NC(I,J)))
C
C     CALCULATE NOISY W'S
C
```

```
      DO 922 I=1,NS
      DO 922 J=1,NF-1
      PC=PN(I,J)
      DP=PN(I,J)-PN(I,J+1)
      IF(DP.GT.PI)PC=PC-TWOPI
      IF(DP.LT.-PI)PC=PC+TWOPI
922   WN(I,J)=WL(J)*PC-WL(J+1)*PN(I,J+1)
      IF(IRA.EQ.0)GO TO 398
C
C     CALCULATE NOISY RELATIVE AMPLITUDES
C
      DO 349 IR1=1,NS
      DO 349 IR2=1,NF-1
349   AN(IR1,IR2)=AN(IR1,IR2)/AN(IR1,IR2+1)
C
C     COMPUTE NEAREST-NEIGHBOR DISTANCES
C     BETWEEN ANY TWO CLASSES
C
398   CALL DIST(IRA,IYW,IYA,A,W,AN,WN,NF,NS,RR,RK,D)
C
C     PERFORM NEAREST-NEIGHBOR CLASSIFICATION
C     AND COMPUTE THE NUMBER OF FALSE ALARMS
C
C     IF ASPECT ANGLES ARE ASSUMED KNOWN THEN
C     CONSIDER ONLY THOSE CLASSES WHOSE ASPECT ANGLES
C     ARE THE SAME AS THAT OF THE TARGET, OTHERWISE
C     CONSIDER ALL CLASSES
C
      KASP=(MAXASP-MINASP)/INCASP+1
      IF(IAK.EQ.0)KASP=1
C
C     FIND THE NEAREST-NEIGHBOR OF THE TEST TARTETS
C
      DO 7263 IKX=1,KASP
      DO 740 IT=IKX,NS,KASP
      DMIN=10000000000.
      DO 860 I=IKX,NS,KASP
      IF(D(I,IT).GE.DMIN)GO TO 860
      DMIN=D(I,IT)
      IMIN=I
860   CONTINUE
      IF(IDIS.EQ.1)PRINT *,' TARGET :',IT,' MIN = ',IMIN
      IF(IDIS.EQ.1)PRINT 730,(D(I1,IT),I1=1,NS)
      IF(IDIS.EQ.2)WRITE(1,730)(D(I1,IT),I1=1,NS)
730   FORMAT(6X,15F5.0,/)
C
C     IF A TARGET IS MISCLASSIFIED INCREASE THE
C     NUMBER OF FALSE ALARMS BY ONE
C
740   IF(IMIN.NE.IT)RMIS=RMIS+1
7263  CONTINUE
888   CONTINUE
C
C     CALCULATE THE MAXIMUM LIKELIHOOD ESTIMATE
C     OF THE ERROR PROBABILITY
```

```
C
      RMIS=RMIS/(NEX*NS)*100.
C
      PRINT 1113,IV,RMIS
1113  FORMAT(' NOISE POWER = ',I3,';  % ERRORS = ',F5.1)
80    CONTINUE
      TYPE *,'DO YOU WANT TO PROCEED ? Y=1 N=0'
      ACCEPT *,IYN
      IF(IYN.EQ.1)GO TO 555
      STOP
      END
C
C     THIS SUBROUTINE CALCULATES THE NEAREST-NEIGHBOR
C     DISTANCES BETWEEN ANY TWO CLASSES IN THE DATA BASE
C
      SUBROUTINE DIST(IRA,IYW,IYA,A,W,AN,WN,NF,NS,RR,RK,D)
      REAL D(18,18),A(18,50),W(18,50),AN(18,50),WN(18,50)
      DO 20 I=1,NS
      DO 20 IT=1,NS
      D(I,IT)=0.
      DO 23 K=1,NF-1
      IF(IYW.EQ.1)D(I,IT)=D(I,IT)+((W(I,K)-WN(IT,K))*RK)**2
      IF(IYA.EQ.1)D(I,IT)=D(I,IT)+(A(I,K)-AN(IT,K))**2
23    CONTINUE
C
C     IF ABSOLUTE AMPLITUDES ARE USED THEN TAKE INTO ACCOUNT
C     THE LAST FREQUENCY.
C
      IF(IYA.EQ.1.AND.IRA.EQ.0)D(I,IT)=D(I,IT)+
     1(A(I,NF)-AN(IT,NF))**2
      D(I,IT)=SQRT(D(I,IT))
20    CONTINUE
      RETURN
      END
C
C     THIS SUBROUTINE ADDS GAUSSIAN NOISE TO THE ORIGINAL
C     DATA FILES TO GENERATE TEST TARGETS
C
      SUBROUTINE MN(VR,IS3,IS4,C,NC,NF,NS,IYA,IYW,IEX,SAP)
      COMPLEX NC(18,50),C(18,50)
      REAL SAP(18)
C
C     THE GAUSSIAN NOISE IS ADDITIVE AND HAS VARIANCE VR
C     AND MEAN 0.
C
C     ASSUME EQUAL AMOUNTS OF NOISE ARE ADDED TO
C     THE REAL PARTS AND THE IMAGINARY PARTS
C     OF THE DATA POINTS
C
      VR1=VR/2.
C
C
      DO 10 I=1,NS
C
C     RESET THE SEEDS FOR EACH TEST TARGET
```

```
C
      IS3=IS3-4
      IS4=IS4-6
      DO 10 J=1,NF
C
C     GENERATE TWO GAUSSIAN NUMBERS
C
      CALL GAUSS(IS3,0.,VR1,S3)
      CALL GAUSS(IS4,0.,VR1,S4)
C
C     GENERATE A TEST TARGET
C
      NC(I,J)=CMPLX(REAL(C(I,J))+S3,AIMAG(C(I,J))+S4)
C
C     IF PHASE RETURNS ARE UNKNOWN THEN SET THEM TO ZERO
C
10    IF(IYA.EQ.1.AND.IYW.EQ.0)NC(I,J)=CMPLX(ABS(C(I,J))+S3,S4)
      RETURN
      END
C
C     THIS SUBROUTINE READS A DATA FILE GENERATED BY
C     THE B3.FOR PROGRAM
C
      SUBROUTINE DATA(MINASP,MAXASP,INCASP,FMIN,FMAX,FINC
     1,NF,NS,C,A,P,IRA)
      INTEGER*2 INFILE(5),FLNAM(5),ASP(13),AIR(4),SHIP(5)
      COMPLEX C(18,50)
      REAL A(18,50),P(18,50),W(18,50)
      REAL*4 AM(801),PH(801)
      DATA ASP/'00','15','30','45','60','75','90',
     1'05','20','35','50','65','80'/
      DATA SHIP/'AD','LR','LB','KA','79'/,AIR/'87','C0','C5','DC'/
      IBASE=0
      TYPE *,' AIRCRAFT CLASSIFICATION ----> TYPE 0'
      TYPE *,' SHIP CLASSIFICATION -----> TYPE 1'
      ACCEPT *,IAS
      IF(IAS.EQ.0)PRINT *,'CLASSIFICATION OF AIRCRAFT'
      IF(IAS.EQ.1)PRINT *,'CLASSIFICATION OF SHIPS'
      IF(IAS.EQ.0)NST=4
      IF(IAS.EQ.1)NST=5
      DO 772 I=1,NST
      IF(IAS.EQ.0)FLNAM(I)=AIR(I)
772   IF(IAS.EQ.1)FLNAM(I)=SHIP(I)
      IF(INCASP.EQ.0)INCASP=1
      IBC=(MAXASP-MINASP)/INCASP
      DO 40 I=1,NST
      DO 111 IAP1=MINASP,MAXASP,INCASP
      IBASE=IBASE+1
      IASP=IAP1/15+1
      INFILE(1)='R:'
      INFILE(2)=FLNAM(I)
      INFILE(3)='FV'
      INFILE(4)=ASP(IASP)
      INFILE(5)=0
      CALL TR(INFILE,AM,PH,TFMIN,TFINC,SF)
```

```
C
C       NOTE THE DATA FILES
C       ARE ALREADY SCALED BY THE SCALE FACTOR
C
        IMAX=(FMAX-TFMIN)/TFINC+1
        IMIN=(FMIN-TFMIN)/TFINC+1
        IC=FINC/TFINC
        NF1=0
        DO 2111 J=IMIN,IMAX,IC
C
C       CONVERT AMPLITUDE  SCALE FORM CM TO M
C       BY DIVISION OF 100
C
        NF1=NF1+1
        A(IBASE,NF1)=10.**(AM(J)/20.)/100.
2111    P(IBASE,NF1)=PH(J)
111     CONTINUE
40      CONTINUE
        NS=IBASE
6664    DO 1436 I=1,NS
        DO 1436 J=1,NF
1436    C(I,J)=CMPLX(A(I,J)*COS(P(I,J)),A(I,J)*SIN(P(I,J)))
        IF(NF.LE.NF1)GO TO 1435
        DO 1437 I=1,NS
        P(I,NF)=0
        A(I,NF)=0
1437    C(I,NF)=0
1435    RETURN
        END
C
C       THIS SUBROUTINE CALCULATES THE VARIANCE OF
C       A SET OF NUMBERS
C
        SUBROUTINE VARN(A,NF,NS,VA,INC)
        REAL A(18,50)
        RMEAN=0
        DO 10 I=1,NS
        DO 10 J=1,NF,INC
10      RMEAN=A(I,J)+RMEAN
        RMEAN=RMEAN/(NS*(NF/INC))
        VA=0
        DO 20 I=1,NS
        DO 20 J=1,NF,INC
20      VA=VA+(A(I,J)-RMEAN)**2
        VA=VA/(NS*(NF/INC))
        RETURN
        END
C
C       THIS SUBROUTINE GENERATES A GAUSSIAN RANDOM NUMBER
C
        SUBROUTINE GAUSS(IS,AM,V,S)
        A=0.0
        DO 50 I=1,12
        A=A+RAN(IS)
50      CONTINUE
```

```
      S=(A-6.)*SQRT(V)+AM
      RETURN
      END
```

```
C
C       THIS SUBROUTINE READS A FILE
C
        SUBROUTINE TR(INFILE,AM,PH,FMIN,FINC,SF)
        INTEGER*2 INFILE(5),LINE2(24)
        INTEGER*4 ID(12)
        REAL*4 AM(801),PH(801)
        INCLUDE 'SYS$LIBRARY:FORIOSDEF'
8106    OPEN(UNIT=8,NAME=INFILE,TYPE='OLD',IOSTAT=IERR,ERR=8100)
        READ(8,30)(ID(I),I=1,12),LINE2,NP,FMIN,FINC,SF
30      FORMAT(12A4,24A2,4A4)
        READ(8,40)(AM(I),I=1,NP),(PH(I),I=1,NP)
40      FORMAT(128A4)
        GO TO 331
8100    IF(IERR.EQ.FOR$IOS_FILNOTFOU)THEN
        TYPE 1112,INFILE
1112    FORMAT(' FILE : ',15A2,' WAS NOT FOUND',//,
     1' ENTER FILENAME AGAIN')
        ELSE IF (IERR.EQ.FOR$IOS_FILNAMSPE)THEN
        TYPE 1113,INFILE
1113    FORMAT(' FILE : ',15A2,' WAS BAD, ENTER NEW FILENAME')
        ELSE
        TYPE *,'UNRECOVERABLE ERROR, CODE=',IERR
        STOP
        ENDIF
        ACCEPT 1114,(INFILE(IIT),IIT=1,14)
1114    FORMAT(14A2)
        GO TO 8106
331     CLOSE(UNIT=8,DISP='SAVE')
        RETURN
        END
C
C       THIS SUBROUTINE DECODES PARAMETERS READ
C       FROM THE DATA FILES, WHICH ARE CODED IN ASCII CODES
C
        SUBROUTINE DCDE(NP,FMIN,FINC)
        COMMON BUFF
        BYTE BUFF(6656)
        INTEGER*4 IMIN,IINC,NP
C
C       NO OF DATA POINTS IS STORED IN THREE CHARACTERS, AND
C       STARTING FREQ AND FREQ INC. IN 5 CHARACTERS
C
        CHARACTER*3 CNL
        CHARACTER*5 CFF,CINC
        EQUIVALENCE (BUFF(124),CNL),(BUFF(131),CFF),(BUFF(140),CINC)
C
C
C       CONVERT CHARACTERS INTO THEIR NUMERICAL EQUIVALENTS
C
        DECODE(3,100,CNL)NP
100     FORMAT(I5)
        DECODE(5,100,CFF)IMIN
        DECODE(5,100,CINC)IINC
        FMIN=FLOAT(IMIN)/1000.
```

```
FINC=FLOAT(IINC)/1000.
RETURN
END
```

```
C
C       PROGRAM NAME : TIME.FOR
C
C
C       THIS PROGRAM CLASSIFIES TARGETS IN THE TIME DOMAIN
C
C
        COMPLEX C(18,50),NC(18,50)
        COMPLEX FFFT(32)
        REAL D(18,18),SFFT(8)
        REAL SP(18),SNP(18)
        COMMON /BLK1/SFFT,FFFT
        TYPE *,' ***** YOU MUST ASSIGN DATA DIRECTORY TO R *****'
        TYPE *,' WANT TO PRINT DISTANCES IN CLASSIFICATION ? Y=1 N=0'
555     ACCEPT *,IDIS
C
C       INPUT TWO ARBITRARY LARGE ODD INTEGERS WHICH
C       WILL SERVE AS SEEDS FOR GENERATING RANDOM NUMBERS
C
        TYPE *,'INPUT 2 ARBITRARY LARGE ODD INTEGERS'
        ACCEPT *,IS3,IS4
C
C       SPECIFY THE MINIMUM, MAXIMUM, AND INCREMENT OF THE
C       ADDITIVE GAUSSIAN NOISE POWERS
C
        TYPE *,'INPUT MIN,MAX,INC OF THE NOISE POWER (DB)'
        ACCEPT *,IV1,IV2,IVT
C
C       SPECIFY TARGET ASPECT ANGLES
C
        TYPE *,'INPUT MIN,MAX,INC OF ASP'
        ACCEPT *,MINASP,MAXASP,INCASP
C
C       SPECIFY FREQUENCIES
C
        TYPE *,'INPUT FMIN,FINC,NO OF FREQ'
        ACCEPT *,FMIN,FINC,NF
C
C       SET THE NUMBER OF CLASSIFICATION EXPERIMENTS
C
        TYPE *,'INPUT NO OF EXPERIMENTS'
        ACCEPT *,NEX
C
        TYPE *,'ASP KNOWN --> TYPE 1'
        TYPE *,'ASP UNKNOWN --> TYPE 0'
        ACCEPT *,IAK
        FMAX=FMIN+(NF-1)*FINC
        PRINT *,' LARGE INTEGERS : ',IS3,IS4
        IF(IAK.EQ.1)PRINT *,' ASP KNOWN'
        IF(IAK.EQ.0)PRINT *,' ASP UNKNOWN'
        PRINT *,' ADDITIVE NOISE ADDED'
        PRINT *,' CLASSIFICATION IN TIME DOMAIN'
        PRINT *,' NO OF EXPERIMENTS ',NEX
        PRINT 2839,FMIN,FMAX,FINC,NF
2839    FORMAT(' FMIN = ',F8.3,' FMAX = ',F8.3,' FINC = ',
```

```
     1F8.3,/,' NO OF FREQ = ',I3)
        PRINT 2849,MINASP,MAXASP,INCASP
2849    FORMAT(' MIN,MAX,AND INC OF THE ASPECTS : ',3I5)
C
C       READ DATA FILES
C
        CALL DATA(MINASP,MAXASP,INCASP,FMIN,FMAX,FINC,
     1NF,NS,C,IRA)
C
C       CALCULATE A COSINE TABLE FOR FAST FOURIER TRANSFORMS
C       BY CALLING A SUBROUTINE IN THE SCIENTIFIC LIBRARY
C
        CALL FORT(FFFT,5,SFFT,0,IFERR)
C
C       CALCULATE SQUARE-ROOTS OF TOTAL SIGNAL POWERS
C
        DO 98274 I=1,NS
        SP(I)=0
        DO 9824 J=1,NF
9824    SP(I)=SP(I)+ABS(C(I,J))**2
98274   SP(I)=SQRT(SP(I))
C
        PRINT *,'NO OF TARGETS ',NS
        PRINT 18220
18220   FORMAT(1X,'****************************************')
C
C       VARY THE NOISE POWERS FROM IV1 TO IV2 DBS
C       AT INCREMENT OF IVT DBS
C
        DO 80 IV=IV1,IV2,IVT
C
C       INITIALIZE THE TOTAL NUMBER OF FALSE ALARMS
C
        RMIS=0
C
C
C       PERFORM CLASSIFICATION EXPERIMENTS NEX TIMES
C
        DO 888 IEX=1,NEX
        IF(IDIS.EQ.1)PRINT *,'****************************************'
C
C       ADD NOISES TO ORIGINAL DATA FILES TO GENERATE
C       TEST TARGETS
C
        VM=10.**(FLOAT(IV)/10.)
        CALL MN(VM,IEX,IS3 TS4,C,NC,NF,NS,SP)
C
C
C       CALCULATE SQUARE-ROOTS OF TOTAL POWERS OF
C       THE NOISY TARGETS
C
        DO 9221 I=1,NS
        SNP(I)=0
        DO 921 J=1,NF
        SNP(I)=SNP(I)+ABS(NC(I,J))**2
```

```
921     CONTINUE
9221    SNP(I)=SQRT(SNP(I))
C
C       COMPUTE CROSS-COEFFICIENTS BETWEEN ANY TWO CLASSES
C
        NB=INT(FMIN/FINC)
479     CALL DIST(C,NC,SP,SNP,NF,NS,D,NB)
C
C       PERFORM TIME-DOMAIN CLASSIFICATIONS,
C       AND COMPUTE NO OF FALSE ALARMS
C
C       IF ASPECT ANGLES ARE ASSUMED KNOWN THEN
C       CONSIDER ONLY THOSE CLASSES WHOSE ASPECT ANGLES
C       ARE THE SAME AS THAT OF A TARGET, OHTERWISE
C       CONSIDER ALL CLASSES
C
        KASP=(MAXASP-MINASP)/INCASP+1
        IF(IAK.EQ.0)KASP=1
C
        DO 7263 IKX=1,KASP
        DO 740 IT=IKX,NS,KASP
        DMAX=-10000000000.
C
C       FIND  A CLASS WHICH HAS THE MAXIMUM CORRELATION
C       WITH A TARGET
C
        DO 860 I=IKX,NS,KASP
        IF(D(I,IT).LE.DMAX)GO TO 860
        DMAX=D(I,IT)
        IMAX=I
860     CONTINUE
C
        IF(IDIS.EQ.1)PRINT *,' TARGET :',IT,' MAX = ',IMAX
        IF(IDIS.EQ.1)PRINT 730,(D(I1,IT),I1=1,NS)
        IF(IDIS.EQ.2)WRITE(1,730)(D(I2,IT),I2=1,NS)
730     FORMAT(6X,15F5.2,/)
C
C       IF A TARGET IS MISCLASSIFIED THEN INCREASE THE
C       NUMBER OF FALSE ALARMS BY 1
C
740     IF(IMAX.NE.IT)RMIS=RMIS+1
C
7263    CONTINUE
888     CONTINUE
C
C       CALCULATE THE MAXIMUM LIKELIHOOD ESTIMATE OF
C       THE ERROR PROBABILITY
C
        RMIS=RMIS/FLOAT(NEX*NS)*100.
C
C
        PRINT 1113,IV,RMIS
1113    FORMAT(' NOISE POWER = ',I5,';  % ERRORS = ',F5.1)
80      CONTINUE
        TYPE *,'DO YOU WANT TO PROCEED ? Y=1 N=0'
```

```
      ACCEPT *,IYN
      IF(IYN.EQ.1)GO TO 555
      STOP
      END
C
C     THIS SUBROUTINE CALCULATES THE CROSS-CORRELATION
C     COEFFICIENTS BETWEEN TWO CLASSES
C
      SUBROUTINE DIST(C,NC,SP,SNP,NF,NS,D,NB)
      REAL D(18,18),SP(18),SNP(18),S(8)
      COMPLEX C(18,50),NC(18,50),RF(50),F(32)
      DO 20 I=1,NS
      DO 20 IT=1,NS
      DO 23 K=1,NF
C
C     CALCULATE PRODUCTS OF RADAR RETURNS OF A CLASS
C     AND COMPLEX CONJUGATES OF A TARGET'S RETURNS
C
      RF(K)=C(I,K)*CONJG(NC(IT,K))
C
23    CONTINUE
C
C     CALCULATE THE INVERSE FAST-FOURIER
C     TRANSFORM ( IFFT ) OF THE PRODUCTS
C
      CALL IDIFT(RF,NF,NB,STM)
C
C     NORMALIZE THE OUTPUTS OF THE IFFT
C
      D(I,IT)=STM/(2.*SP(I)*SNP(IT))
C
20    CONTINUE
      RETURN
      END
C
C     THIS SUBROUTINE ADDS GAUSSIAN NOISE TO THE ORIGINAL
C     DATA FILES TO GENERATE TEST TARGETS
C
      SUBROUTINE MN(VR,IEX,IS3,IS4,C,NC,NF,NS,SP)
      COMPLEX NC(18,50),C(18,50)
      REAL SP(18)
C
C     THE GAUSSIAN NOISE ARE ADDITIVE AND HAS VARIANCE VR
C     AND MEAN 0.
C
      VR1=VR/2
      DO 10 I=1,NS
C
C     RESET SEEDS FOR EACH CLASS
C
      IS3=IS3-4
      IS4=IS4-2
      DO 10 J=1,NF
C
C     GENERATE TWO GAUSSIAN NUMBERS
```

```
C
      CALL GAUSS(IS3,0.,VR1,S3)
      CALL GAUSS(IS4,0.,VR1,S4)
C
C     GENERATE A TEST TARGET'S RETURN
C
10    NC(I,J)=CMPLX(REAL(C(I,J))+S3,AIMAG(C(I,J))+S4)
C
      RETURN
      END
C
C     THIS SUBROUTINE READS DATA FILES GENERATED BY PROGRAM
C     B3.FOR
C
      SUBROUTINE DATA(MINASP,MAXASP,INCASP,FMIN,FMAX,FINC
     1,NF,NS,C,IRA)
      INTEGER*2 INFILE(5),FLNAM(5),ASP(13),AIR(4),SHIP(5)
      COMPLEX C(18,50)
      REAL A(18,50),P(18,50),W(18,50)
      REAL*4 AM(801),PH(801)
      DATA ASP/'00','15','30','45','60','75','90',
     1'05','20','35','50','65','80'/
      DATA SHIP/'AD','LR','LB','KA','79'/,AIR/'B7','C0','C5','DC'/
      IBASE=0
      TYPE *,' AIRCRAFT CLASSIFICATION ------> TYPE 0'
      TYPE *,' SHIP CLASSIFICATION ------> TYPE 1'
      ACCEPT *,IAS
C
C     NST = NO OF TARGETS
C
      IF(IAS.EQ.0)NST=4
      IF(IAS.EQ.1)NST=5
C
C     GENERATE FILE NAMES
C
      DO 772 I=1,NST
      IF(IAS.EQ.0)FLNAM(I)=AIR(I)
772   IF(IAS.EQ.1)FLNAM(I)=SHIP(I)
      IF(INCASP.EQ.0)INCASP=1
      DO 40 I=1,NST
      DO 111 IAP1=MINASP,MAXASP,INCASP
      IBASE=IBASE+1
      IASP=IAP1/15+1
      INFILE(1)='R:'
      INFILE(2)=FLNAM(I)
      INFILE(3)='FV'
      INFILE(4)=ASP(IASP)
      INFILE(5)=0
C
C     READ A FILE
C
      CALL TR(INFILE,AM,PH,TFMIN,TFINC,SF)
C
C     NOTE THE INPUT FILES
C     HAVE ALREADY BEEN SCALED BY THE SCALE FACTOR
```

```
C
      IMAX=(FMAX-TFMIN)/TFINC+1
      IMIN=(FMIN-TFMIN)/TFINC+1
      IC=FINC/TFINC
      NF1=0
      DO 2111 J=IMIN,IMAX,IC
C
C     CONVERT AMPLITUDE SCALE FORM CM TO M
C     BY DIVISION OF 100
C
      NF1=NF1+1
      A(IBASE,NF1)=10.**(AM(J)/20.)/100.
2111  P(IBASE,NF1)=PH(J)
111   CONTINUE
40    CONTINUE
      NS=IBASE
6664  DO 1436 I=1,NS
      DO 1436 J=1,NF
1436  C(I,J)=CMPLX(A(I,J)*COS(P(I,J)),A(I,J)*SIN(P(I,J)))
      IF(NF.LE.NF1)GO TO 1435
      DO 1437 I=1,NS
      P(I,NF)=0
      A(I,NF)=0
1437  C(I,NF)=0
1435  RETURN
      END
C
C     THIS SUBROUTINE GENERATES  GAUSSIAN RANDOM NUMBERS
C     WHICH HAVE A VARIANVE V AND MEAN AM
C
      SUBROUTINE GAUSS(IS,AM,V,S)
      A=0.0
      DO 50 I=1,12
      A=A+RAN(IS)
50    CONTINUE
      S=(A-6.)*SQRT(V)+AM
      RETURN
      END
C
C     THIS SUBROUTINE CALCULATES THE INVERSE
C     FOURIER TRANSFORM OF A SET OF COMPLEX DATA POINTS
C     AND FIND THE MAXIMUM OF THE RESULTS
C     IT ASSUMES THAT THE DATA POINTS ARE SYMMETRIC
C     AROUND ZERO FREQUENCY
C
      SUBROUTINE IDIFT(RF,NF,NB,STM)
      COMPLEX F(32),RF(50)
      REAL S(8)
      COMMON /BLK1/S,F
      NP=32
      DO 40 I=1,NP
40    F(I)=(0.,0.)
      K=0
      DO 50 I=NB+1,NB+NF
      K=K+1
```

```
      F(I)=RF(K)
50    F(NP+2-I)=CONJG(RF(K))
C
C     CALL A STANDARD IFFT ROUTINE IN THE SCIENTIFIC
C     LIBRARY
C
      CALL FORT(F,5,S,2,IFERR)
      IF(IFERR.NE.0)PRINT *,' ERR IN IFFT'
C
C     FIND THE MAXIMUM OF THE OUTPUTS OF THE IFFT
C
      STM=-10000.
      DO 500 I=1,NP
500   IF(REAL(F(I)).GT.STM)STM=REAL(F(I))
      RETURN
      END
```

END

FILMED

2-86

DTIC